Delivery of nucleic acids in brain ischemia mediated by dendrimers: The challenge of crossing the blood-brain barrier

Beatriz Maria Lopes Custódio

Master Thesis

Integrated Master in Bioengineering

Molecular Biotechnology

Supervisor: Dr. Ana Paula Pêgo

Co-supervisor: Dr. Sofia Santos

September 2018

This work was financially supported by:

By INFARMED (project FIS-2015-01_CCV_ 20150630-88); National Funds through FCT – Fundação para a Ciência e a Tecnologia (PTDC/CTM-NAN/3547/2014); projects NORTE-01-0145-FEDER-000008 and NORTE-01-0145-FEDER-000012, supported by Norte Portugal Regional Operational Programme (NORTE 2020), under the PORTUGAL 2020 Partnership Agreement, through the European Regional Development Fund (ERDF) and FEDER - Fundo Europeu de Desenvolvimento Regional funds through the COMPETE 2020 - Operacional Programme for Competitiveness and Internationalisation (POCI), Portugal 2020, and by Portuguese funds through FCT/MCTES in the framework of the project "Institute for Research and Innovation in Health Sciences" (POCI-01-0145-FEDER-007274).

This page was intentionally left in blank.

Abstract

Ischemic stroke is a pathology with high economical and social impact in today's western-world society with the lack of effective therapies and the persistence of the affected patients who remain, to this day, still untreated.

One of the most promising approaches to promote the improvement of a stroke's outcome relies on neuroprotection. Worldwide studies have exposed a huge number of molecules with neuroprotection potential for ischemic stroke, contrasting with their failure in clinical applications, mainly, due to their low bioavailability in the brain, limited blood-brain barrier permeability and blood stability, as well as their high cytotoxicity. Consequently, there has been a permanent effort in creating strategies to improve these molecules' characteristics, so they can be used for this purpose. Nanomedicine has been revealing itself as the most capable field to address these caveats, since nanoscale biomaterials can provide a promising delivery platform (nanocarriers) for brain therapeutic substances such as drugs, proteins and nucleic acids.

Here, we tested commercially available generation 4 poly(amino amine) (PAMAM) and generation 3 PEGylated Gallic Acid-Triethylene Glycol Ester (PEG-GATGE) dendrimers as potential carriers of therapeutics. The last ones were the main focus of this project, once they have been recently proposed by our group, constituting a new family of fully degradable dendrimers. These are currently being explored as carriers of therapeutic nucleic acids (named as dendriplexes) to be applied by intravenous administration in the aftermath of an ischemic stroke.

Regarding central nervous system therapies aimed to be administrated by intravenous route, it is imperative to assess the permeability through the blood-brain barrier (BBB). It is well-known that, after an ischemic stroke, there is a temporary disruption of the BBB which can be a window of opportunity for nanoparticle delivery.

Concerning that, a previously developed *in vitro* BBB model was used to test dendrimers and dendriplexes ability to permeate under physiologic and ischemic conditions, which were induced by oxygen and glucose deprivation, as it happens after a vessel occlusion in ischemic stroke. Studies were started with the commercially available dendrimers (PAMAM) tethered with the fluorophore molecule rhodamine, where it was possible to verify higher permeation of the dendrimers under ischemic conditions. Subsequently, similar experiments were done with PEG-GATGE dendrimers complexed with nucleic acids (siDNA), however it was not possible to determine a permeability profile but an endocytic profile under different stimuli (normoxia and

hypoxia). In ischemic conditions, the dendriplex endocytosis-mediated uptake increases, possibly due to metabolic mechanisms alterations induced by hypoxia. The assessment of the dendriplexes permeation through the BBB should continue in the future to understand deeply their ability to permeate the BBB after intravenous administration.

For further *in vivo* studies with dendriplexes, a global ischemic zebrafish larvae model was developed in order to mimic the characteristic BBB disruption as it happens in humans after an ischemic stroke. The ischemia was induced to 4 days post fertilization animals by oxygen deprivation for 4 hours in a successfully validated hypoxia chamber. Imaging analysis was improved during the model establishment and higher quality imaging was verified *in vivo* under a fluorescence confocal microscope. However, results are still not conclusive as additional experiments should be done, accompanied by image quantification to determine BBB disruption. Overall these results, although in their infancy, show the promise of the proposed dendrimer system and open important avenues for the assessment of these newly proposed biocarriers.

Key words: Ischemic stroke, Dendrimers, Blood-brain barrier, Blood-brain barrier permeability, *In vitro* blood-brain barrier model, *In vivo* global ischemic zebrafish larvae model

Resumo

Atualmente, o acidente vascular cerebral (AVC) é uma patologia com elevado impacto económico e social no mundo ocidental. A persistência de pacientes por tratar deve-se à falta de terapias efetivas.

Uma das abordagens mais promissoras para a melhoria dos efeitos induzidos pelo AVC assenta no desenvolvimento de terapias neuroprotetoras. Inúmeros estudos têm descrito o potencial de diversas moléculas para este propósito, no entanto a maioria é caracterizada pelo insucesso em ensaios clínicos, devido à sua baixa biodistribuição no cérebro, permeabilidade à barreira hematoencefálica e estabilidade no sangue, bem como elevada citotoxicidade. Por isso, a procura de estratégias para melhorar as características destas moléculas tem sido um esforço constante. A nanomedicina tem-se revelado promissora na colmatação destas fraquezas, uma vez que os biomateriais à nanoescala podem ser utilizados como plataforma de entrega de substâncias terapêuticas ao cérebro, por exemplo fármacos, proteínas e ácidos nucleicos.

Neste trabalho, testámos dendrímeros comerciais de geração 4, poly(amino amine) (PAMAM), e dendrímeros sintetizados de geração 3, PEGylated Gallic Acid-Triethylene Glycol Ester (PEG-GATGE), como potenciais transportadores de moléculas terapêuticas. Estes últimos são o foco principal do projeto, uma vez que foram recentemente propostos pelo nosso grupo, constituindo uma nova família de dendrímeros completamente degradáveis. Estes estão a ser explorados como transportadores de ácidos nucleicos para administração intravenosa após AVC, sob a forma de dendriplexos.

Como terapia para o sistema nervoso central a ser administrada intravenosamente, é imperativo estudar a sua permeabilidade através da barreira hematoencefálica. Está descrito uma abertura temporária desta barreira após AVC isquémico, que pode ser vista como uma janela de oportunidade para a entrega das nanopartículas.

Posto isto, os dendrímeros e dendriplexos foram testados num modelo *in vitro* da barreira hematoencefálica de modo a avaliar a sua capacidade de permeação em condições fisiológicas e isquémicas (induzidas por privação de oxigénio e glucose, como acontece após a oclusão venosa em AVC). Estes estudos iniciaram-se com os dendrímeros comerciais (PAMAM) funcionalizados com um fluoróforo, a rodamina, nos quais foi possível verificar maior permeabilidade em condições de isquemia. Seguidamente, experiências similares foram realizadas com os dendrímeros PEG-GATGE complexados com ácidos nucleicos (siDNA). No entanto, não foi possível

determinar o perfil de permeabilidade, mas sim, um perfil de endocitose quando sujeitos a diferentes estímulos (normoxia e hipoxia). Em condições de isquemia, a entrada das nanopartículas por endocitose aumenta, possivelmente devido a alterações metabólicas induzidas pela hipoxia. O estudo da permeabilidade da barreira hematoencefálica aos dendriplexos deve continuar, de forma a perceber detalhadamente a sua capacidade de permear esta barreira após a administração sistémica.

Para futuras experiências *in vivo* com os dendriplexos, um modelo global de isquemia em larvas de *zebrafish* foi desenvolvido, de forma a mimetizar a disrupção característica da barreira hematoencefálica após AVC isquémico. A isquemia foi induzida por privação de oxigénio durante 4 horas em animais com 4 dias após a fertilização, numa câmara de hipoxia validada com sucesso. A análise por imagem foi melhorada durante o estabelecimento do modelo, sendo que imagens com qualidade superior foram obtidas *in vivo* recorrendo a um microscópio confocal de fluorescência. No entanto, os resultados não foram conclusivos e futuras experiências devem ser realizadas, acompanhadas por análise de imagem para determinar a disrupção da barreira hematoencefálica.

Apesar de ainda terem de ser explorados, estes resultados validam o conceito proposto para os sistemas dendríticos e apresentam métodos promissores de análise para os mesmos.

Palavras-chave: Acidente vascular cerebral isquémico, Dendrímeros, Barreira hematoencefálica, Permeabilidade da barreira hematoencefálica, modelo *in vitro* de barreira hematoencefálica, modelo *in vivo* de isquémica global em larva de *zebrafish*

Acknowledgements

No final desta etapa, um obrigado não chega para agradecer a todas estas pessoas que me acompanharam durante estes 5 anos e, especialmente, nesta reta final.

Em primeiro lugar, um grande obrigado às minhas orientadoras, Ana Paula Pêgo e Sofia Santos, pela oportunidade que me deram em participar neste projeto que tanto me desafiou e me ensinou. Um especial agradecimento pela ajuda e pelo apoio ao longo destes meses, sem vocês não seria possível este resultado final.

A todo o grupo nBTT que me acolheu carinhosamente e que foi incansável em ajudar-me sempre que precisei, um enorme obrigada. Foi também a vossa boa disposição que tornou tudo isto possível.

Ao grupo 'Vertebrate Development and Regeneration', IBMC/i3s e outros utilizadores da *zebrafish facility*, um obrigado pelo acolhimento e pela disponibilidade nas experiências com o *zebrafish*. À Joana Marques, um enorme obrigado por toda a ajuda e tempo despendido neste desafio com os nossos peixinhos!

A todas as pessoas que conheci nestes últimos 5 anos e sempre me ajudaram, especialmente à Ana Beatriz, à Cláudia, ao Luís, ao Gonçalo, à Mariana e à Ana Luísa, um muito obrigada. Valeu a pena mudar-me para o Norte do país para vos conhecer!

Ao Alex, um indescritível obrigado pelo apoio ao longo de todo este processo, especialmente pelo ânimo e carinho nas fases menos boas.

Por último, mas, de todo, não menos importante, aos meus pais, a quem devo isto e muito mais, um gigante obrigado pelo apoio incessante e a oportunidade que me deram para delinear o meu Futuro. E aos meus irmãos, que apesar da inevitável distância, me têm acompanhado nesta caminhada. A toda a restante família: avós, tios e primos, também um especial obrigado.

This page was intentionally left in blank.

Index

List of Figures

This page was intentionally left in blank.

Abbreviations list

AMPA	α-amino-3-hydroxy-5-methyl-4-propionate
ATP	Adenosine triphosphate
BaiTS	Biodegradable dendrimers for Targeted neuroprotective therapies in Stroke
BBB	Blood-brain barrier
CNS	Central nervous system
DLS	Dynamic scattered light
DMEM	Dulbecco's modified Eagle medium
dpf	Days post fertilization
EB	Evans blue
ECM	Extra-cellular matrix
FBS	Fetal bovine serum
FCT	Fundação para a Ciência e Tecnologia
G	Generation
GFAP	Glial fibrillary acidic protein
HBSS	Hank's Balanced Salt Solution
HEPES	4-(2-hydroxyethyl)-1-piperazineethanesulfonic acid
HMWM	High-molecular weight molecules
i.c.	Intracranial
i.n.	Intranasal
i.p.	Intraperitonial
i.v.	Intravenous
i3S	Instituto de Investigação e Inovação em Saúde
INEB	Instituto Nacional de Engenharia Biomédica
JAM-1	Junctional adhesion molecule-1
LD50	Medium lethal dose
MGCs	Mixed glial cells
MMPs	Matrix-metalloproteases
NA	Nucleic acid
nBTT	nanoBiomaterials for Targeted Therapies
NMDA	N-methyl-D-aspartate
NVU	Neurovascular unit
OGD	Oxygen and glucose deprivation
ON	Overnight

OPCs	Oligodendrocyte progenitor cells
PAMAM	Poly(amino amine)
PBS	Phosphate buffered saline
PDI	Polydispersity
PDL	Poly-D-lysine
PECAM-1	Platelet endothelial cell adhesion molecule-1
PEG	Poly(ethylene glycol)
PEG-GATGE	PEGylated gallic acid-triethylene glycol ester
PEG-PAMAM-5(6)-ROX	Rhodamine labeled PEGylated PAMAM
PEPE	Poly(ether)-copoly(ester)
PET	Polyehtylene terephthalate
PFA	Paraformaldehyde
PPI	Poly(propylene imine)
PLL	Poly-(L-lysine)
P/S	Penicillin/streptomycin
PTU	N-phenylthiourea
rCBF	Regional cerebral blood-flow
RGD	Arginylglycylaspartic acid
ROS	Reactive oxygen species
ROX	Rhodamine
SDS	Sodium dodecyl sulfate
TBE	Tris/Borate/EDTA
TEER	Transendothelial electrical resistance
TJ	Tight junction
tPA	Tissue plasminogen activator
WT	Wild type
ZO	Zonula occludens

Introduction

1.1. Stroke

Stroke is one of the world's biggest killers and cause of long-term disability in the western world with a huge social and economic impact. [1]–[3]. The worldwide incidence of this disease is highly related with prevalence of specific risks and genetic factors as well as the ability to clinically manage stroke. [3], [4]

Stroke can be either ischemic or hemorrhagic, depending on its causes. Between 80 and 90% of strokes are ischemic, caused by a transient or permanent brain arterial occlusion, restricting the blood flow to the brain. [5]–[8] Only a residual percentage of strokes are hemorrhagic, caused by a blood vessel leakage and consequent blood accumulation in the tissue creating swelling and increasing pressure. [9], [10]

The different consequences of each subtype of stroke lead to an independent management of these events in terms of therapies. [3] Due to the highest prevalence of ischemic stroke and to the fact that the only pharmacological treatment is not effective in all stroke patients, it has been a preferential target to the development of new therapeutic approaches. [7]

1.1.1. Ischemic stroke

Brain cells have a high metabolic rate and are mainly dependent on aerobic metabolism (oxidative phosphorylation) to obtain energy which leads to approximately 20% of the overall body oxygen consumption by the central nervous system (CNS). [10], [12], [13] The restriction of blood flow to any part of the brain leads to an inadequate oxygen and glucose input which rapidly compromises the tissue homeostasis. Following that, a complex and heterogeneous pathophysiological cascade of events starts, such as energy failure, excitotoxicity, peri-infarct depolarization, inflammation and cell death (necrosis or apoptosis). Ischemic cascade can last hours or even days, during and after vessel occlusion (Figure 1). [7], [8], [13], [14]

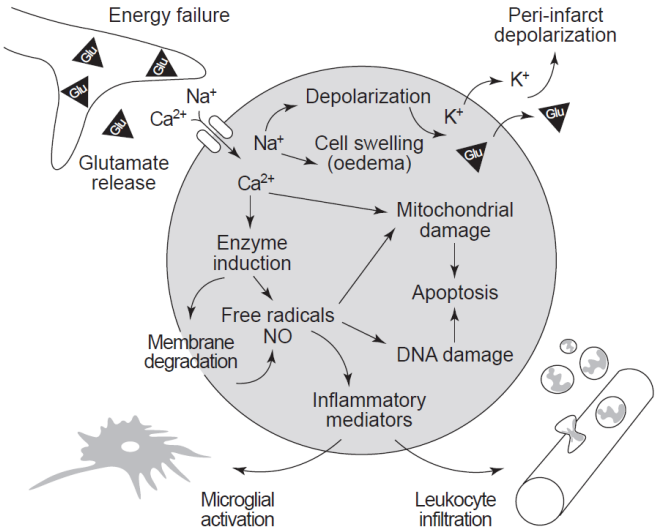

Figure 1 – Overview of the cascade events after an ischemic stroke (adapted from [13])

The core of brain infarct, closer to the occluded vessel, immediately experience cell death and it progresses over time to the surrounding area (ischemic penumbra). Ischemic penumbra is the area between the irreversible damaged core and the normal brain which has constrains in blood flow supply but energy metabolism is in part preserved. This area of the brain suffers a remodeling during the time after ischemic injury because of the activated mechanisms in ischemic cascade. [10], [14]

The pathological event starts with bioenergetic failure. Neurons are the most affected cells once they are highly dependent on oxygen and glucose for adenosine triphosphate (ATP) production for impulse transmission which requires the maintenance of ionic gradients through the membrane and presynaptic reuptake of excitatory amino acids. [10], [15] The loss of membrane ion pump both in neurons and glia lead to the loss of potassium (K^+) in return with sodium (Na^+),

chloride (Cl^-) and calcium (Ca^{2+}) and consequent cell swelling due to the inflow of water (cytotoxic edema). Also, the neuronal depolarization activates somatodendritic and presynaptic voltage-dependent Ca^{2+} channels, inducing the release of excitatory amino acids as glutamate to the extracellular space (excitotoxicity). The uncontrolled release of the referred amino acid activates glutaminergic calcium and monovalent ions receptor, such as N-methyl-D-aspartate (NMDA), α-amino-3-hydroxy-5-methyl-4-propionate (AMPA) or kainate receptors, increasing the influx of Na^+ and Ca^{2+} and, consequently, worsening the cytotoxic edema and promoting apoptosis mechanisms. [10], [13], [15]

The increase of Ca^{2+} intracellular levels initiates cytoplasmic and nuclear events by the activation of many enzymes such as proteases, kinases, phospholipases, endonucleases and cyclooxygenases. These include enzymes able to degrade cytoskeletal proteins, extracellular matrix proteins, membrane structures and also other cellular components, with the extensive production of reactive oxygen species (ROS) which overpowers the cell antioxidant capacity, specially neurons which have low antioxidative defense. Additionally, inflammation is triggered and ultimately the ischemic cascade leads to cell damage and death. [13], [14]

All mechanisms involved in ischemic stroke result in an impairment of brain cells and neurological deficits as clinical outcomes. The neurological improvement and recovery is dependent on cell recovery and remodeling in the ischemic penumbra, so that this tissue should be the target for any therapy after ischemic event. [13], [14], [16]–[18]

1.1.2. Current and emerging therapies

Current treatments for ischemic stroke aim to improve, in a safe manner, the clinical outcome after vessel occlusion. [19] Presently, there are no treatments that aim to protect neurons nor at promoting neural tissue repair and/or regeneration.

The available therapies are based on the "recanalization hypothesis", enabling the opening of occluded vessels for salvaging of the neurons and glial cells in the ischemic penumbra. [10], [20] Options are limited to pharmacological thrombolysis (using tissue plasminogen activator (tPA)), or mechanical thrombolysis (exploring mechanical thrombectomy devices). [21], [22]

tPA is an antithrombotic agent that is injected in the blood flow after an ischemic stroke to degrade the clot, so that the penumbra tissue is re-perfused and the oxygen and glucose levels are reestablished. [23] However, there are some drawbacks that should be taken in account when using antithrombotic agents in these patients. Treatment is limited to a narrow window of time

(until 4.5 hours after stroke), once their efficiency diminishes with the treatment delay [19], [21], [23], [24]; and there is the risk of hemoharrage which limits the therapy to a small number of patients (less than 10%) [7], [25]. Despite the favorable clinical outcome in the patients where the treatment is effective, the recanalization efficacy is modest, especially in large vessel occlusions, with only 40% cases of success. [19], [26]–[28] Consequently, research in pharmacological thrombectomy therapies continues, in order to have a more effectiveness in a longer window of time and with reduced side effects, as examples of novel fibrinolytic agents like desmoteplase, urokinase and prourokinase. [28], [29]

It has been recognized the advantage of the mechanical thrombectomy devices regarding the clinical outcomes in ischemic stroke therapies, due to their higher rates of reperfusion and the increase in indirect salvaging of the ischemic penumbra after longer periods of time. [19], [26], [30]–[32]

Available therapies allow the reperfusion of affected tissues, improving patients clinical outcome but they are still very limited once mechanisms of ischemia remain active. [15], [20], [33] Therefore, it remains the need of an urgent therapy to mitigate the distention of the ischemic core to the ischemic penumbra area. [19], [34], [35]

In the last decades, there has been an explosion in neuroprotective strategies, which target the penumbra area controlling cellular events in acute ischemia and stabilizing penumbra environment, once neurons around the ischemic core can survive for hours after the ischemic event. They can be a key element in stroke therapy, drawn to be used as alternatives or adjuvants to available therapies however, their success is still dependent on the time window of intervention. The number of possibilities is large due to the complexity of the ischemic event, where many molecular targets can be chosen for neuroprotection, such as neurotrophic stimulation, excitotoxicity mechanisms, calcium influx, ROS and nitric oxide production, inflammatory response and apoptosis. [13], [15], [35], [36]

Despite the intense research in these new approaches, therapies for brain ischemia are restricted to recanalization approaches with huge limitations. It makes the ischemic stroke one of the greatest health-care challenge, with very low approved clinical treatments, where there are many molecules with therapeutic potential but lack of clinical potential specially due to low crossing of the blood-brain barrier (BBB) and brain biodistribution. [7], [37] So, there is an imperative necessity to the development of new approaches which comply with clinical requirements. Recently, nanomedicine has taken notable advantage in this area since nanoscale biomaterials provide a promising delivery platform (nanocarriers) for brain therapeutic substances such as drugs, proteins and nucleic acids (NA), improving brain bioavailability, BBB permeation, blood

stability and cytotoxicity outcomes. All these characteristics are recognized to aid a therapeutic molecule to reach the target and be effective. Various materials have been tested as nanocarrier systems, which are commonly based on polymeric, lipid and/or metallic compounds. [37], [38]

1.1.2.1. Dendrimers

Dendrimers are a powerful class of polymer-based 3D nanoscale structures and attractive candidates for drug delivery systems due to their exceptional and tunable structural characteristics. As unique nanomaterials, dendrimers have a small size (nanoscale), a well-defined and globular shape, a low polydispersity and multiple functionable branches. [38]–[40] Dendrimers are composed by a central core - atom or molecule with at least two reactive groups -, repeating monomer units covalently attached to the core and concentrically organized in layers called “generations” (G), and many functional groups exposed on the surface (Figure 2). Reactive functional groups present in the external part of the dendrimer confer it polyvalence, allowing the creation of multivalent molecules which can deliver therapeutic molecules as well as mimic and target several biological systems. [40]–[42] For example, by improving brain bioavailability, BBB permeation, blood stability and cytotoxic outcome, which is the focus of this work.

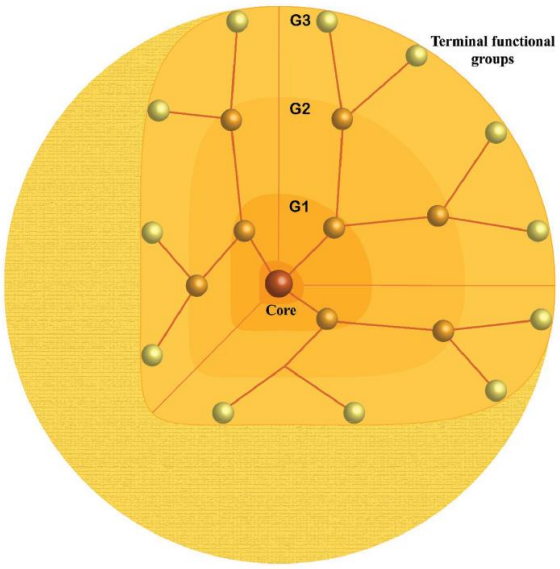

Figure 2 – Schematic representation of a G3 dendrimer structure (adapted from [40])

Dendrimer synthesis can be done by two different approaches: divergent or convergent. The divergent procedure consists in the growth of structure layer-by-layer from the core to the surface by adding repeating monomer units. Each monomer layer represents one generation of the dendrimer and the number of layers will determine the G number and, consequently, the size

of the molecule. Alternatively, the convergent route is based on the synthesis of dendrons (dendritic branches) which are then attached to the functional core. [40], [41]

Biologically active compounds or therapeutic molecules can be connected to the dendrimers in different ways depending on molecule characteristics: 1) encapsulated into the dendrimer structure or 2) chemically linked or physically adsorbed to external part of the dendrimer. [42], [43]

The extensively researched dendrimers for CNS applications are the poly(amino amine) (PAMAM) dendrimers, however there are others being explored such as poly(propylene imine) (PPI), poly(L-lysine)-based (PLL), carbosilane and poly(ether)-copoly(ester) (PEPE). [40], [42]

CNS therapeutic/diagnosis approaches using nanocarriers should comply several requirements such as biocompatibility, ability to transport and protect cargos and capability to reach CNS and the cell population of interest. Moreover, when designing CNS regeneration studies, it is important to consider biodegradability of the systems. [40], [44] And lack of biodegradability is one of the major drawbacks in the popular dendrimers in biomedical applications, once they have high stability under physiological conditions which could lead to bioaccumulation and consequent cytotoxicity. [41], [45]

To overcome this issue, there are several biodegradable dendriplexes being explored. The project BaiTS - Biodegradable dendrimers for Targeted neuroprotective therapies in Stroke, within the framework of which this thesis was conducted, aims at the development of fully biodegradable dendrimers able to transport therapeutic nucleic acids to improve neuron survival, neurite growth and synaptic plasticity in penumbra area after ischemic stroke.

It was reported in our group a PEGylated Gallic Acid-Triethylene Glycol Ester (PEG-GATGE) dendrimer G3 (Figure 3A), a fully biodegradable dendrimer due to the inclusion of hydrolysable ester bonds in its structure (unpublished data). In the physiological environment, enzymatic cleavages are expected to degrade the dendrimer in small fragments able to be eliminated by metabolic pathways. [44], [45]

Despite the challenging preparation due to its easy degradation during the synthesis, purification and functionalization steps, a fully biodegradable dendrimer was successfully synthetized (unpublished data). The dendrimer can be functionalized in the periphery of its branches with several molecules of interest, such as functional groups, target molecules and fluorescence molecules for tracking purposes. Here, they were functionalized with benzylamine groups (cationic) by a “click” chemical reaction (Figure 3B) to complex and deliver NA and to act as non-viral vectors in gene therapeutic applications. When mixed in an appropriate buffer, NAs link to the functionalized dendrimers by electrostatic interactions and form nanosized structures named

as “dendriplexes”, protecting their NA cargo from endonuclease degradation (Figure 3C). [40], [45] The formation of dendriplexes-NA complexes lead to a charge neutralization, however cationic proprieties are preserved once the molar ratio between the cationic groups from the dendrimer and phosphate groups from the NA (N/P ratio) is higher than 1. [41], [45]

The hydrophobicity of the aromatic groups and the electrostatic interactions with the end of the dendron and NAs, when forming the dendriplexes, lead to the exposure to the surface of the poly(ethylene glycol) (PEG) molecules. These molecules mask the dendriplexes’ positive charge and improve solubility, due to their hydrophilicity. Moreover, resident time in systemic circulation is increased which enhance the uptake by the cells of interest. [37], [38], [41], [45]

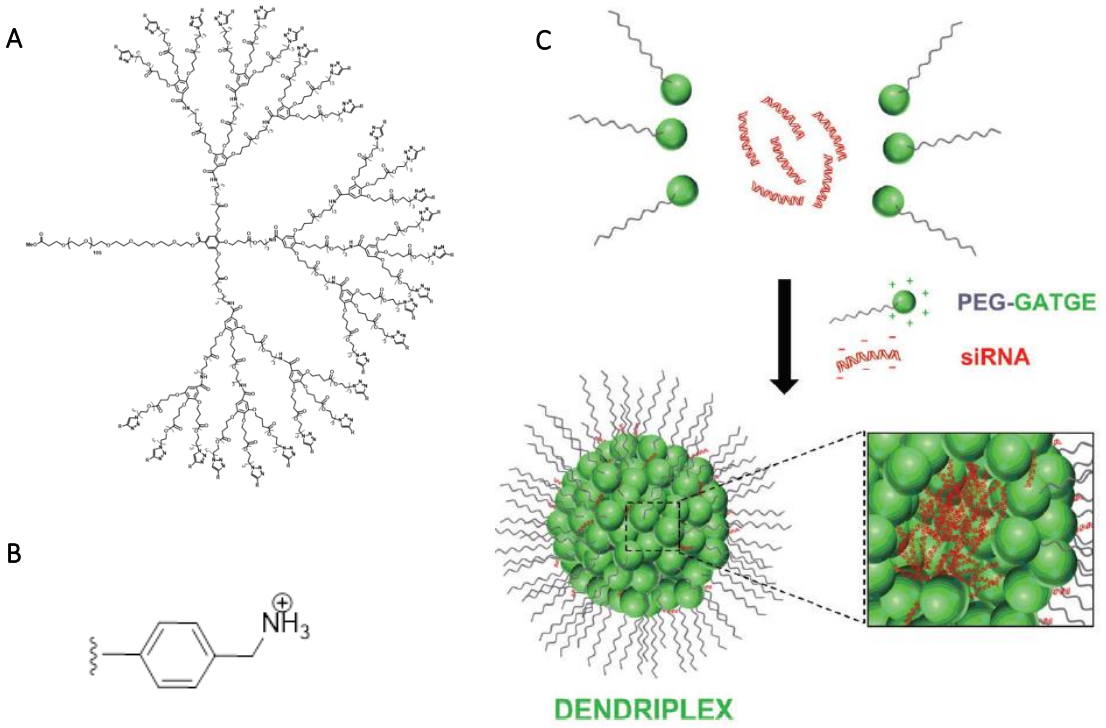

Figure 3 – A: Chemical structure of the G3 PEG-GATGE dendrimer; **B**: Dendrimer functionalization group – Benzylamine; **C**: Schematic representation of the formation of dendriplexes (PEG-GATGE complexed with NA) (adapted from [45])

It was also shown the ability of these biodegradable vectors to be internalized by mammalian cells and it is expected that they promote the intracellular release of the NA and, so, they achieve a high transfection efficiency. Provided that, the described nanoparticles are promising for gene therapy in the CNS and, when conjugated with a neuroprotective NA, they may improve clinical outcome after ischemic stroke.

1.2. Blood-brain barrier

When developing minimally invasive strategies to reach brain parenchyma, the intravenous administration is the one most commonly considered route. There is a challenge in reaching this tissue, as almost no molecules have the ability to cross the BBB. It arises the need to study and assess the BBB, a dynamic interface between the blood and the brain tissue, in order to predict brain biodistribution. [37], [46], [47] Regarding the project where this work is inserted, an intravenous gene therapy for neuroprotection after ischemic stroke, it is crucial to analyze BBB characteristics in physiological conditions and after ischemic injury for a better understanding of particles behavior and permeability when reaching the BBB.

1.2.1. Brief description

The BBB is a dynamic barrier on which depends part of the homeostasis of the CNS. It is a physical barrier between blood flow and brain tissue, mainly in charge of the supply of nutrients and oxygen to the CNS, to maintain the osmotic pressure in the brain interstitial fluid and to protect neurons from potentially harmful substances present in the blood by controlling the influx and efflux of molecules and ions. [12], [48]–[50]

The anatomic structure of the BBB lays on a single layer of brain microvascular endothelial cells surrounded by astrocytic end-feet, pericytes and the noncellular basement membrane ensheathing pericytes and endothelial cells. (Figure 4) These key components, neighbored by microglia and neurons, form a neurovascular unit (NVU), an integrated system with a central role in the maintenance of brain tissue homeostasis. [8], [12], [46], [50]

BBB endothelial cells are joined with complex tight junctions (TJ) structures, sealing gaps between adjacent cells, restringing paracellular diffusion mostly of hydrophilic molecules (>400 Da) and increasing transendothelial electrical resistance (TEER). TJ are a complex of highly specialized proteins modulated by intra and extracellular pathways such as transmembrane proteins (junctional adhesion molecule-1: JAM-1, occludin and claudins) and cytoplasmic proteins (zonula occludens-1 and -2: ZO-1 and ZO-2, cingulin, AF-6 and 7H6) linked to the cytoskeleton. Otherwise, transcellular transport is limited by the restrict processing of pinocytotic vesicles, the high content in enzymes capable to digest many exogenous toxins, substances and xenobiotics and the enrichment in polarized and energy-dependent efflux transporters such as P-glycoprotein. [12], [18], [37], [46], [47], [50]

Astrocytes, with a BBB coverage estimated at 99%, are essential for BBB function and maturation by the secretion of specific biochemical factors that upregulate tight junctions and polarized transporters expression and they assist the transport through capillary walls. [12], [47], [48], [51] Pericytes are attached to the abluminal membrane of endothelial cells with an irregular pattern, cover only 30% of the barrier. Their function is not clearly described, however it is believed to regulate capillary blood flow and help in maturation and maintenance of barrier properties, both in normal and pathological conditions. [12], [47], [48] Neurons are important regarding to communication, with important effects in barrier proprieties maintenance. [47] Extracellular matrix supports endothelial cells and can regulate them through matrix proteins. [12]

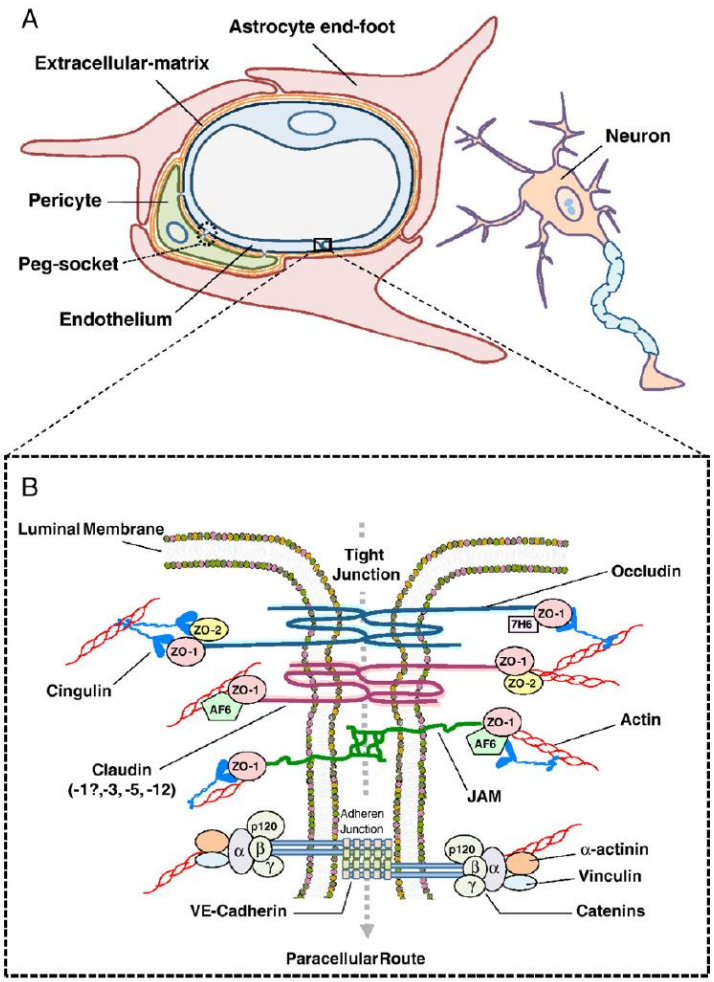

Figure 4 – Schematic representation of the NVU (adapted from [18]). **A**: Transversal view of a brain capillary. **B**: Tight junction composition and organization.

Regarding BBB features and mechanisms to deal with exogenous substances that reach brain through blood which ensure an incredible protection, most of the CNS designed therapies fail

because of its poor bioavailability in the area of interest, due to the difficulty in crossing this highly impermeable barrier. [46], [50], [52]

1.2.2. BBB IN STROKE

The interruption of blood flow in ischemic conditions, i.e. depletion of oxygen and essential nutrients such as glucose, as well as the reperfusion, in natural or under therapeutic conditions, interferes with cellular metabolism, not only at neuronal level, but also at other NVU components. [8], [12]

Many studies report a BBB disruption after hypoxia conditions, as in ischemic stroke, and consequent increase of the barrier permeability which could vary between 15% and 66% depending on stroke severity and timepoint of measurement. However, it is not a singular event, but a phasic one, due to its dependence in different mechanisms and signals during the ischemia and eventual reperfusion (Figure 5). [14], [18]

It has been shown that tight junctions are dynamic structures with the ability to be modulated in normal and pathological conditions. [18], [53] Right after the ischemic injury, in the core of ischemic zone, the endothelium suffers a metabolic dysregulation which leads to TJ disassembly and accumulation of bradykinin, vascular endothelial growth factor, thrombin and activated proteases. On the other hand, vessels located in penumbra zone are managed by molecular events occurring during ischemic cascade. [14], [18]

As deeply explain in section 1.1.1., one of the consequences of energy depletion in the ischemic insult is the cytotoxic edema which causes cell swelling due to the rapid and uncontrolled influx of water into glial and neuronal cells, leading to the narrowing of internal capillary diameter. [18], [54] Also, matrix-metalloproteases (MMPs), enzymes activated in the early cascade, digest the endothelial basal lamina, creating damages in the BBB structure and the detachment of some cells of the NVU, ultimately, marked as a deregulation of TJ and a BBB permeability increase. [12], [14], [18] Finally, ROS accumulation in penumbra tissues induce TJ impairment followed by increasing of paracellular permeability. [55]

Despite the BBB damage induced by vessel occlusion itself, reperfusion contribute to an extra damage: the reperfusion injury. [14] After reperfusion, it is possible to record three significant BBB openings: one associated to the rapid elevation of regional cerebral blood-flow (rCBF) when circulation is restored; and then a “biphasic” permeability response around 5 and 72h.

The first BBB significant increase permeability phase occurs minutes after reperfusion due to the sharp increase of pressure and consequent acute disruption of TJ. The reassembly of TJ is unclear, however the BBB permeability is in part reestablished and there is a remodeling of the NVU. [18]

At 3-8h pos-reperfusion, there is the first opening of the biphasic permeability phase, once it happens right after an hypoperfusion state which increases oxidative stress, enzymatic degradation of the endothelial extra-cellular matrix (ECM) and the adhesion and inflammatory activity by leukocytes. Leukocytes infiltrate into the endothelium barrier to reach brain parenchyma aided by the release of oxidants, proteolytic enzymes and inflammatory cytokines, which compromise the integrity and function of the BBB. [14], [18], [53], [56]

The BBB disruption lead to the extravasation of blood proteins and fluid into the brain parenchyma, which progressing elevates the brain water content and intracranial pressure, event known as vasogenic edema. [14], [18], [51], [53], [54] Angiogenesis and increase of intracranial pressure due to cerebral edema (cytotoxic and vasogenic edema) correspond to the final phase of BBB opening, approximately 18-96h after reperfusion. In this final phase, there is a disassembly and assembly of TJ which affects paracellular permeability conducted by molecular and chemical deregulation and it is not necessarily a reestablishment of BBB. [18]

All these BBB opening events are directly correlated with brain area affected and ischemic injury severity. [18]

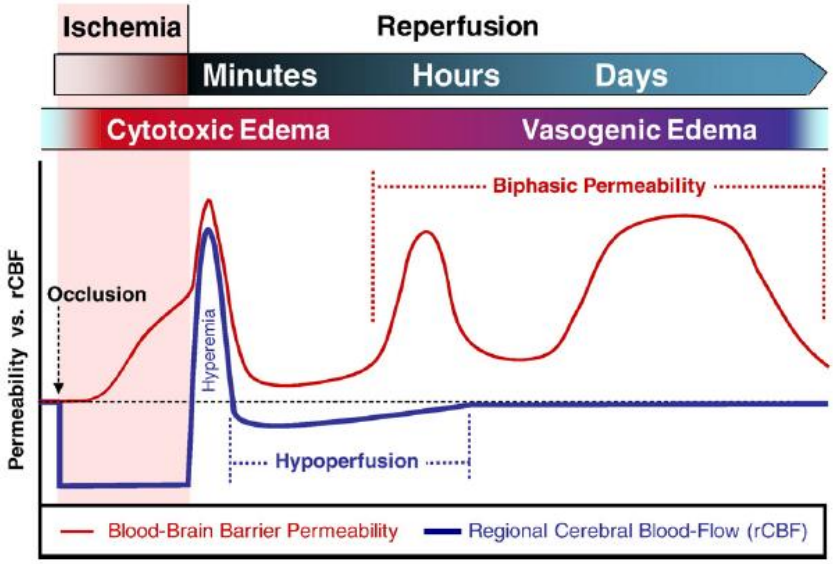

Figure 5 – BBB opening events after a ischemic stroke and during reperfusion (adapted from [18])

The increase of TJ permeability after ischemic stroke can be used as a window of opportunity to deliver brain therapeutic agents, such as neuroprotective molecules, which otherwise would be excluded from the brain. [37], [53], [57]

1.3. BBB MODELS

The determination of a compound biodistribution in CNS is extremely important and it is mainly determined by BBB permeation. [37] So it is necessary to have *in vitro* and *in vivo* BBB models as screening tests in pre-clinical trials to verify their ability to cross the BBB.

1.3.1. *IN VITRO*

During the early phase of a therapy development, direct *in vivo* testing is not viable in many cases. *In vitro* models can mimic essential *in vivo* characteristics and provide a medium to high-throughput data in an economical way, avoiding many ethical constrains. [37], [50] So, much research effort has been directed to the development of functional BBB in vitro model for rapid drug screening. [47]

Due to the complexity of the NVU, there are many variables that can be played when mimicking the BBB. The most common model into the scientific community is based on a Transwell® system, traditionally with a compartment simulating blood and the other mimicking the CNS. [37], [47]

Endothelial cells are an essential component of the BBB, so that all BBB models are primarily based on these cells. Mono-cultures of brain endothelial cells on the apical side of a semipermeable membrane are the simplest permeation BBB model and therefore highly suitable for high-throughput screening. Although, many *in vivo* physiologic properties are lost when cultured alone owning to the absence of other NVU cellular components. [37], [49], [50]

The above described problem can be overcome by doing co- or triple-cultures of endothelial cells with cells belonging to NVU, once the crosstalk between its components is essential for BBB characteristics maintenance. [50] Co-cultures consist in culturing endothelial cells with other component of the NVU (astrocytes, pericytes or neurons), while, in triple-cultures, it is added 2 types of NVU cells to endothelial ones. The increase of complexity is a significant disadvantage when developing a high-throughput model, once it reduces the ability to reproduce it. So, most BBB studies, that uses other NVU cell besides endothelial cells, are based on co-culture models. [47], [50]

NVU cells, as astrocytes, pericytes or neurons are seeded on the abluminal side of the insert, either on the bottom of the well (non-contact culture) or directly on the membrane (contact culture). Non-contact cultures only ensure that endothelial cells are affected and regulated by chemical gradients induced by factors released to the culture medium. On the other hand, in contact cultures, endothelial barrier is not only regulated by chemical factors but also physical stimuli by cell processes through the membrane. [47] Restrictive barrier proprieties are highly

influenced by the astrocytes secreting factors, but also physical signals by contact stimuli. [8] Whereas pericytes where recently described to be critical in BBB differentiation and pinocytosis reduction. [46] So, despite the importance of other NVU cell types in BBB maintenance, referred two are the most common in co-cultures when mimicking the BBB.

Recently, it had been reported some new dynamic and microfluidic models able to mimic *in vivo* blood flow, which presented promising results in barrier tightness when compared to co-culture static models. Although, they are still in an early phase of development and, at least for now, they are not suitable for high-throughput studies. [50]

BBB models are validated using different features mainly to determine the high junctional tightness such as TEER measurement [47], permeability studies with hydrophilic low-molecular weight tracer molecules [48] and analysis of TJ protein expression [50].

These cell models can differ depending on the cell origin and type (cell line or primary cells), influencing the expression of transporters and the tightness of the endothelial layer. [37] Immortalized endothelial cell lines are the most used, once they are simpler and cheaper to handle. However, TEER values are low when compared with *in vivo* values. Nevertheless, primary cells, when cultured *ex vivo*, lose some key characteristics, as changes in phenotypic expressions, which could determine the success of the model. [47] Additionally, the coating of the insert semipermeable membrane can be determinant in BBB features, once ECM proteins can influence cell signaling events able to regulate TJ proteins. [50]

Even though there are many drawbacks and variables using this type of models, they were design to account either passive diffusion through a transcellular way and active transport without the influence of physiological factors existing *in vivo*, so they can be used as high-throughput screening models. [37]

1.3.2. *In vivo*

Despite the possible answers to be collected with *in vitro* BBB models, *in vivo* experiments allow studies in brain natural environment with the complexity of the integrated NVU, overcoming many *in vitro* limitations. Therefore, potential therapeutic agents may be tested in *in vivo* models before translation to clinics. [37], [46], [47]

Within the *in vivo* studies using novel approaches, such as dendrimers for CNS applications, the BBB permeability and the brain biodistribution is a common assay. In Table 1 it is reviewed the validation of dendrimers for CNS applications using different in vivo models and routes of administration.

Table 1 - Description of some in vivo studies with dendrimers where BBB permeability and/or brain biodistribution are assessed. Abbreviations: intracranial (i.c.); intranasal (i.n.); intraperitonial (i.p.); intravenous (i.v.); generation (G).

Dendrimer - Generation	Functionalization	Animal	Route of administration	Aim of the study	Reference
Poly(amino amine) - PAMAM					
PAMAM – G2		Rat	Brain injection	Gene delivery after ischemic stroke	[58]
PAMAM – G3		Mouse	i.v.	Deliver anti-cancer drug across the BBB	[59]
PAMAM - G4	Angiopep; PEG	Mouse	i.v.	Brain-targeted gene therapy	[60]
	RGD; PEG	Mouse	i.p.	Brain tumor-targeted therapy	[61]
	Serine-Arginine-Leucine peptide; PEG	Mouse	i.v.	Brain-targeted gene therapy	[62]
	Cy-5	Mouse	i.p.	Neonatal white matter injury treatment	[63]
	Magnetofluorescent nanoworms	Mouse	i.c.	Protein-target knockdown	[64]
	Biotin	Rat	i.v.	Brain biodistribution studies	[65]
	Arginine	Rat	i.c.	Neuron-targeted gene therapy	[66]
		Rabbit	Subarachnoid administration	Brain inflammatory cells-targeting in cerebral palsy	[67]
	Hydroxyl groups; Mannose	Rabbit	i.v.	Brain inflammatory cells-targeting in cerebral palsy	[68]
	Hydroxyl groups	Rabbit	i.v.	Delivery platform for neuroinflammation suppression in cerebral palsy	[69]
		Dog	i.v.	Drug delivery platform for brain injury following circulatory arrest treatment	[70]

(Table 1) contd…

Dendrimer - Generation	Functionalization	Animal	Route of administration	Aim of the study	Reference
PAMAM - G5	Transferrin; PEG	Mouse	i.v.	Brain-targeted gene therapy	[71]
	Lactoferrin; PEG	Mouse	i.v.	Brain-targeted gene therapy	[72]
		Rat	i.n.; i.p.	Drug delivery platform into the brain	[73]
PAMAM – G4 and G6	Hydroxyl groups	Dog	i.v.	Delivery platform for brain injury following circulatory arrest treatment	[74]
Poly(propylene imine) - PPI					
PPI - G3	Lactoferrin; Diamobutyric groups	Mouse	i.v.	Brain-targeted gene therapy	[75]
	Lactoferrin	Mouse	i.v.	Gene therapy in brain cancer, Alzheimer's and Parkinson's diseases	[76]
PPI - G4	Maltotriose; Fluorescent units	Rat	i.p.	Brain therapeutic platforms able to cross the BBB	[77]
Carbosilane					
Carbosilane - G2		Mouse	Retro-orbital injection	Brain-targeted gene therapy	[78]

Even though there are not many studies using zebrafish for nanoparticles biodistribution in brain or their permeability through the BBB, the animal model is starting to be more used due to its simplicity. [79] Also, many studies have reported the ability of the organism for a quick and reliable toxicity studies even using dendrimers. [80], [81]

1.3.2.1. Zebrafish model

There are different *in vivo* models used in CNS research not only focused on therapeutic approaches but also on the study of BBB. One such *in vivo* model is Zebrafish (*Danio rerio*), a widely used model not only in vertebrate studies but also in neuroscience studies. [79], [82]–[84] This is mainly due to the high similarity between this specie and human genomes [85], low-cost and easy maintenance and high fertility that is not possible with other vertebrates [86]. In

addition, when studying zebrafish in the early development, such as embryos and larvae, there is a huge advantage in imaging, since they are transparent allowing the use of standard tools. [46] Even more, regarding to drug screening, there is a high similarity between these organisms and humans, once many drug binding sites have similar aminoacidic sequences. [86], [87] Considering these characteristics zebrafish can be used as a high-throughput *in vivo* model for diverse investigation studies including CNS research. [88]

Regarding to the BBB, almost all vertebrate animals have a BBB functionally similar [89], [90] so as the zebrafish BBB, that is functional and structurally homologous to human's, since it reproduces the organizational features such as the presence of tight junctions, the similar fluid system including choroid plexus and ventricular system and the high sequence similarity to human transporters [46], [91], [92]. It was previously described that this barrier is established 3 days post fertilization (dpf) when tight junction proteins Claudin-5 and ZO-1 can be detected in some cerebral vessels. [46], [82], [91], [92] However, at the third dpf even with the exclusion of some molecule sizes, BBB is not totally functional, once only some cerebral vessels express TJ proteins, it maturates between 3 and 10 dpf. [92]

Zebrafish is naturally resistant to hypoxia, keeping the aerobic metabolism even in low oxygen (O_2) levels comparing to normoxic water (≈7.5 mg/L O_2). [93] Despite that, it has been described as an *in vivo* model for drug screening with potential applications under hypoxic conditions, when overcome the threshold for hypoxia tolerance. [93], [94] Also, it has been shown some important factors in zebrafish that are characteristic to human ischemic stroke such as collateral circulation and autoregulatory capacity. [86]

Even though it is not described a hypoxic-ischemic model using zebrafish larvae, Yu *et al.* [94] published a global ischemic model using zebrafish adults. The model is based on simplicity, once it does not use invasive procedures to induce ischemia but oxygen deprivation.

Aim of the thesis

2

The present thesis has been conducted in the framework of the project BaiTS - Biodegradable dendrimers for Targeted neuroprotective therapies in Stroke, which aims at the production of biodegradable dendrimers for NA coding neuroprotective proteins delivery after ischemic stroke. These systems are proposed to be intravenously injected in the early stage of ischemic injury to rescue neurons from the hostile environment in the ischemic penumbra.

Taking into consideration the proposed route of administration, it is imperative to assess the permeation of the developed dendritic system through the BBB. Therefore, the main goal of this dissertation was to determine the permeation profile of the developed nanoparticles under stroke conditions, both *in vitro* and *in vivo*. In order to fulfill the proposed objective, the experimental work was divided in two main parts:

1. Study the ability and mechanisms of the commercial dendrimers (PAMAM) and dendriplexes (fully biodegradable dendrimers developed in our group complexed with NA) to permeate a compromised BBB *in vitro* model based on the co-culture of endothelial cells and astrocytes under oxygen and glucose deprivation conditions.
2. Establish in the lab a larvae zebrafish *in vivo* model of ischemia and assess the dendrimers permeation through the BBB and brain bioavailability after administration.

This page was intentionally left in blank.

3 Materials and methods

3.1. *In vitro* model

3.1.1. Rat astrocyte isolation and culture

Rat primary astrocytes were kindly provided by Eva Carvalho (nBTT, INEB/i3s). Concisely, cells were isolated from Wistar Han rat pups in post-natal day 2, as previously described [95], [96]. After thorough meninges removal and cortex dissection, cortices were digested by mechanical digestion, followed by enzymatical digestion (0,0025% (w/v) trypsin (27250018, Gibco) in Hank's Balanced Salt Solution (HBSS) without calcium and magnesium (H2387, Sigma-Aldrich), and 0.001mg/mL DNase I (Applichem LifeSciences) for 15 minutes at 37°C. Then, they were homogenized in Dulbecco's modified Eagle medium (DMEM) Glutamax (high glucose) (31966-021, Gibco) supplemented with 10% (v/v) heat-inactivated fetal bovine serum (FBS) (F7524, Sigma-Aldrich) (inactivated at 56 °C for 30 minutes) and 1% (v/v) penicillin/streptomycin (P/S) (L0022, BioWest), and centrifuged at 500g for 10 minutes. The supernatant was discarded, the pellet of mixed glial cells (MGCs) re-suspended in serum supplemented DMEM and then filtered through a 40 µm nylon cell strainer to remove large cell clusters. The cells were plated in T75 cell culture flasks and maintained in culture for 14 days, with culture medium change every 2-3 days. At day 14 after plating, a pre-shake of the MGC cultures (210 rotations per minute (rpm) at 37°C for 2 hours) was performed to remove most loosely adherent microglia cells. Then, the plate was shaken overnight (230 rpm at 37°C) to further detach microglia and oligodendrocyte progenitor cells (OPCs). The shaken T75 were then cultured at 37°C, 5% CO_2 and weekly shaken. After the third shake, the remaining cells are mainly astrocytes. To obtain pure astrocytes, cells were trypsinized and seeded on new T75 flasks at least three times. Astrocytes were maintained in culture or frozen for future use.

All experiments involving animals and their care were performed in agreement with institutional ethical guidelines (IBMC/INEB/i3S), the EU directive (2010/63/EU) and Portuguese law ('Decreto de Lei' 113/2013). All procedures involving animals were conducted by FELASA C graded researchers, and all efforts were made to minimize the number of animals used as well as their suffering.

3.1.2. Endothelial cell culture

Immortalized mouse brain endothelial cells (bEnd.3) (American Type Culture Collection, USA) were cultured in DMEM Glutamax supplemented with 10% heat-inactivated FBS and 1% P/S in a humidified chamber at 37°C and 5% CO_2. The culture medium was changed every 2 or 3 days and cells were harvested when confluent using 0.25% trypsin/EDTA solution with 0.05% glucose (T4799, Sigma-Aldrich).

3.1.3. Model setup

The used in vitro BBB model, based on a Transwell® model, was previously established [97] and optimized by Débora Moreira [98].

Firstly, 12-well inserts (polyethylene terephthalate – PET) with pore size of 0.4 µm (313580, Falcon) were coated with poly-D-lysine (PDL, 6.7 µg/cm^2, P6407, Sigma-Aldrich) on the abluminal side for 1 hour at room temperature (RT). After rinsing three times with sterile distilled water, the luminal side of the insert was coated with type I rat tail collagen (6.7 µg/cm^2 in 0.1M acetic acid, C7661, Sigma-Aldrich) overnight (ON) at 4°C. The inserts were rinsed again and left drying in the flow hood.

Primary rat astrocytes (passage 4-8) were seeded on the abluminal side of the insert with 4x10^4 cells/cm^2 and incubated in a humified chamber at 37°C and 5% CO_2 for 2 hours for the cells to adhere. Inserts were flipped and placed in a proper 12-well plate with DMEM Glutamax supplemented with 10% FBS and 1% P/S for 2 days in a humidified chamber at 37°C and 5% CO_2. Then, endothelial cells, bEnd.3, were seeded on the luminal side of the inserts with a density of 1x10^5 cells/cm^2. Co-cultures were maintained for 7 days in a humidified chamber at 37°C and 5% CO_2. Every 2 or 3 days, the medium was carefully changed, both on the luminal and abluminal sides of the inserts, by 50% fresh medium (DMEM Glutamax supplemented with 10% FBS and 1% P/S) and 50% conditioned medium from astrocytes which were cultured on a 24-well culture plate on the same day and density as the ones on the insert.

3.1.4. 2D controls

In 2D controls, the culture conditions were kept the same as done with the Transwell® *in vitro* model, to be able to draw conclusions between them. Cell culture coverslips (83.1840.002, Sarstedt) were coated with PDL or collagen in the same conditions as the membrane of the insert (described in section 2.1.2.). In coverslips coated with PDL, primary rat astrocytes were seeded on a density of $4x10^4$ cells/cm^2 and incubated in a humidified chamber at 37°C, CO_2 for 9 days. And the coverslips coated with collagen were seeded with bEnd.3 ($1x10^5$ cells/cm^2) and incubated in a humidified chamber at 37°C, CO_2 for 7 days. Cell culture medium was changed, in both cultures, every 2 or 3 days for 50% fresh medium and 50% astrocyte-conditioned medium, as done for the insert experiments.

3.1.5. Oxygen and glucose deprivation

To mimic ischemic stroke conditions and induce the BBB disruption, the *in vitro* BBB model, described previously in section 2.1.2., was subjected to oxygen and glucose deprivation (OGD) on the 7^{th} day.

On the day before the treatment, DMEM low-glucose (11966-025, Gibco) supplemented with 1% (v/v) P/S was deoxygenized ON in a humidified chamber at 37°C, 0.1% O_2 and 5% CO_2 (hypoxia chamber). On the 7^{th} day of the co-culture, the culture medium was carefully removed and cells were rinsed once with pre-warmed phosphate buffered saline (PBS). Then, deoxygenized, serum- and glucose-free DMEM was added to both insert and well and cells were incubated in the hypoxia chamber for 4 or 12 hours. As controls, co-cultures were incubated with 50% fresh and 50% conditioned medium for 4 or 12 hours at 37°C and 5% CO_2 in a humidified chamber with O_2.

3.1.6. Transendothelial electrical resistance measurements

TEER values were measured using the Millicell® ERS-2 (Merck Millipore, USA).

Before and after cells were subjected to OGD conditions and their controls, they were taken from the respective incubator to RT for 15 min. After that, pre-sterile STX01 electrode was perpendicularly placed in the insert and well, so that the longer tip touched the bottom of the well and the shorter tip did not touch the insert cell layer. The resistant measurements were done in the ohm (Ω) mode and in three different areas of each insert. Unit area resistance was calculated for each measurement by subtracting TEER value of blank inserts (PDL and collagen

coated inserts without cells and incubated with 50% fresh and 50% conditioned medium), followed by Equation 1.

Unit area resistance ($\Omega.cm^2$) = R x A **Equation 1**

where measured resistance is represented by R (Ω) and A represents the effective membrane area of the insert (0.9 cm^2).

3.1.7. Paracellular permeability evaluation

After TEER measurements in the co-cultures, the paracellular permeability to sodium fluorescein was analyzed. Cell culture medium was removed, cell layers were carefully rinsed twice with pre-warmed HBSS with Ca^{2+} and Mg^{2+} (14025-050, Gibco) and inserts were placed in a new plate. To each well, 1 mL of pre-warmed HBSS was added and, to the luminal side of the insert, 1 mL of sodium fluorescein (F6377, Sigma-Aldrich) solution (100 µg/mL in HBSS). Cells were incubated in a humidified chamber at 37°C and 5% CO_2. Every 30 min for 4 hours, abluminal concentration of fluorescein was determine by taking four 100 µL aliquots of well medium of each sample and measuring its fluorescence (λ_{exc}=485 nm; λ_{em}=535 nm) using a spectrophotometer microplate reader (SynergyMX, Biotek). Total removed solution (400 µL) from abluminal side was replaced between measurements with fresh pre-warmed HBSS.

To determine the fluorescein coefficient of permeability, a series of calculations were done. Firstly, cleared volume of fluorescein was calculated according Equation 2. Then, cleared volume was divided by assay time (Equation 3) to determine the volume of fluorescein that passes the barrier over time (PS). Lastly, the permeability coefficient (P) was calculated using Equation 4.

$$\text{Cleared volume } (\mu L) = \frac{C_{abluminal} \times V_{luminal}}{C_{luminal}} \qquad \textbf{Equation 2}$$

where $C_{abluminal}$ is the measured fluorescein concentration in the luminal side of the insert, $V_{luminal}$ the volume of fluorescein solution added to the top of the insert and $C_{luminal}$ the concentration of fluorescein solution added to the insert.

$$PS\ (\mu L/s) = \frac{\text{Cleared volume}}{\text{time}} \qquad \textbf{Equation 3}$$

$$P\ (cm/s) = \frac{\frac{1}{\frac{1}{PS_{sample}} - \frac{1}{PS_{blank}}}}{A_{insert}} \qquad \textbf{Equation 4}$$

where PS_{sample} corresponds to the volume of fluorescein that passes through the cell barrier under normoxia or OGD conditions, PS_{blank} to the volume of fluorescein that passes through the insert

without cells and only with coatings (PDL and collagen) and A_{insert} indicates the area of the insert (0.9 cm^2).

3.1.8. PAMAM dendrimers

A) Rhodamine-labelling and PEGylation

Generation 4 (G4) of an amine-terminated PAMAM (PAMAM-NH_2) (Dendritech, Inc.) dendrimers were labelled with Rhodamine using 5(6)-Carboxy-X-rhodamine N-succinimidyl ester (5(6)-ROX) (sc-210422, Santa Cruz Biotechnology, Inc.) and PEGylated with methoxy PEG Succinimidyl Carboxymethyl Ester (MeO-PEG-NHS) (Jenkem Technology USA) (performed by Victoria Leiro, nBTT, INEB/i3S). Amine groups from PAMAM-NH_2 reacted with the succinimidyl ester groups, yielding stable amide bonds. Briefly, a 5(6)-Carboxy-X-rhodamine N-succinimidyl ester (1.2 equivalents) solution was added drop by drop to a PAMAM-NH_2 solution (1 equivalent), both in dry DMSO, and the reaction mixture was magnetically stirred at RT for 12h under inert atmosphere (Ar). The resulting mixture was transferred into a dialysis membrane tubing (3500 MWCO) (Jenkem Technology) and purified by dialysis against deionized water during 48h (water changes were carried out every 4 h, except during ON). Finally, the resulting solution was freeze-dried yielding the PAMAM-5(6)-ROX conjugate as a dark pink powder (96% yield).

In order to get the PEGylation of the previous conjugate, MeO-PEG-NHS (10 equivalents) was added to a PAMAM-5(6)-ROX (1 equivalent) solution in dry DMSO. The reaction mixture was magnetically stirred at RT for 12h under inert atmosphere (Ar) and protected from light. Next, the previously described procedure for the purification by dialysis was followed. After freeze-drying of the corresponding dialyzed solution, PEG-PAMAM-5(6)-ROX conjugate was obtained as a dark pink foaming solid (91% yield), which was stored at -20°C, and protected from light until further use.

3.1.9. G3 PEG-GATGE dendrimers

A) Dendrimer Synthesis

G3 PEG-GATGE dendrimers were kindly provided by the chemical-production team in our group (Victoria Leiro, Natália Magalhães, Ana Spencer and Cristiana Sousa, nBTT, INEB/i3S). Briefly, PEG-dendritic block copolymers with terminal azides were obtained through a divergent strategy. The

dendritic core/monomer was synthesized from commercially available gallic acid and triethylene glycolazide. The block copolymer of generation one (PEG-[G1]-N3) was obtained from PEG-NH2 and 3 equivalents of monomer 3. PEG-[G1]-N3 terminal azides were subjected to a catalytic hydrogenation, followed by the treatment of the resulting triamine with 6 equivalents of monomer 3 as previously done, leading to generation two PEG-[G2]-N3. Applying the same sequence of reactions (hydrogenation - amide formation - precipitation) to PEG-[G2]-N3 (18 equivalents of monomer 3) leads to the third generation, PEG-[G3]-N3. This process had an overall yield of 68%.

The dendrimer surface functionalization was performed using the Cu (II)-catalyzed Huisgen cycloaddition with the alkynated ammonium salt (benzyl-amine). The reaction was carried out with $CuSO_4$ (5 mol% per azide) as source of cooper and sodium ascorbate (25 mol% per azide) as reducing agent, in DMF:H_2O 1:1 (RT, 48h). Both products were characterized by H^1 NMR (D_2O) and FTIR microscopy (KBr technique).

B) Dendriplexes formation

Dendriplexes were prepared with 5 or 20 N/P ratio, where N corresponds to the primary amines in the dendritic copolymer and P is the number of phosphate groups in the siDNA backbone. N/P5 was used in the first experiments (here, the TJ analysis) and N/P20 was used for the remained. The dendritic copolymer solution (6 mg/mL) was prepared in nuclease-free water (1039498, Qiagen) and filtered with 0.45 µm PTFE (polytetrafluoroethylene) membrane (514-0069, VWR). For dendriplex preparation, an optimized buffer, HEPES 20 mM (4-(2-hydroxyethyl)-1-piperazineethanesulfonic acid) with 5% glucose (G6152, Sigma-Aldrich), was used, where dendrimers and siDNA-cy5 (75868515, IDT) were mixed. The sample was vortexed for 10 seconds (middle velocity) and incubated at room temperature for 30 minutes before adding to the cells.

To characterized dendriplexes, size, polydispersity (PDI) and zeta potential of complexes were measured by Ana Spencer, nBTT, INEB/i3s using a dynamic light scattering instrument (Zetasizer Nano ZS, Malvern Instruments, UK) at 633 nm, following the manufacturer's instructions.

3.1.10. Nanoparticles permeability assay

After treatments described in section 2.1.5., cell culture medium was removed, cell layers were carefully rinsed twice with pre-warmed HBSS with Ca^{2+} and Mg^{2+} and inserts were placed in a new 12-well plate.

A) PAMAM dendrimers

To each well, 1 mL of pre-warmed HBSS with Ca^{2+} and Mg^{2+} was added and, to the luminal side of the insert, 0.5 mL of PEG-PAMAM-5(6)-ROX solution (0.01 mg/mL). Cells were incubated in a humidified chamber at 37°C and 5% CO_2 for 1 or 4 hours.

Fluorescence detection

The well medium (abluminal side) was collected and the fluorescence was quantified. To quantify the samples, a calibration curve was done measuring the fluorescence of successive dilutions of the solution added to the inserts (0.01 mg/mL in HBSS). Rhodamine was the molecule for fluorescence to be detected (λ_{exc}=552 nm; λ_{em}=598 nm) using a spectrofluorometer (Fluoromax-4, Horiba).

B) Dendriplexes

To each well, 1 mL of pre-warmed HBSS with calcium and magnesium was added and, to the luminal side of the insert, 0.25 mL of dendriplexes solution (4 µg siDNA/mL; 0.2 mg dendrimer/mL – N/P20; 0.05 mg dendrimer/mL – N/P5) diluted in HBSS with Ca^{2+} and Mg^{2+}. Cells were incubated in a humidified chamber at 37°C and 5% CO_2 for 4 hours.

Fluorescence detection

After the 4h incubation, the well medium (abluminal side) was collected. Dendriplexes were, firstly, decomplexed by adding sodium dodecyl sulfate (SDS) in a final concentration of 0.1% (v/v) (05030, Sigma-Aldrich) for 30 minutes and, then, the fluorescence of cy-5 (λ_{exc}=640 nm; λ_{em}=663 nm) was detected by a spectrofluorometer (FLuoromax-4, Horiba).

To quantify the samples, a calibration curve was done by successive dilutions of the solution added to the inserts. The fluorescence was quantified after and under the same procedure as samples.

Sample concentration

The well medium (abluminal side) was collected and samples were concentrated by ultrafiltration with Amicon® Ultra-0.5 centrifugal filter unit 10 kDa (UFC501024, Merck Millipore) at 4000 rpm for 10 minutes.

Polyacrylamide gel electrophoresis assay

Polyacrylamide gels, with 4% stacking and 15% resolving gel, were prepared in Tris/Borate/EDTA (TBE buffer, MB27701, NZYTech). After 30 min incubation with 0.1% SDS, samples (concentrated or non-concentrated) were loaded with 6 µL of loading buffer (MB13101, NZYTech) and the electrophoresis run at 100V for 30 minutes. The gels were stained with SYBRGold® nucleic acid stain (S11494, Invitrogen), diluted in TBE buffer (1:10 000) for 20 minutes and visualized using GelDoc XR imager (BioRad).

3.1.11. Immunocytochemistry

On the 7th day of co-cultures and 2D control with bEnd.3 or on 9th day of the 2D control with astrocytes, with and without exposure to the nanoparticles, cells were fixed with 4% paraformaldehyde (PFA) (158127, Sigma-Aldrich) for 15 min at RT and, then, rinsed three times with 1X PBS. After, immunocytochemistry was performed as described below.

A) Tight Junctions

To avoid non-specific protein absorption, cultures were incubated with 10% (v/v) FBS in PBS (blocking buffer) for 60 min at RT. After that, cell layers were incubated ON at 4°C with mouse Alexa Fluor® 488-conjugated anti-Claudin-5 (352588, Invitrogen) (1:100) and rabbit anti-ZO-1 (161-7300, Invitrogen) (1:100) diluted in blocking buffer. On the next day, samples were rinsed three times with PBS and incubated with goat anti-rabbit Alexa Fluor® 594 (A11072, Life Technologies) (1:1000) diluted in 5% FBS in PBS for 60 minutes at RT. The secondary antibody was washed out and nucleus was stained with Hoechst (1:10000) for 15 minutes.

B) Cell phenotype

For cell permeabilization, cultures were incubated with 0.2% (v/v) Triton X-100 (234729, Sigma-Aldrich) in PBS for 10 minutes at RT. To minimize non-specific protein adsorption, cells were incubated for 60 min at RT with the blocking buffer (3% bovine serum albumin (BSA, 42235S, VWR), 5% horse serum (26050-070, Gibco) and 0.05% Triton X-100 in PBS). Cells were, then, incubated ON at 4°C with goat anti-platelet endothelial cell adhesion molecule-1 (PECAM-1, sc-1506, Santa Cruz Biotechnology, Inc.) (1:50) and rabbit anti-glial fibrillary acidic protein (GFAP, ab7260, Abcam) in blocking buffer. On the next day, samples were rinsed three times with PBS

and incubated with donkey anti-goat Alexa Fluor® 488 (A11055, Life Technologies) (1:1000 in blocking buffer) for 60 minutes at RT. After, cell layers were incubated with donkey anti-rabbit Alexa Fluor® 647 (A31573, Life Technologies) (1:1000 in blocking buffer) or goat anti-rabbit Alexa Fluor® 594 (1:1000 in blocking buffer) according to the first antibody. The secondary antibody was washed out and nucleus was stained with Hoechst (1:10000) for 15 minutes.

C) Early endocytic markers

For cell permeabilization, cultures were incubated with 0.1% (v/v) Triton X-100 in PBS for 10 minutes at RT. To minimize non-specific protein adsorption, cells were incubated for 60 min at RT with the blocking buffer (5% donkey serum (D9663, Sigma-Aldrich) in PBS). Cells were, then, incubated ON at 4°C with rabbit anti-clathrin heavy chain (4796P, Cell Signaling Technology) (1:50 in blocking buffer) or rabbit anti-caveolin (3267P, Cell Signaling Technology) (1:400 in blocking buffer). On the next day, samples were rinsed three times with PBS and incubated with donkey anti-rabbit Alexa Fluor® 488 (A11034, Life Technologies) (1:1000) diluted in blocking buffer for 60 minutes at RT. The secondary antibody was washed out and nucleus was stained with Hoechst (1:10000) for 15 minutes.

D) Confocal microscope imaging

For confocal imaging, stained cells in membranes or coverslips were mount on a microscope slide with Fluoromount™ Aqueous Mounting Medium (F4680, Sigma-Aldrich) and observed under a confocal microscope, TCS SP5 (Leica Microsystems, Germany) using the 63x objective and 1x zoom. In every field imaged, several images were taken in the z-axis with the step size of 1.22 µm.

3.2. *In vivo* model

3.2.1. Animals

Zebrafish (*Danio rerio*) experiments were done according with the European Directive 2010/63/EU and the Portuguese law, 'Decreto Lei' 113/2013, on the protection of animals used for scientific purposes.

Animals were kept in a 20L tank at 28±0.5°C, pH=7.3-7.5, in a 14:10h light:dark cycle, and in a semi-closed water system with aeration and mechanical and biological filtration. Fishes were fed twice a day with a commercial diet. Male and female fish at a proportion of 2:3 were reared ON in a smaller tank for spawning after room light onset. Embryos were collected and kept at 28±0.5°C in E3 medium (5 mM NaCl, 0.17 mM KCl, 0.24 $CaCl_2$, 0.33 $MgSO_4$ and 0.01% methylene blue in deionized water) with 0.003% (m/v) N-Phenylthiourea (PTU) (P7629, Sigma-Aldrich) to prevent pigmentation.

3.2.2. Hypoxia chamber

Hypoxic chamber was adapted from the experimental system used by Yu et al. [94]. A 100 mL glass Erlenmeyer was used, that was filled until its maximum capacity (100 mL) with embryo swimming medium E3 medium with PTU. A rubber lid was used to keep the chamber air-proofed and two needles as air ports: one connects the medium with a nitrogen tank (N_2) and the other one the air space inside to the open air. (Figure 6) To determine the best time point for inducing hypoxia in medium N_2 was flushed (flowing pressure approximately 0.4 bar) into the chamber for 4, 5, 10 or 15 minutes with one vigorous shake at half time of flushing. Before the end time point, the needle connected to the air inside was firstly removed and then the N_2 needle.

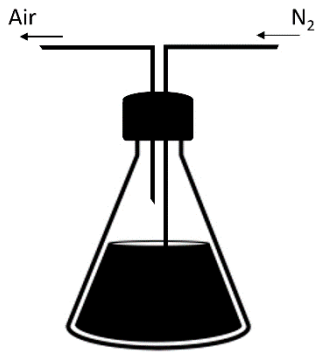

Figure 6 – Schematic representation of the developed hypoxia chamber.

A) Oxygen measurements

Due the the absence of a chamber incorporable oximeter electrode, an external one was used (DWI Oxygen Electrode Chamber, Hansatech Instruments). Two methods were initially tested to take samples from the hypoxia chamber with the lid closed and after opening the lid. The first one was done with a needle and a syringe. The second method was by taking the sample, carefully with a pipette after opening the lid. The lid was left opened between measurements (2, 5, 10 and 20 min).

B) Hypoxia treatment

4 dpf zebrafish larvae was placed in the hypoxia chamber after 4 min of N_2 bubbling by opening the rubber lid. After 2 minutes, the chamber was sealed from the air and placed at 28±0.5°C. for 9, 15, 20, 30, 40, 60, 120, 150, 180, 240 minutes or 24 hours. After, larvae were transferred to normal (oxygenated) E3 medium with PTU and the medium was changed once to reestablish the normoxic conditions, until the imaging procedure was done.

3.2.3. BBB disruption assay

The chorion of the animals with 2 dpf was removed before experiments to approximate with the 4 dpf (naturally without chorion on this stage of development).

A) Evans blue in the swimming medium

2 and 4 dpf animals were exposed to Evans blue dye (E-2129, Sigma-Aldrich) (λ_{exc}=470 and 540 nm; λ_{em}=680 nm) solutions for 30 minutes at three concentrations: 1%, 0.1% and 0.01% in E3 medium with PTU.

Animals were anesthetized by adding tricaine (ethyl 3- aminobenzoate; E10521, Sigma-Aldrich) into the swimming medium and observed under a fluorescence stereomicroscope (Leica M205 FA, Leica Microsystems).

B) Evans blue injection

2 and 4 dpf animals were injected with 5-10 nL of 1% Evans blue solution in 0.9% NaCl sterile solution using a standard zebrafish microinjection apparatus. Animals were kept ON at 28±0.5°C

in E3 medium with PTU and *ex vivo* (section 2.2.5.) and live (section 2.2.6.) confocal imaging was performed as described below.

C) BBB DISRUPTION CONTROLS

As a positive control of BBB disruption, 4 dpf animals were injected with 5-10 nL of Bradykinin solution (B3259, Sigma-Aldrich) (0.2 mM in 1% Evans blue in 0.9% NaCl sterile solution) using a standard zebrafish microinjection apparatus. Animals were kept ON at 28±0.5°C in E3 medium with PTU and live (section 2.2.6.) confocal imaging was performed as described further.
As a negative control, animals were kept ON at 28±0.5°C in E3 medium with PTU and live (section 2.2.6.) confocal imaging was performed as described below.

3.2.4. PAMAM DENDRIMER INJECTION

2 and 4 dpf animals were injected with 5-10 nL of PAMAM solution (in a final ratio of 10 mg/kg in 0.9% NaCl sterile) using a standard zebrafish microinjection apparatus. Animals were kept ON at 28±0.5°C in E3 medium with PTU and live (section 2.2.6.) confocal imaging was performed as described further.

3.2.5. *EX VIVO* IMAGING

Animals were fixed with 4% PFA ON at 4°C and, then, rinsed three times with PBS 1X. The yolk was removed due to its autofluorescence, so imaging artefacts are prevented. Fish were placed in a slide microscope soaked in 50% (v/v) glycerol (G5519, Sigma-Aldrich) in PBS solution. Animals were observed under a TCS SP5 (Leica Microsystems, Germany) using the 10X or 20X objective with 1X zoom, where several images were taken in the z-axis with the step size of 1.51 µm.

3.2.6. LIVE IMAGING

Animals were anesthetized by adding tricaine to the swimming medium and placed in a 35 mm glass bottom dish (81158, ibidi). A drop of pre-heated (37°C) 6% low-melting agarose (39346-81-1, Cleaver Scientific) solution was put on the animal and the larvae were immediately oriented with dorsal-side-up. This procedure was done to immobilize fish for imaging and, once the room is at 21°C, it solidifies on top of it. Animals were observed under a TCS SP5 (Leica Microsystems,

Germany) using the 20X objective and 1.85X of zoom, where several images were taken in the z-axis with the step size of 1.51 µm.

3.3. Statistical analysis

All statistical analyses were performed with the GraphPad Prism 7 Software (Prism 7 for windows, version 7.00, GraphPad Software, Inc.). The number of independent experiments for each condition (n) is described in correspondent figure legend. Data is presented as mean±standard deviation (SD). Independent one-way or two-way analysis of variance (ANOVA) statistical analysis and post-hoc tests, such as Tukey and Sidak's multiple comparison tests, were performed with the significance level set at 0.05.

This page was intentionally left in blank.

Results and Discussion 4

4.1. Dendrimer/dendriplex BBB permeation *in vitro* studies

To assess the dendrimers/dendriplexes BBB permeation potential we explored a co-culture BBB *in vitro* model that has been previously established and optimized in our group [97]. Briefly, the model is based on a Transwell® system where mouse brain endothelial immortalized cells (bEnd.3) are cultured on the luminal side of the insert and primary rat astrocytes on the abluminal side. In the present study the co-cultures were kept in contact with astrocyte conditioned medium and maintained for 7 days in culture in order to upregulate TJ proteins and decrease paracellular permeability [98].

4.1.1. BBB disruption analysis under oxygen and glucose deprivation

As described in section 1.2.2., BBB suffers various disruptions after an ischemic stroke event. Here, to induce the a similar effect, co-cultures were subjected to glucose and oxygen deprivation (OGD), as previously explored [98], but for different period of times to optimize BBB disruption. The model is constituted by endothelial cells and astrocytes and the impairment of each cell type could influence the barrier integrity. Yang *et al.* [99] reported a permeability change in a culture of immortalized brain endothelial cell line (bEnd.5) after 2h of exposure to OGD conditions. However, concerning to primary astrocytes, the cell swelling, and consequent astrocyte-feet detachment [18], started to be registered only at 12h in Yu *et al.* study [100]. In the previous work [98], 4 hours was the used OGD period, and, based on the literature and acquired results [101]–[104], we decided to compare with a longer timepoint regarding the barrier tightness effects. Concisely, the co-cultures were incubated in glucose and serum-free cell culture medium in a

hypoxia chamber (humidified chamber at 37˚C, 0.1% O_2 and 5% CO_2) for 4 or 12 hours. After OGD, different assays were preformed to evaluate the BBB cohesivity.

TEER is a widely used quantitative method to determine the quality of a BBB *in vitro* model, which, by measuring the electrical resistance through the cell layers (between electrodes), can indicate the barrier integrity. [47], [50] After the OGD treatment, TEER decreased in these co-cultures, when comparing to the control condition (Figure 7). When the referred conditions are maintained for 4 hours, TEER decreases in, approximately, 21% but without significant statistical differences whereas the treatment for 12 hours lead to a decrease in, approximately, 51%. The significative TEER decrease when co-cultures are treated for 12 hours of OGD conditions, led us to conclude that under these conditions there is a robust compromise in barrier integrity as it happens after an ischemic stroke.

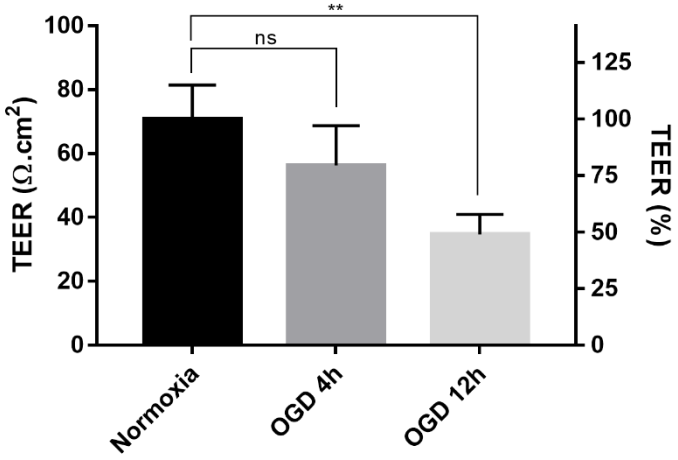

Figure 7 – *Co-culture TEER values dependent on time of the OGD treatment.* Cultures were submitted to different OGD times and compared with the normoxia control under normal culture conditions. Reading the left axis, it presents the TEER values. And reading the right axis, it represents, the percentage in TEER reduction. **P<0.01; ns: not significant; (Normoxia: n=6 with triplicates, OGD 4h: n=4 with triplicates; OGD 12h: n=2 with triplicates).

Although it is not possible to measure BBB TEER in humans, registered TEER values in mammals can reach 8000 Ω.cm^2. Considering the impossibility to accomplish these values in an *in vitro* model, many studies use models with TEER values, around hundreds Ω.cm^2, for drug screening assays. [37], [47], [50] Here, the TEER average value for the barrier under physiologic conditions was 71± 11 Ω.cm^2 which is in accordance with the reported published data [97] and the previous experiments [98]. Moreover, TEER decreased with the OGD treatment in a time-dependent manner.

Barrier tightness and, consequently, TEER are influenced by many factors, for example cell confluency, cell origin, primary culture or cell line and ECM coatings, which can explain

differences in TEER values. [47], [105] Endothelial cells used in this model (bEnd.3, immortalized cell line) are known to present low TEER values in mono-cultures Transwell® systems which are usually around 50 $\Omega.cm^2$. [47]–[50], [106] Also, it was previously shown by Tilling et al. [105] that cell support proteins has high influence in TEER regulation. In studies using porcine endothelial primary cells, cells seeded on rat tail collagen type I, coating as used in this study, showed a decrease in TEER comparing to collagen type IV, fibronectin and laminin. These can be justified by the structural architecture of ECM components, once collagen type I forms a fibrillar structure whereas natural collagen type V ECM of NVU organizes in a polymer network structure. [50], [105]

Despite the above described influencing characteristics, there are also other variables which affect TEER values. For example, measurements with different equipment, equipment position in relation to cells, temperature and cell handling during measurement can change TEER results disallowing tightness deduction and comparison. [48].

So, although TEER is a simple way to measure barrier tightness, it is not enough to conclude about it selectivity. [47], [48] Selective permeability to specific hydrophilic marker substances, which passively diffuses through paracellular route, such as Lucifer yellow (444 Da), sodium fluorescein (376 Da) and mannitol (180 Da) can be additionally measured. [47], [48], [50] Following the previous experiments [98], the sodium fluorescein dye was used to determine barrier paracellular permeability.

As expected, in every condition, the fluorescein concentration increases in the abluminal side over time (Figure 8A). However, it is noticeable that, after 12 hours of OGD conditions, the rate of fluorescein passage is higher comparing to other conditions. This is confirmed by the calculation of the permeability coefficient (Figure 8B), done after 60 and 240 minutes of sodium fluorescein exposure. Permeability coefficient under normoxic conditions after 60 or 240 min, $2.7\pm0.3 \times 10^{-6}$ cm/s and $2.3\pm1.2 \times 10^{-6}$ cm/s, respectively, defines a tight cell barrier as verified before and described in literature [50], [97], [98]. The OGD exposure for 4 hours does not reveal significative effects in sodium fluorescein permeability, however, after 12 hours of OGD, it can be noticed an increase of paracellular permeability, $9.9\pm4.5 \times 10^{-6}$ cm/s (calculated at 240 min), that indicates barrier tightness compromise.

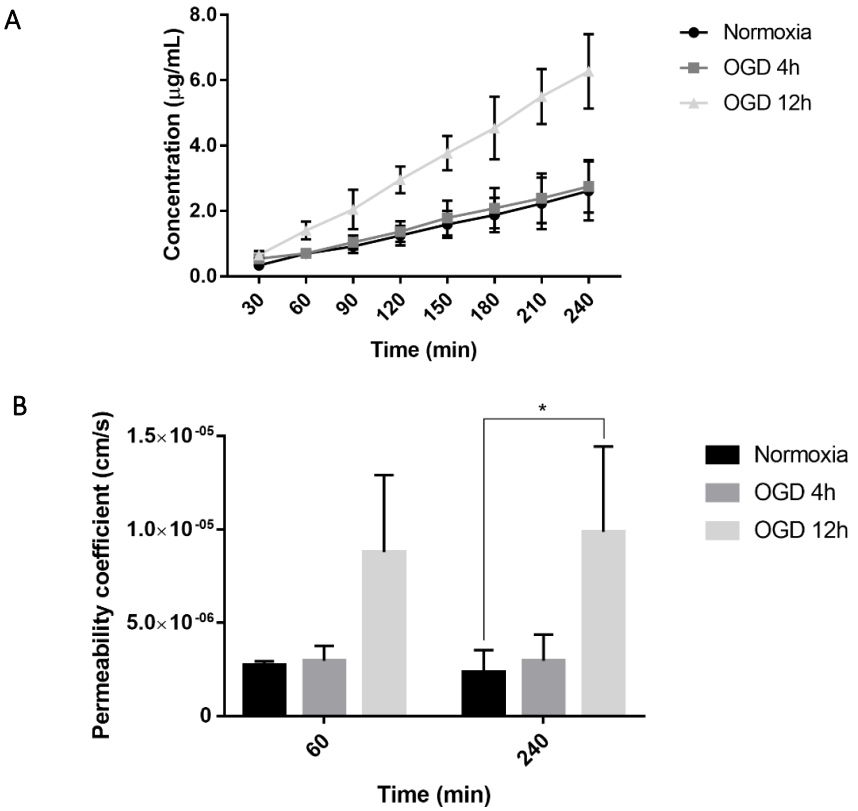

Figure 8 – *Paracellular permeability evaluation using sodium fluorescein.* Cultures were submitted to different OGD times and compared with the normoxia control under normal culture conditions. The fluorescein concentration on the abluminal side was measured over time. **A**: Cumulative concentration of fluorescein that passes through the membrane under studied conditions. Normoxia and OGD 4h results were not statistical significantly different, however Normoxia and OGD 12h treatment was with $P<0.0001$. **B**: Permeability coefficients after 60 and 240 min in contact with fluorescein. There are no statistically significant differences over time. *$P<0.05$ (Normoxia: n=3 with triplicates; OGD4h and OGD12h: n=2 with triplicates).

We have noticed that there was some medium evaporation and/or medium loss in the Transwell® membrane between measurements that was not considered in calculations. This can lead to a larger standard deviation and some inaccuracy, though similar to all 3 conditions. In order to overcome this issue, an experiment could be performed where we would read the different time points only one time, without medium collection and replenishment between measurements.

As described in section 1.2.2., the BBB disruption related to pathology is, in part, caused by TJ disassembly. This event increases the barrier permeability, which could be a window of opportunity to delivery neuroprotective NA complexed with dendrimers (named dendriplexes). Based on the described results, OGD treatment for 12 hours, showed significant differences in barrier disruption. This was the used timepoint to mimic ischemic stroke conditions in further experiments with dendriplexes.

In this context, it is important to analyze TJ protein expression after OGD, such as Claudin-5 and ZO-1 that are commonly used as qualitative markers in BBB tightness. [47]–[50] In Figure 9, the downregulation of both Claudin-5 and ZO-1 TJ proteins in endothelial cells after OGD is notable when compared to endothelial cells in normoxia co-cultures, as described before by Koto *et al*. [107] using bEnd.3 mono-cultures under hypoxia conditions. Also, in normoxic conditions, the expression of Claudin-5 is located nearby the cytoplasmic membrane with a continuous pattern (Figure 9A, white arrows), as expected [18], [107] indicating that the BBB is correctly established, while after OGD this is lost with a disrupted expression of Claudin-5. The same should be observed using ZO-1 and, in injury or proliferation conditions, it is described that ZO-1 have nuclear co-location [12], however the staining did not show the expected cell pattern in normoxia conditions and so the immunocytochemistry analysis will be conducted with another antibody.

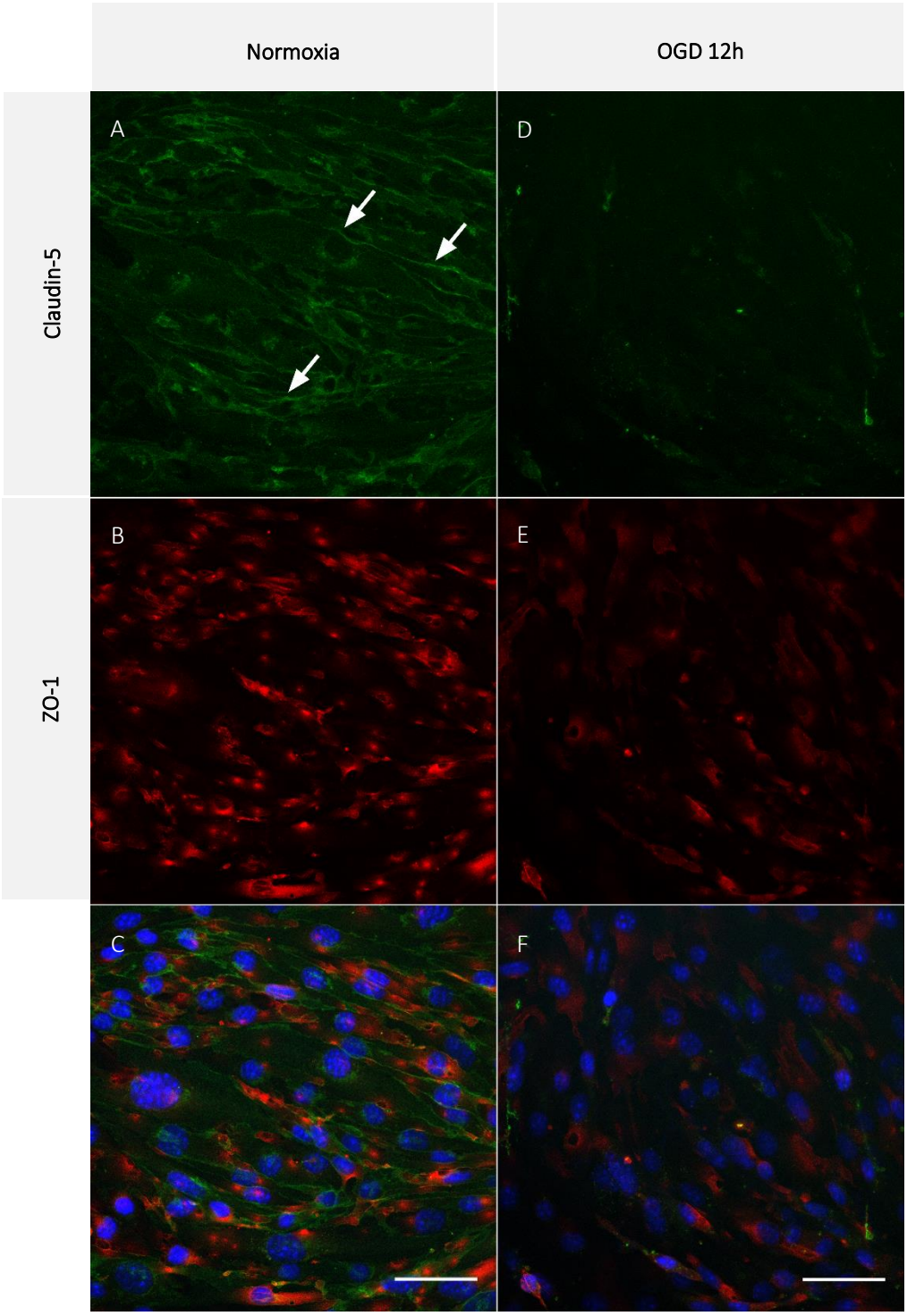

Figure 9 – *TJ proteins expression under physiological and ischemic stroke conditions.* Immunolabelling of Claudin-5 and ZO-1 after normoxia culture or OGD for 12 hours treatment. **A, D**: Claudin-5 staining (green) after normoxia or 12 hours OGD, respectively. **B, E**: ZO-1 staining (red) after normoxia or 12 hours OGD, respectively. **C, F**: Merge of previous described staining and cell nuclei (Hoechst, blue) after normoxia or 12 hours OGD, respectively. Scale bar: 50 µm

4.1.2. BBB PERMEABILITY TO DENDRIMERS

4.1.2.1. PAMAM DENDRIMERS

To establish the permeability assay for the dendrimers, we performed a pilot experiment for optimizations using a commercially available dendrimer – G4 PAMAM that was further PEGylated and labelled with Rhodamine, here referred as PEG-PAMAM-5(6)-ROX, before testing our synthetized dendrimers . Characterization performed in our group by DLS regarding size showed that these dendrimers had a hydrodynamic size of 24.2 ± 16.2 nm [108]. For these studies, earlier established OGD conditions were tested (OGD for 4 hours) [98]. Although this is not the best time period for BBB disturbances, notice that the TEER decrease is not significant (Figure 7) and there are not differences in the fluorescein assay (Figure 8), we knew that tight junctions were altered [98] and so this could result in interesting differences regarding the dendrimer BBB crossing. Succinctly, described co-cultures were treated under physiologic conditions (normoxia), whereas others were subjected to an OGD environment for 4 hours. After that, endothelial cells were exposed to a dendrimer solution for 1 or 4 hours and different tests were performed to determine nanoparticle permeation. After the contact with the dendrimers, the medium from the abluminal side of the insert was collected and fluorescence determined. Comparing the exposure duration, 4 hours of contact presents lower permeability coefficients than 1 hour contact (Figure 10), which could be due to the recovery of the barrier after returning to normoxia, decreasing therefore the permeability over time. Concerning to normoxia and OGD cultures, there are no statistical significative differences in each timepoint (Figure 10). Possibly, the OGD period should be extended to 12h in order to see higher disturbances, which should result in higher PAMAM crossing.

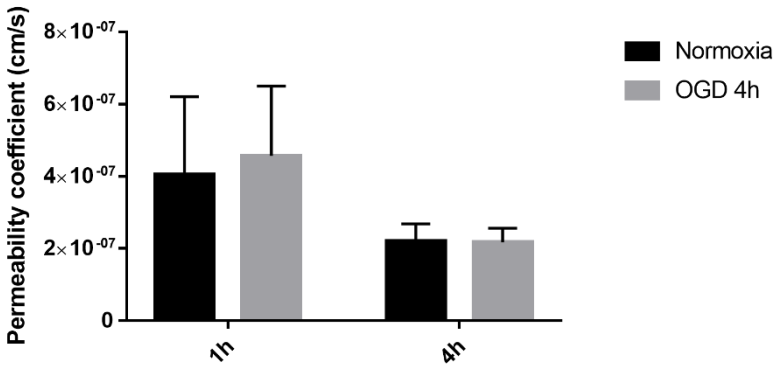

Figure 10 – *In vitro BBB model permeability coefficient to PEG-PAMAM-5(6)-ROX after inducing ischemic stroke conditions*. Cultures were submitted to 4 hours of OGD and normoxia conditions and, then, exposed to the nanoparticles solution for 1 or 4 hours to determine permeability coefficient. There were no statically significant results between conditions. (n=2 with triplicates).

Even though described results should be repeated to diminish the errors associated with the model, dendrimers' paracellular permeability are not to be significantly affected by a 4 hours OGD treatment. Nevertheless, present results do not allow conclusions about transcellular permeability. In order to assess transcellular way that is known as a route for nanoparticles to reach the brain parenchyma [37], [109], confocal images of the different cell layers in study – endothelial cells and astrocytes – were obtained. They allow the analysis of the permeation profile through the barrier (Figure 11) and draw conclusions about differences between conditions, as previously done by Tian *et al.* [110].

It was previously hypothesized in our group that the pathological barrier recovers and tends to equal the physiological barrier's coefficient of permeability. [98] In previous data (data not shown, [98]), it was verified that OGD cultures had higher permeability coefficients after 1 hour of contact with nanoparticles than normoxia ones. So, co-cultures that were that period in contact with PAMAM dendrimers were further analyzed.

Since nanoparticles have only a 1h contact period with cells, and as it is possible to see their fluorescence in the porous of the supportive membrane (Figure 11, white arrows) and even on the astrocyte layer (Figure 11B and C, bottom). Regarding the OGD treatment for 4 hours, it appears to increase the permeability of the rhodamine labeled particles in this transport, since more pores are stained and there is a higher density of dendrimers on the astrocyte layer. As explained before, during OGD, TJ suffers a deregulation mediated by different factors, which ultimately lead to a disassembly and downregulation of TJ proteins expression. This disturbance of the physiological homeostasis induce an increasing in paracellular permeability, once the space between cells tend to increase. [37], [53], [57] These results fit better with a transport through a paracellular mechanism, however, we cannot exclude the possibility of a transcellular pathway.

The paracellular transport of the dendrimers, it should only represent a small part of the fate of the studied nanoparticles in the first hour. With the paracellular route highly restricted in the BBB, nanocarriers can promote substances permeability through the transcellular way. [37], [44] Increased permeability of nanoparticles by these pathway occur specially with positively charged nanoparticles enhancing the electrostatic interactions with the cell membrane (negatively charged) and consequently increasing the endothelial uptake [38], as it can be observed in Figure 11B and C (Top). This process could be followed by endothelial exocytosis, that allow the transcytosis of dendrimers and passage through the insert membrane. [44] Concerning to the differences between OGD treatment and control cells, the first ones seem to have higher internalization of the nanoparticles. This could be justified by the activation of the metabolic cascade after OGD which leads to NVU components deregulation with high impact in endothelial

cells. [53] Few studies report the impact of induced-hypoxia in nanoparticles uptake and retention, however Brownlee *et al.* [111] describe the increase of endocytosis and exocytosis of tested polystyrene nanoparticles in cells under hypoxia environment. So, oxygen depletion treatment could not only induce an increase in paracellular permeability but also in a transcellular way, resulting in a augmentation of nanoparticles uptake.

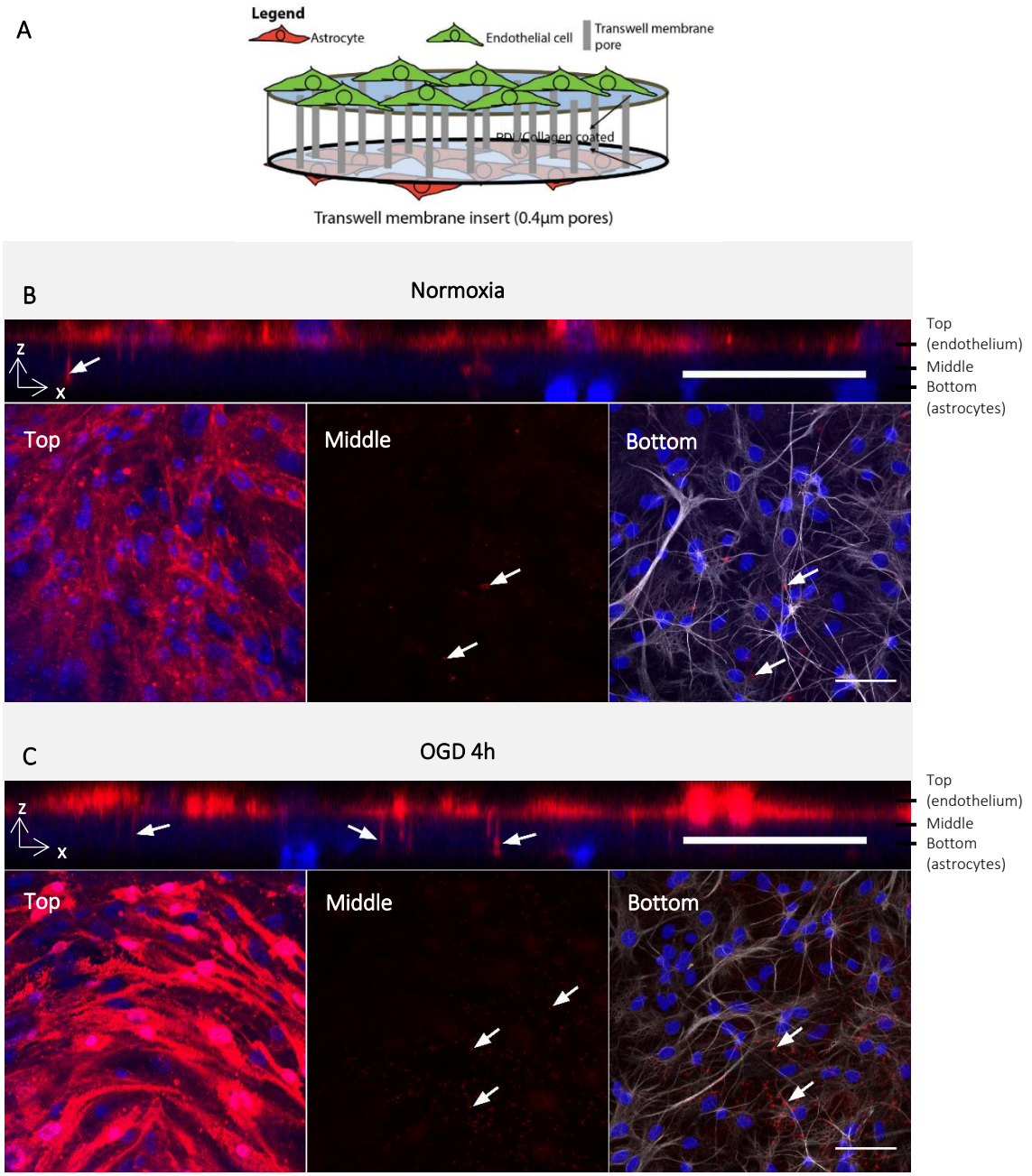

Figure 11 – *In vitro BBB permeability to PEG-PAMAM-5(6)ROX dendrimers under physiological (normoxia) and ischemic conditions (OGD).* **A**: Schematic representation of the insert membrane (adapted from [110]) **B** and **C**: Orthogonal representation done with confocal microscopy images of the insert after 1h contact with PEG-PAMAM-5(6)ROX (red), nuclei stained with Hoechst (blue). And confocal microscopy images of different levels of the insert membrane: endothelial cells (top); insert membrane (middle); astrocytes (bottom) – stained with GFAP (grey). Scale bar: 50 µm.

4.1.2.2. Dendriplexes

The set-up for PAMAM permeation analysis was aimed to be applied to our patented dendrimers complexed with a NA as a cargo. For that, the dendrimers should be labeled with a fluorescent tracker on their branches or instead in their cargo, the NA. To mimic a potential therapeutic NA, a test double stranded siDNA molecule labeled with Cy-5 was used for simplicity and economical reasons.

Briefly, siDNA (negatively charged) links with dendrimer branches (positively charged) by electrostatic interactions and allow the formation of nanoparticles (dendriplexes) that result from the complexation of the NA and dendrimer units (Figure 3C). After complexation, dendriplexes have a nanometric scale (55-65 nm), as previously characterized in our group (data not shown). Also, it is known that the ratio between amines (from functional group of the dendrimers) and phosphates (from NA) (N/P) influence the dendriplexes assembly, the particles characteristics and their behavior in biological environment. After a set of tests performed by other elements of our group, for example particle complexation efficiency, size, cell internalization and transfection, hemolysis and toxicity assays, it was selected a N/P with interest characteristics for intravenous administration in ischemic stroke applications, N/P 20 (data not shown).

The PAMAM permeability assay was adapted to dendriplexes, using optimized conditions. Succinctly, co-cultures were treated under physiologic conditions (normoxia), whereas others were subjected to an OGD environment for 12 hours (optimized condition). After that, endothelial cells were exposed to the dendriplex solution for 4 hours and the tests were performed to determine nanoparticle permeability. Since it is not known the permeability profile during time, the longest timepoint (4h) was chosen to perform the permeability assay.

For permeability determination, medium from the well (abluminal side) was collected and fluorescence was directly measured in a fluorimeter. With this approach, it was not possible to detect fluorescence from siDNA fluorochrome due to dendrimer influence by quenching the cy-5 signal. For a real detection, dendriplexes were dissociated by adding SDS, which disrupted the nanoparticles, as done before [45], by competing with NA in electrostatic interaction leading to its release. Here, it was possible to detect the fluorescence, but it was under the equipment limit of detection (data not shown). Alternative methods for sample analysis were tested for a more sensitive detection, including a polyacrylamide gel assay for NA detection and quantification with or without sample concentration by ultrafiltration. In this case, the NA sample concentrated was also under the limit of this method detection even after 30x concentration (data not shown). So, although it was not an ideal alternative for quantification, luminal solution from the insert was

collected to indirectly infer the quantity of nanoparticles lost i.e that are in the cells or passed through the membrane (cleared dendriplexes) (Figure 12), knowing that 1 µg of siDNA (complexed with dendrimers) was added to each insert. Notice that without cells, the dendrimer freely diffuses through the membrane. In the presence of the tight barrier the dendrimer does not freely cross but can associate with cells leading to the same decrease. After OGD the associated dendrimer can further cross the co-culture towards the abluminal side and the decrease in the luminal side would be the same. No conclusions can be taken from that information without cell analysis.

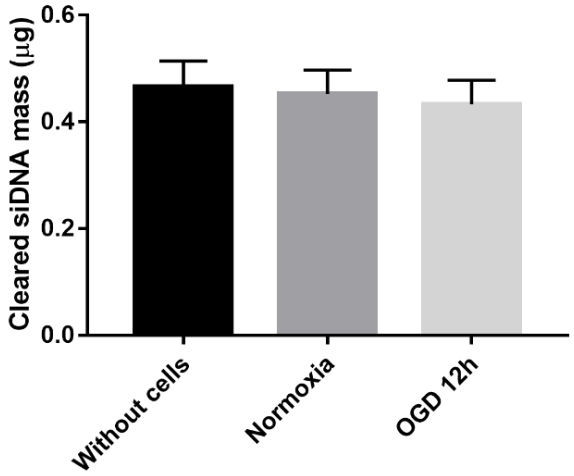

Figure 12 – *Cleared siDNA mass complexed in dendriplexes through the in vitro BBB model.* Luminal medium fluorescence was quantified to determine the cleared mass of siDNA (what is inside the cells, on the membrane and passes to the abluminal side). There were no statically significant results between conditions. (n=2 with triplicates).

Therefore, cells were stained to analyze the permeability profile, as previously done with PAMAM (Figure 13). Both under normoxia and OGD conditions, it was not possible to detect dendriplexes on the membrane nor on the astrocytes (Figure 13), which impedes to draw conclusions about transcellular permeability in a short timepoint.

PECAM-1 expression increased in endothelial cells subjected to OGD conditions (Figure 13C, top). The literature is not consistent regarding this issue. Studies, using stem-cell derived human microvascular endothelial cell line and brain microvascular endothelial cells, report no changes in PECAM-1/CD31 expression exposure to hypoxia conditions. [112], [113] Whereas, *in vivo* experiments where ischemic brain infraction is induced or animals were subjected to low oxygen levels, expression of PECAM-1 seems to enhance. [107], [113] Further studies should be done regarding the PECAM-1 expression in OGD conditions, with and without dendriplexes exposure, to clarify the here described observations.

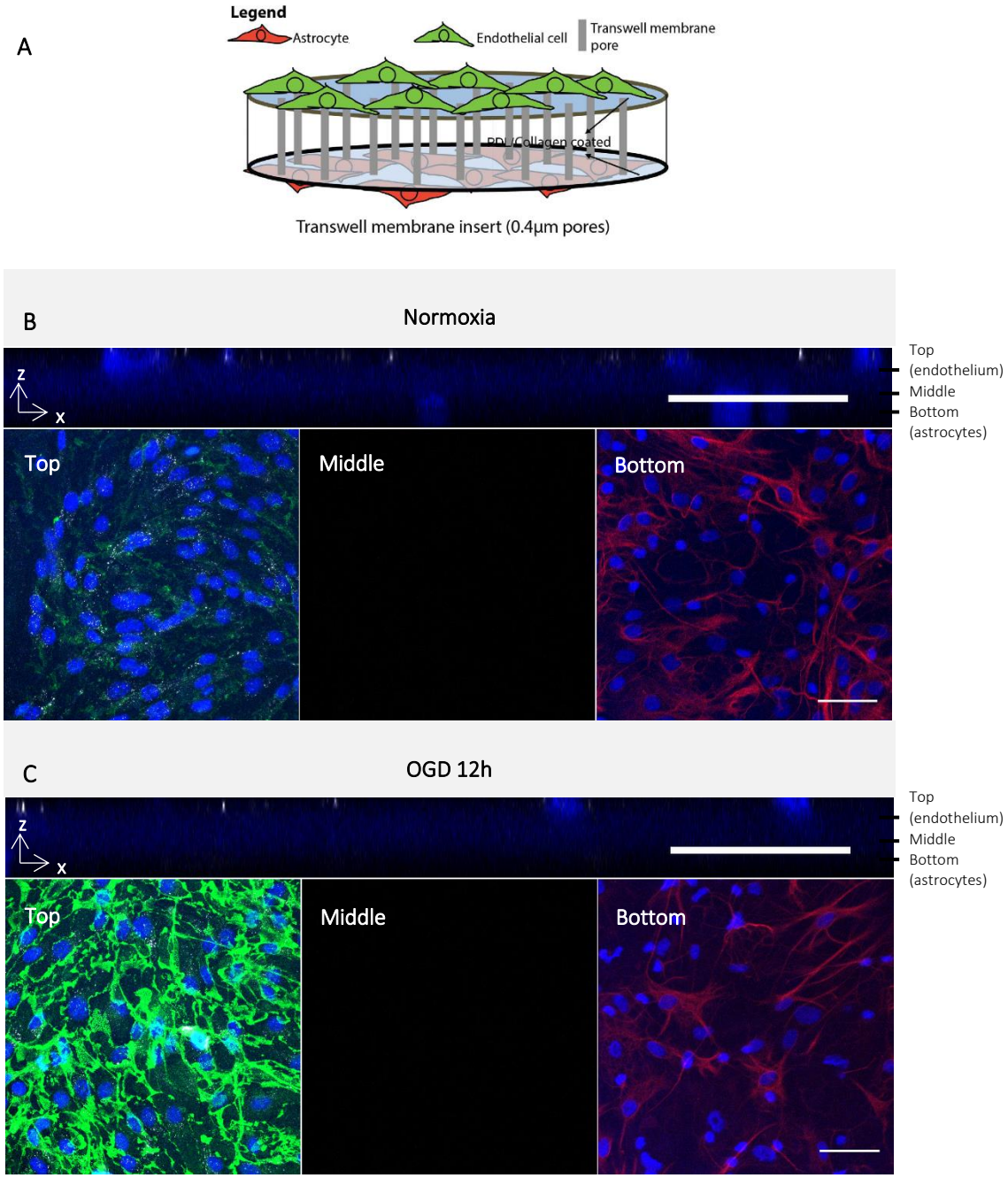

Figure 13 - *In vitro BBB permeability to dendriplexes under physiological and ischemic stroke conditions*. **A**: Schematic representation of the insert membrane (adapted from [110]) **B** and **C**: Orthogonal representation done by confocal microscopy images of the insert after 4h contact with dendriplexes (grey), nuclei stained with Hoechst (blue). And confocal microscopy images of different parts of the insert membrane: endothelial cells (top) – stained with PECAM-1 (green); insert membrane (middle); astrocytes (bottom) – stained with GFAP (red). Scale bar: 50 µm.

The differences in PAMAM dendrimers and dendriplexes permeation can be associated wit their different dynamics when in contact with cells. During the comparison of both nanoparticles, it is

important to be aware of their differences, such as different generation leading to distinct sizes and charge densities, as well as contrasting organizational structures.

Concerning obtained results, experimental design should be improved for dendriplexes detection in the abluminal side of the insert by increasing the time of contact or changing the labeled method. In the first case, it is important to underline that the thickness of the membrane do not reflect the *in vivo* ECM which is much thinner. [50] On the other hand, it would be more accurate to track the dendrimers instead of the NA to detect the nanoparticles without the possibility of causing its disassembly.

Regarding the difficulties during this process and to have the idea of the internalization profile of this particles, 2D controls were done only under normoxic conditions to evaluate each cell (endothelial cells and astrocytes) behavior when in contact with dendriplexes. In Figure 14, dendriplexes can be detected in the both types of cells.

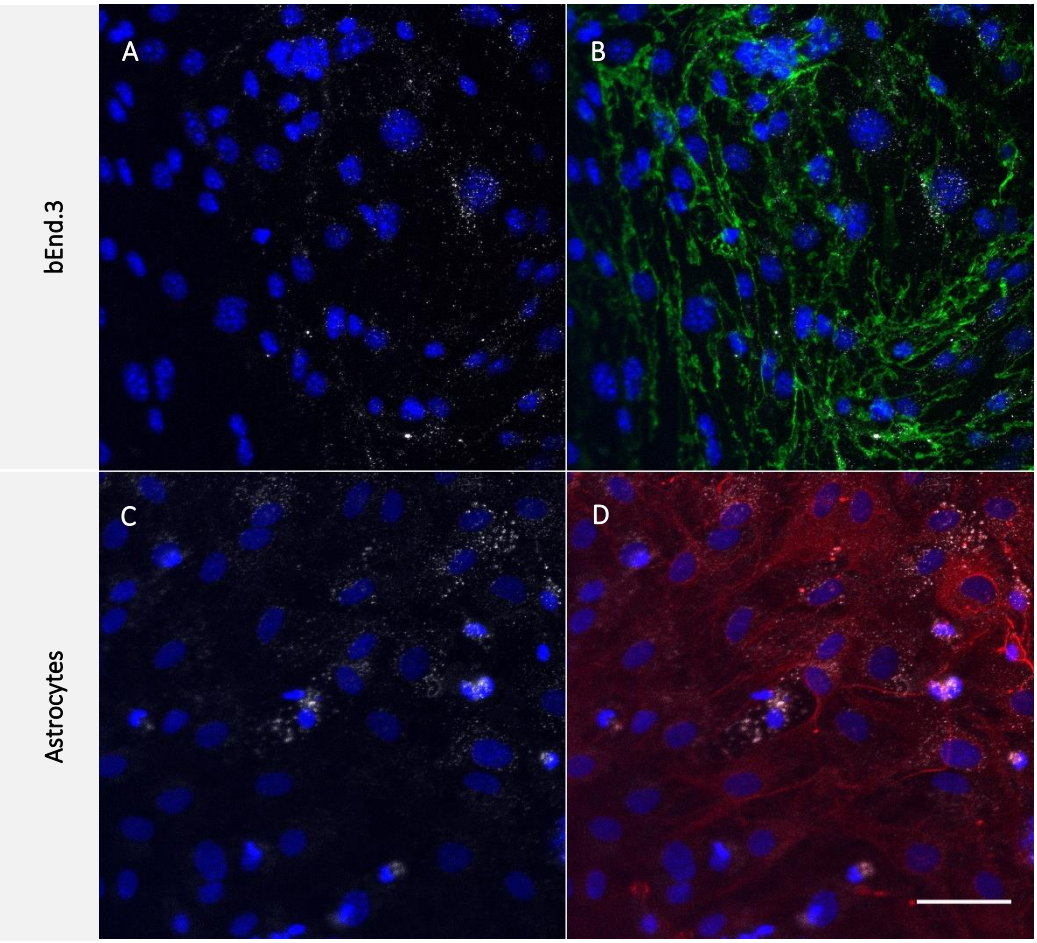

Figure 14 – *2D dendriplex internalization controls of endothelial cells (bEnd.3) and astrocytes*. Confocal microscopy images of endothelial cells (bEnd.3, A and B) and rat primary astrocytes (C and D) after 4h of contact with dendriplexes (grey). **A** and **C**: Cell nuclei stained with Hoechst (nuclei, blue) and internalized dendriplexes (grey); **B**: Merge of image A with PECAM-1 (green) staining in endothelial cells; **D**: Merge of image C with GFAP (red) staining in primary rat astrocytes.

Dendriplexes were designed to be a non-invasive technique to pass through the barrier, once themselves are not intended to cause BBB disruption [114]. This could be a huge advantage in the area, since BBB induced disruption, even temporary, could carry a significant risk for patient. [50] To confirm that BBB characteristics are not impaired by cell contact with dendriplexes, several tightness assays should be performed after dendriplexes contact, such as TEER measurement, sodium fluorescein permeation and TJ expression. Exploratory experiments were done concerning this issue, with only a TJ protein (ZO-1) staining (Figure 15). We have observed that the TJ location is preferably in the periphery of the membrane after 4 hours of contact with dendriplexes in OGD conditions (Figure 15D) than under normoxic conditions (Figure 15A). Comparing both conditions, the recovery of TJ protein expression and localization could be related to dendriplexes effects either on normoxia or OGD conditions. Regarding that, it would be necessary a parallel co-culture without these nanoparticles and subjected to the same treatment conditions to compare with obtain results. Further experiments should be done concerning the effect of dendriplexes in barrier tightness, once they were designed to permeate the BBB without disturbing it.

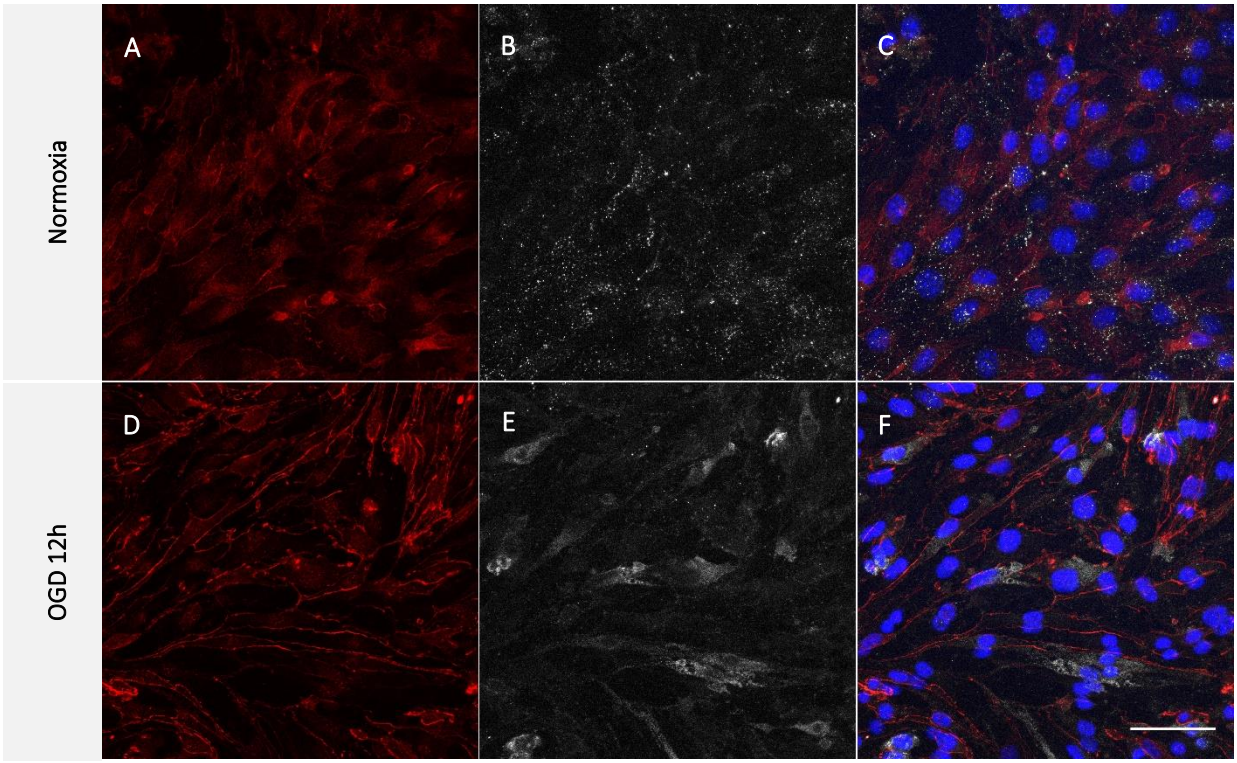

Figure 15 – *Influence of dendriplexes in ZO-1 expression after OGD treatment in the BBB model*. Confocal microscope images of endothelial cell layer after 4 hours contact with dendriplexes. **A** and **D**: ZO-1 staining (red) in bEnd.3 cells under normoxia and OGD conditions, respectively. **B** and **E**: Dendriplexes (grey) internalized by bEnd.3 cells under normoxia and OGD conditions, respectively. **C** and **F**: Merge of previously described channels with nuclei staining (Hoechst, blue).

As previously referred for PAMAM dendrimers, it is known that nanoparticles can stimulate vesicular transport in order to reach brain parenchyma, starting with endocytosis and followed by transcytosis through the BBB. [43], [44], [109] Looking at Figure 15, the internalization profile of dendriplexes seemed different between normoxic and OGD cultures. Regarding studies with cancer cells which describes a down-regulation of endocytic proteins during hypoxia [115], [116], it was hypothesized that OGD conditions could induce a cell membrane deregulation and, therefore, nanoparticles could enter the cell by diffusion, an effect compatible with the observed staining. Concerning that, endocytosis studies were performed to understand the differences between internalization profiles.

In present results, under normoxic conditions, expression of early endocytic markers (clatherin and caveolin) is low when compared to OGD conditions (Figure 16).

Endocytic vesicles coated with clathrin are characteristic from a receptor-mediated endocytosis, whereas caveolin coated vesicles are formed during the random uptake soluble molecules, non-receptor-mediated endocytosis. [43] Studies in nanoparticle endocytosis refer that it is mainly mediated by receptors, once BBB endothelial cells are characterized by few caveolae. [38], [43], [44] So, we expect that, at least under normoxic conditions, the endocytosis is receptor-mediated, although, this has to be confirmed by inhibition studies.

In OGD conditions, dendriplexes internalization increases as verified before (Figure 16), which was not according to the formulated hypothesis, but occurs by a vesicular endocytosis, receptor and non-receptor mediated. As previously described, hypoxia-induce changes have impact in energy dependent activities, as endocytosis, due to the reduced synthesis of ATP. [115], [116]. So, the dendriplexes uptake was expected to be lower in OGD conditions. A recent study in endocytosis and exocytosis of nanoparticles under hypoxia conditions, using breast cancer cells, corroborates the obtained results by an increasing of uptake when cells are exposed to low oxygen levels, once cells increase the capacity of nanoparticles uptake. This can be explained by metabolic alterations in endocytic receptor uptake and signaling as well as interferences in intracellular traffic. The recycling of transmembranar proteins stimulate endocytic proteins as Caveolin-1, inducing endocytic pathways. In this study, it was also demonstrated an increase in exocytosis under hypoxic conditions. [111] Considering that, the OGD treatment has an impact in dendriplexes uptake by a transcellular way. Further studies should be done in exocytosis, once it was described to be also affected and can influence the passage through the BBB *in vitro* model.

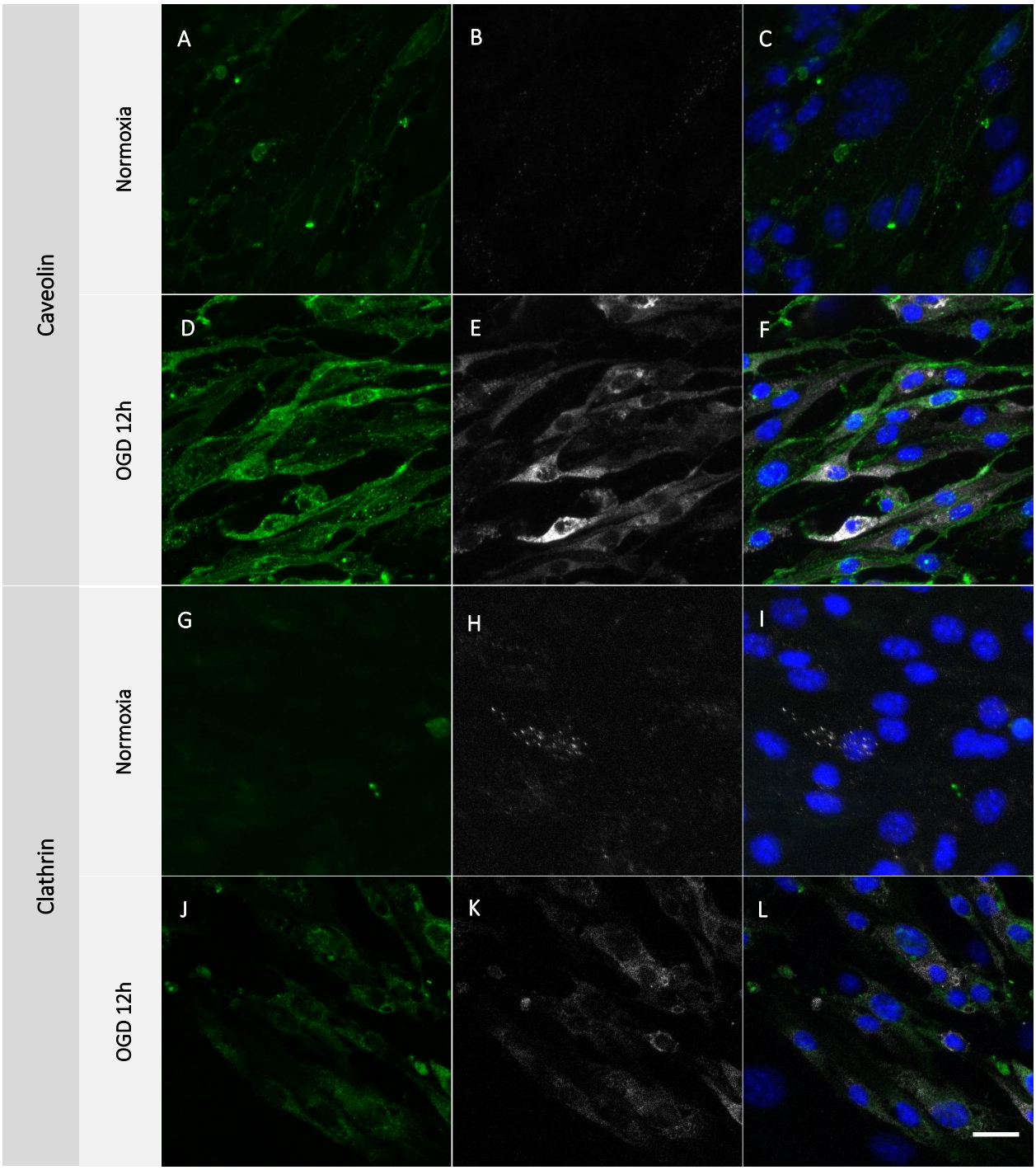

Figure 16 – *Endosomal markers expression after dendriplexes exposure under normoxic and OGD conditions*. Confocal microscope images of endothelial cell layer after 4 hours contact with dendriplexes. **A** and **D**: Caveolin staining (green) in bEnd.3 cells under normoxia and OGD conditions, respectively. **G** and **J**: Clathrin staining (green) in bEnd.3 cells under normoxia and OGD conditions, respectively. **B**, **E**, **H** and **K**: Dendriplexes (grey) internalized by bEnd.3 cells under normoxia and OGD conditions. **C**, **F**, **I** and **L**: Merge of previously described channels with nuclei staining (Hoechst, blue). Scale bar: 20 µm

4.2. *IN VIVO* MODEL

A second aim of this project was the establishment of an *in vivo* model using zebrafish larvae to study the dendriplexes permeation capacity through the BBB, either under physiologic or ischemic conditions.

To the best of our knowledge there is no report on the use of zebrafish larvae to study the bioperformance of nanoparticles in the context of ischemia pathologies. In fact, the number of studies involving nanoparticles being tested in the zebrafish is very limited. Studies with these organisms have huge advantages and could be a promising model for drug screening in ischemic injured brain applications.

As described in section 1.3.2.1., the zebrafish BBB has similar characteristics to the human BBB, which are already established in an early development stage. Taking this into account, to develop the stroke BBB model, we first studied the BBB maturation during development to establish a timepoint where molecules are size excluded from paracellular route.

4.2.1. VERIFICATION OF BBB MATURATION

As previously described, the zebrafish BBB starts expressing TJ proteins 3 dpf and maturation process prolongs until 10 dpf. Although, in earlier stages of development, TJ expression only happens in some cerebral vessels, many molecules are described to be sized excluded from paracellular transportation at these stages. [46], [82], [91], [92]

One indicator of BBB disruption is the extravasation into brain parenchyma of high-molecular weight molecules (HMWM) present in the blood, such as albumin. [82], [117] According that, several molecule tracers can be used to study permeability through barriers. Regarding to the BBB, Evans blue (EB) (961 Da) is a global standard tracer and it has high affinity to serum albumin (EB-albumin complex 68 kDa). So, when administrated systemically it behaves as a HMWM and it does not cross the BBB when this is intact. However, if EB is in the bloodstream and there is a BBB disruption, a dye leakage into brain parenchyma can be noticed. [117]

Therefore, to verify BBB permeability to HMWM, two zebrafish ages were chosen (Figure 17): one before (2dpf) and other after (4 dpf) the theoretical start of maturation and EB was used as a trace marker for BBB disruption. Here, it was expected that, before BBB maturation, there is a dye leakage into brain parenchyma and, after that, staining should be confined to blood vessels. An earlier stage of development during the BBB maturation was chosen since many ethical constrains arises after 5 dpf.

Initially, as pilot studies, EB was added to the larvae zebrafish swimming medium in different concentrations and timepoints, as previously done by Eliceiri *et al*. [118], since molecules in the swimming medium have the ability to cross larvae skin and reach the bloodstream. [118]–[120] However, *in vivo* observations under the fluorescence stereoscope microscope were not conclusive, since they did not allow to a clear verify the entrance of the dye into the blood stream and there were no observational differences of coloration between timepoints in the brain area (see Supplementary Data, Figure S1).

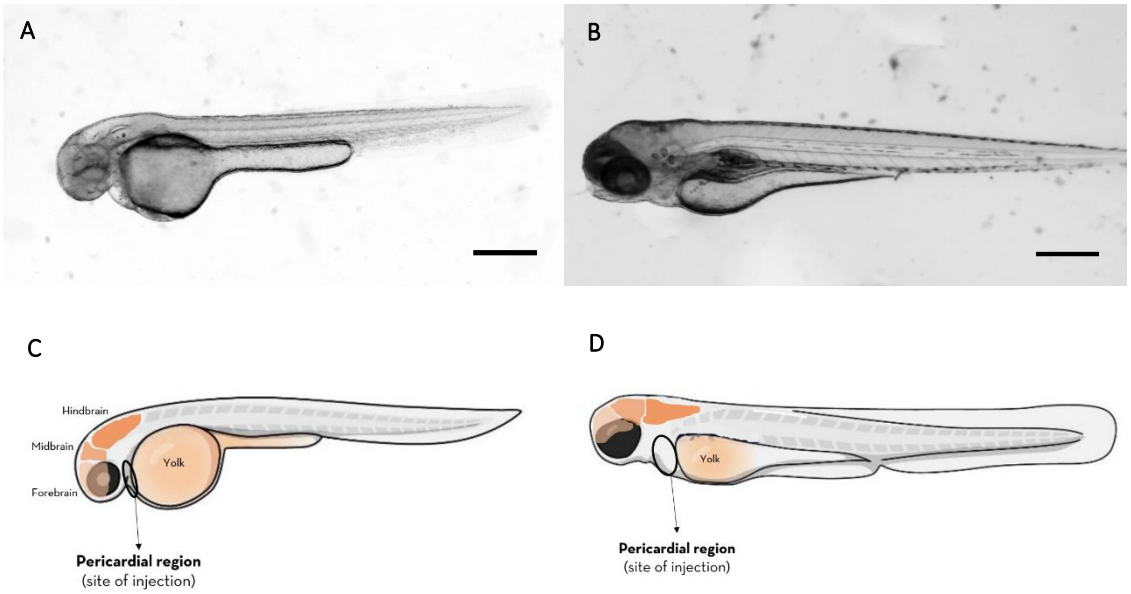

Figure 17 – *Zebrafish in both (2 and 4 dpf) stages of development*. **A** and **B**: *In vivo* zebrafish images.. **A**: zebrafish embryo 2dpf after chorion removal; **B**: zebrafish larvae 4dpf. Scale bar: 250 µm **C** and **D**: Schematic representation of tested zebrafish organisms and different parts of their brains, where is highlighted the pericardial regional (site of injection) (adapted from [121]). **C**: zebrafish embryo 2dpf after chorion removal; **D**: zebrafish larvae 4dpf.

So, to guarantee that EB enters the systemic circulation and permeates into the tissues through the blood vessels, the dye was injected in the pericardial region [120] where heart and pericardium co-localize (Figure 17C and D). In this case, under the stereoscope fluorescent microscope, it was possible to see the dye in circulation, however no significant observational differences were registered between treatments and controls as well as between development states (see Supplementary Data, Figure S2). This can be justified by the high thickness of the specimen not able to be observed with a regular fluorescent microscope/stereomicroscope.

Concerning the brain thickness and to better dissect the signal, animals were fixed and observed *ex vivo* under the confocal fluorescence microscope to be able to analyze each layer of the tissue. Results showed a clear difference between 2 and 4 dpf concerning to brain staining (Figure 18).

As expected in a non-mature BBB, as the one from 2 dpf animals, EB permeate through the blood vessels into brain parenchyma. Whereas, on the 4th with the expression of some TJ protein, the intensity of the staining in the brain parenchyma abruptly decreases with the exclusion of HMWM from the paracellular route.

For the next experiments, to establish the zebrafish ischemia model, the 4dpf stage of development was used, as the BBB is able to exclude HMWM and, therefore, we can study the effect on BBB disruption due to hypoxia.

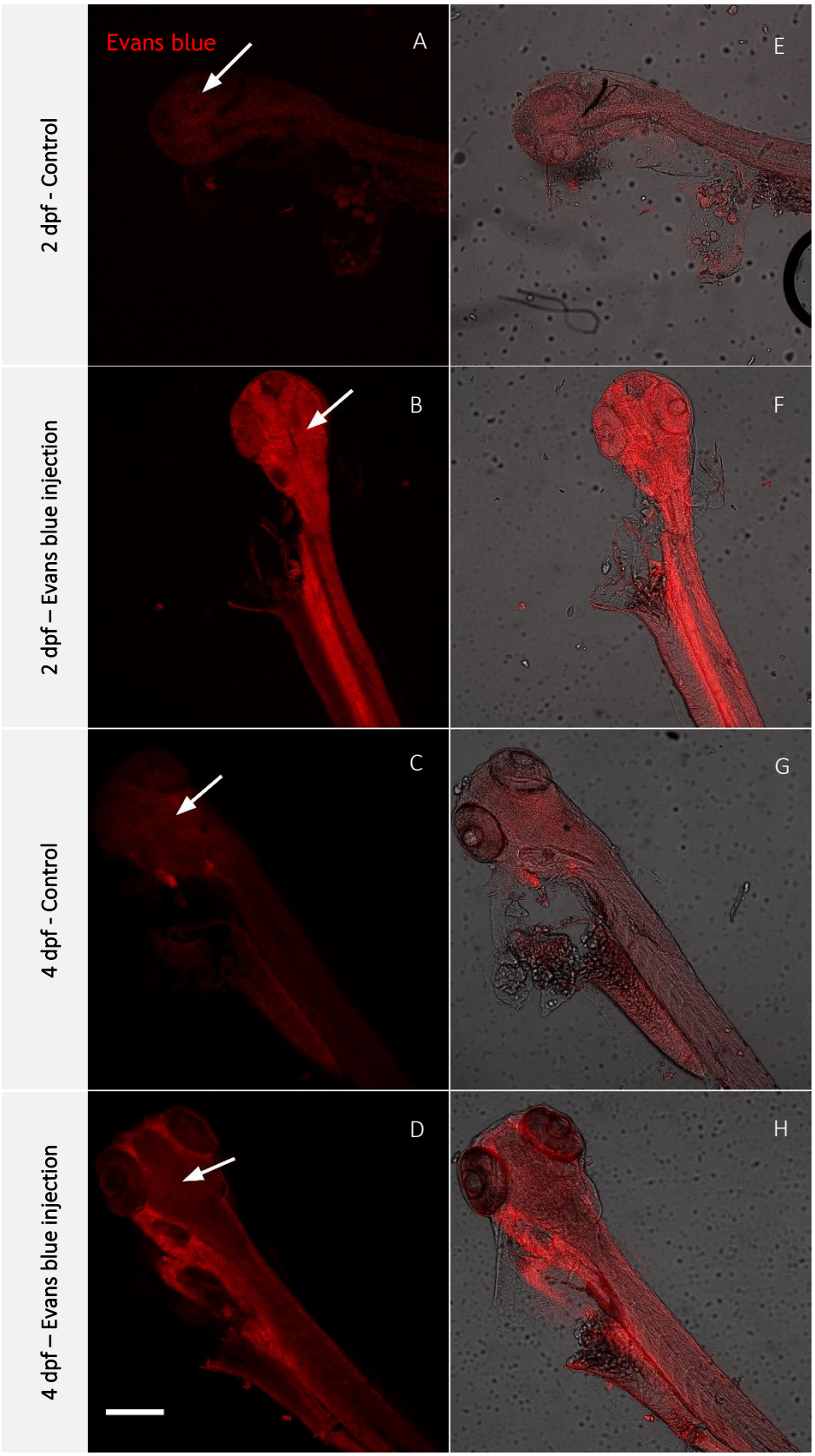

Figure 18 – *EB permeability depending on the stage of development. Ex vivo* 2 and 4 dpf zebrafish confocal fluorescent microscopy images after injection. **A**, **C**: Zebrafish with 2 and 4 dpf, respectively, injected with of 0.9% NaCl (control) solution **B**, **D**: Zebrafish with 2 and 4 dpf, respectively, injected with EB solution. **E**-**H**: EB labeling merge with brightfield image. Scale bar: 250 µm

4.2.2. BBB disruption model

As previously described in section 1.2.2., in humans, oxygen and glycose deprivation after a vessel occlusion triggers a cascade of metabolic effects with affects not only cells in the brain parenchyma by also the components of the NVU. Ischemic event, consequently, leads to various openings of the BBB by TJ deregulation.

Ischemic stroke animal models can be divided in two types: focal or global ischemia. Focal ischemic injury is characterized by a reduction of the blood flow in a delimited area of the brain. On the other hand, a global ischemic injury corresponds to a reduction of blood flow in the entire brain or a depletion of oxygen in circulating blood. [94], [122] When developing an *in vivo* model for ischemic stroke with zebrafish larvae, which confer huge advantages as referred in the introduction section, it is however difficult to induce a focal ischemic stroke done by vessel occlusion, either by making a cerebral thromboembolism or mechanically. So, based on simplicity, tests were performed in zebrafish larvae by oxygen deprivation in the same way as done with zebrafish adults by Yu et al. [94].

4.2.2.1. Hypoxia chamber

To induce oxygen deprivation to the zebrafish larvae, a hypoxic chamber was implemented (Figure 6) and optimized to mimic ischemic conditions. According to the Committee on Environment and Natural Resources concentrations of O_2 below 2 mg/L of O_2 are considered hypoxic. In global cerebral ischemia, oxygen dissolved level drops to 0.6-0.8 mg/L (near complete oxygen depletion). [94]

In the absence of an incorporable oximeter into the chamber, an external one was used. Samples were taken from the chamber by i) opening it and pipetting a sample or ii) aspirating with a syringe. This last one showed a high air incorporation and, consequently, an increase of oxygen levels when used. In this first experiment (see Supplementary Data, Figure S3), N_2 bubbling times were: 5, 10 or 15 minutes and the oxygen levels were lower than 0.6 mg/L. Therefore, bubbling time was decreased to 4 min and oxygen levels reached values between 0.6 and 0.8 mg/L (like global ischemic stroke conditions) (Figure 19). Notice that to take samples for oxygen levels determination in tis experiments, the rubber lid was taken and left opened for 10 min. This is acceptable as we assume that oxygen equilibration with the air is not a fast process and so when placing the animals inside, the oxygen should be similar.

The opening of 2 min was enough to put zebrafish inside the chamber and airproof seal the chamber to reduce oxygen incorporation. So, it was established that in every assay, chamber will be opened for 2 min to add the larvae, therefore the incorporation will be the same every time.

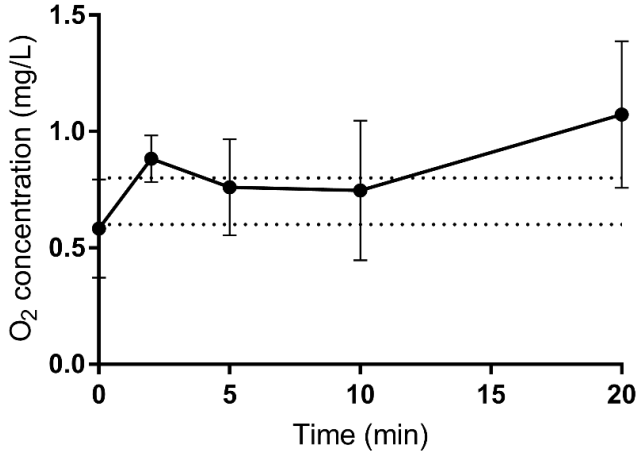

Figure 19 – *Dissolved oxygen concentration after chamber opening.* Hypoxia chamber was bubbled with N_2 for 4 min, the lid was opened and samples were carefully taken, in every timepoint, to an external oxygen reader with a pipette (data results from reading of 3 different flasks).

4.2.2.2. Effects of oxygen deprivation on the BBB

Shortly, the optimized hypoxia chamber was opened and zebrafish with 4 dpf were placed carefully inside to avoid oxygen incorporation into the medium. Animals were left inside for different timepoints and injected with EB in the pericardial site to assay BBB disruption.

Initially, the hypoxia assay was done according to Yu et al. [94], by performing treatments for 9 and 15 min. Larvae injected with the dye were *ex vivo* imaged and there was no observational difference for EB staining between normoxia and hypoxia at the brain parenchyma (see Supplementary Data, Figure S4).

Yu et al. [94] described a high mortality rate of this assay in zebrafish adults, however, with larvae, we did not obtain the same mortality results. According to this information, the lethal dose (LD50) of the treatment was established (Figure 20) to provide information about the best timepoint for treatment. The mortality seems to reach a plateau from 120 minutes in a hypoxia environment, which extends, at least, until 1440 minutes (24h). In small larvae, the diffusion of the oxygen from the medium through the skin is sufficient for metabolic needs, however in hypoxia environments, animals in these state of development have the endogenous capacity of larvae to survive for long times, contrary to the zebrafish adults. [123]–[125]

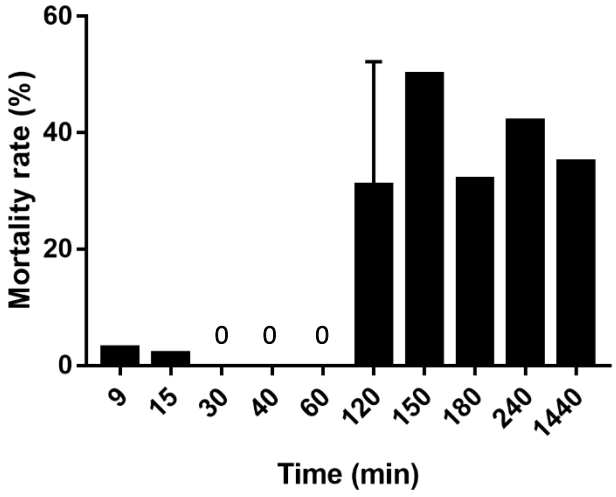

Figure 20 – *Mortality rate after oxygen deprivation.* The mortality rate was determined after zebrafish larvae exposure to low-oxygen medium for different periods. (All timepoints except 120 min: n=1, one independent experiment with 50 animals each; 120 min: n=2 with 50 animals each)

Alive animals after the treatment were injected with EB solution in order to determinate BBB disruption. Observing *ex vivo* images it seems that BBB is not disrupted after 2 hours of hypoxia. However, to identify a clear dye leakage to the brain parenchyma, we investigated blood vessels in higher detail. Although it is possible to identify blood vessels in both conditions – normoxia and hypoxia for 2h (120 min) - (Figure 21, white arrows), it is difficult to outline a dye leakage profile when animals are treated.

To increase the possibility of having a BBB disruption and to overcome these image limitations in *ex vivo* imaging, an in vivo imaging was performed with the animals treated under 240 min (4h) of hypoxic conditions. The image procedure was done according to Nishimura *et al.* [117], which consists in anesthetize the animals and immobilize them under the confocal microscope. In our work, 4 dpf animals were treated under hypoxic conditions for 4 hours, injected with EB and in the next day observed under the confocal microscope. EB stays in circulation complexed with albumin until it reaches a vessel opening and could leakage through it. Considering that the BBB opens in different phases as described previously, in section 1.2.2., animals were left in oxygenated medium overnight to analyze the overall leakage after an induced global ischemic stroke.

Live images were obtained in wild type (WT) animals under physiologic (normoxia) and global ischemic conditions (hypoxia) (Figure 22). Using this method, there is a clear reduction of the background when comparing with fixed animals (Figure 21), once the dye coloration is highly restricted to brain blood vessels (Figure 22, white arrows). In hypoxia for 4 hours, it was expected a leakage of EB dye, however, by observing the images, it is not possible to take conclusions

without quantification. The idea for images quantification passes through the segmentation of the blood vessels, in a restricted area of the brain and, with that, to determine the average fluorescent intensity of dye in the brain parenchyma to be able to compare with other conditions. Despite the necessary optimizations with this method, the aim is to track the path of dendriplexes into the animal after intravenous injection and determine their leakage into the brain parenchyma. So, an endogenous staining of blood vessels would be valuable to verify the actual location of the nanoparticles in the brain (blood vessels or brain parenchyma). According to that, a zebrafish line with fluorescent labeled blood vessels were used (zebrafish transgenic line ED141B [126]) (see Supplementary Data, Figure S5). BBB maturation experiments were repeated with transgenic animals (see Supplementary Data, Figure S6).

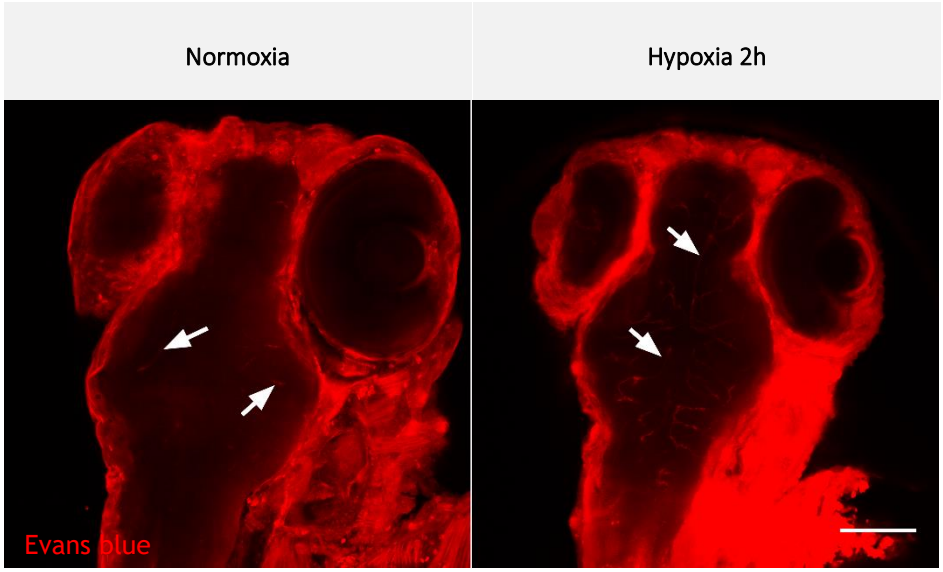

Figure 21 – *Ex vivo analysis of BBB disruption after oxygen* deprivation. Confocal microscope images after EB (red) injection in 4 dpf animals subjected to normoxic (A) and hypoxic (2h - B) conditions, where white arrows point brain blood vessels. Scale bar: 100 µm

In preliminary tests, we used a positive control to confirm the BBB disruption. There are many candidates used as coadjutants in brain targeted therapies, which creates a temporary disruption of the BBB and allow the delivery of therapeutic compounds, such as methamphetamines and bradykinin [127], [128] Here, one used bradykinin to create a disruption model, as done before with animal models, including zebrafish larvae [82], [129] to compare with hypoxia treated animals. Bradykinin is a biologically active compound released by endothelial cells as result of a metabolic deregulation after ischemic stroke injury, causing TJ disassemble and BBB disruption. [55], [57]

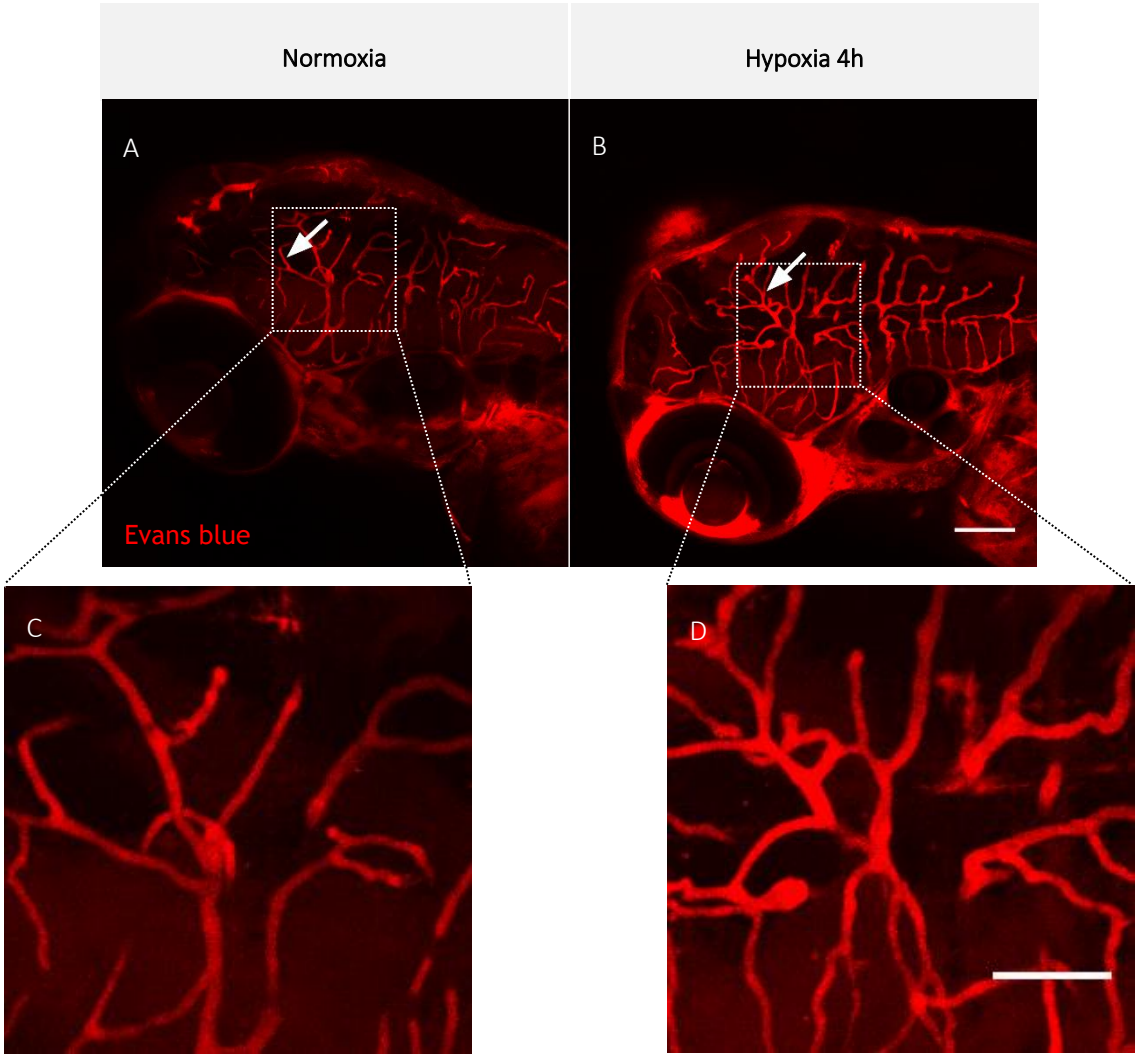

Figure 22 – *In vivo analysis of BBB disruption after oxygen* deprivation. Confocal microscope images after EB (red) injection in 4 dpf animals subjected to normoxic (A, C) and hypoxic (4h – B, D) conditions. Scale bar (A and B): 100 µm; Scale bar (C and D): 50 µm

The difficulties in comparing animals and conditions remains even using the transgenic animals, as expected (Figure 23). There are many factors that could improve imaging analysis and should be taken into account. The fish position can give different image outcomes, so it should be uniformized, which can be done by using zebrafish imaging plates that are able to position animals for live imaging. Considering that BBB maturation starts at 3 dpf and extends until 10 dpf [92], in the studied timepoint, there is still lack of TJ expression enabling some BBB extravasation even in negative control animals, once the dye exclusion is not total. So, experiments should be performed with animals in later stage of development.

Despite the achieved results and conclusions, the challenge will continue. However, the creation of a global ischemia model induced by hypoxia in larval zebrafish to use in ischemic stroke studies seems not to be far.

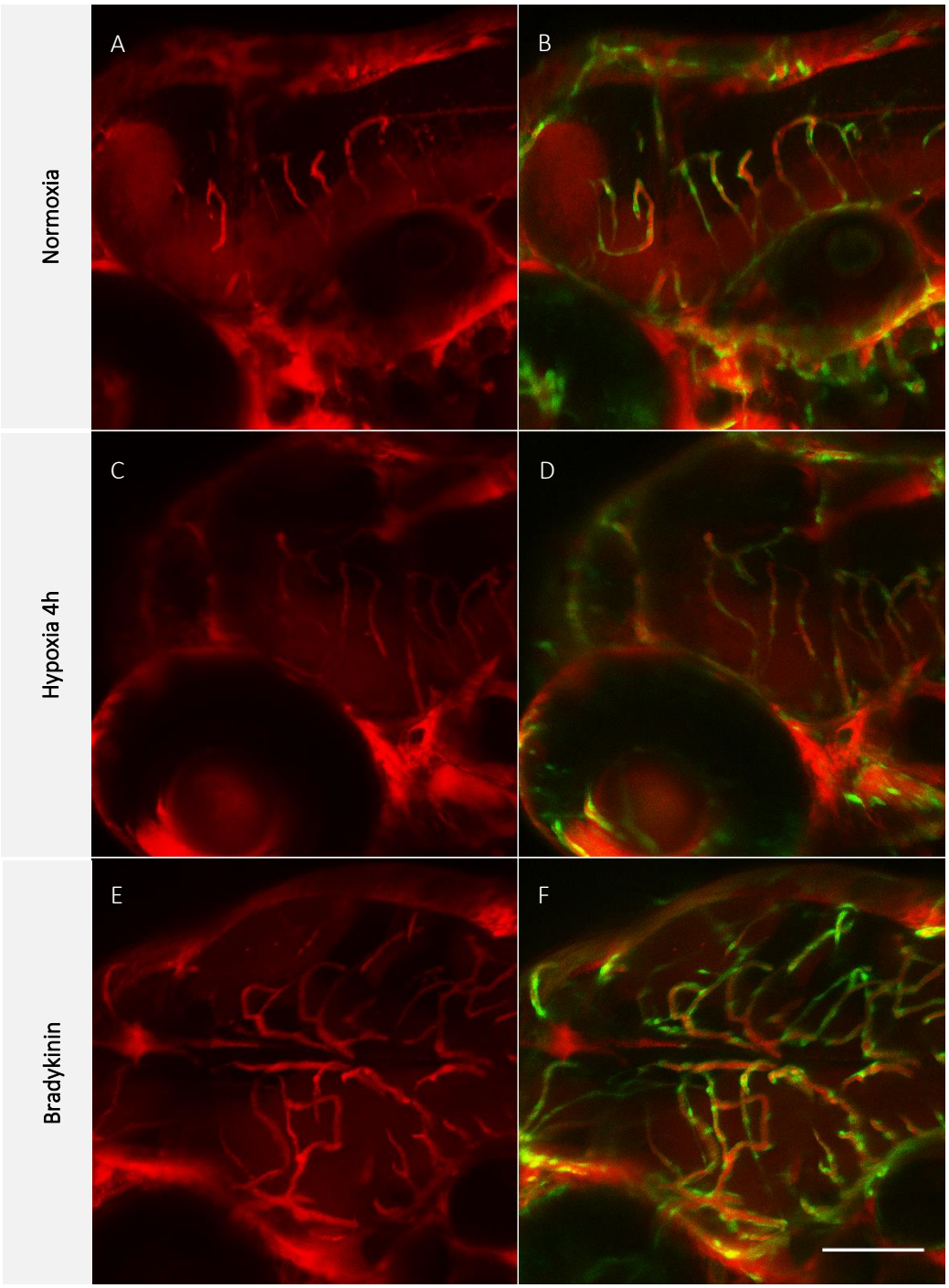

Figure 23 - *In vivo imaging of zebrafish larvae under normoxic, hypoxic conditions and after bradykinin exposure.* Confocal microscope images of the transgenic animal injected with EB (red) after different treatments: normoxia (A and B), Hypoxia for 4 hours (C and D) and Bradykinin (E and F). **A**, **C** and **E**: EB (red) dye in the animal brain area. **B**, **D** and **F**: Merge of EB staining (red) with endogenous staining of blood vessels (green). Scale bar: 100 µm

4.2.2.3. BBB PERMEABILITY TO DENDRIMERS AND DENDRIPLEXES

A preliminary test with dendrimers was done by injecting a PEG-PAMAM-5(6)-ROX solution into the transgenic vessel labeled animals. However, it was difficult to distinguish the vessel fluorescence from dendrimer fluorescence due to an organism residual expression of fluorescence in the same channel as these PAMAM dendrimers. This invalidated the collected data, as one was not able to identify the nanoparticles due to the fluorescence of the vascular tissue in the same wave length of the dendrimers (data not shown).

Further experiments should be done changing the fluorescent tracer marker or using the developed dendrimers complexed with a labelled nucleic acid.

This page was intentionally left in blank.

Conclusions and Future perspectives

5

5.1. *In vitro* model

The BBB *in vitro* model was successfully replicated and improvemented regarding OGD treatment were obtained with significate differences in cell characteristics and barrier tightness.

The PAMAM permeability assay allowed the observation of particles permeating through the membrane and differences between conditions (normoxia vs hypoxia) could be detected. As expected, after OGD conditions, the passage of nanoparticles through the BBB is increased, which is reflected in a higher density of PAMAM in the membrane porous and the astrocyte layer. The same was expected for our fully biodegradable dendrimer complexed with nucleic acid (the dendriplexes), however this was not observed. Possibly particles characteristics may have influenced their dynamic and this should be considered when comparing both results, since these are from different generations and have distinct organization structures (as they are complexed with nucleic acids), size and charge densities.

Regarding the dendriplex permeability profile, under different cell stimuli - normoxia and OGD, the pattern of internalization is different. After OGD, the internalization of nanoparticles increases due to metabolic mechanisms alterations. It was firstly hypothesized that dendriplexes could enter endothelial cells by diffusion after OGD treatment due to the compromise of the cell membrane, however, using early endocytic markers, it was shown an increase in endocytosis. Dendriplexes diffusion capacity should be further analyzed by adding a positive control which induces membrane destabilization, for example surfactants, to compare the permeability profiles.

Despite the dendriplexes uptake by endothelial cells, no particles were detected either on the astrocyte layer nor on the abluminal side, however it was demonstrated that astrocytes have ability to internalize dendriplexes. An increased crossing may be achieved by the prolongation of the assay time, in order to allow endothelial exocytosis and passage through the membrane. The

exocytosis should be also studied in the reversable way, i.e. the recycling of nanoparticles by returning them to the blood compartment. This process is intended to be further studied by pulse chase analysis that, succinctly consists in successively exposing the cells to labelled nanoparticles for a specific period of time followed by exposure to unlabeled nanoparticles and removal of particles solution to quantify labelled nanoparticles and know what is exocytosed to the luminal compartment.

Also, the effect of dendriplexes in barrier tightness should be deeply evaluated to check that they do not disturb the barrier and to confirm the safety of using dendriplexes for ischemic stroke applications via intravenous route.

After the improvement of the permeability assay, we intend to do triple cultures with the BBB co-culture and neurons. These last on the well bottom (abluminal side), in order to analyze the neuronal dendriplex internalization after the passage through the BBB model. Further, a functional NA will be used and transfection effects will be assessed.

5.2. *IN VIVO* MODEL

We have established a novel in vivo zebrafish ischemic model on the 4th dpf. Although hypoxic-induced *in vivo* model with zebrafish larvae looks promising for ischemic stroke studies, there are further experiments to be done to validate this model.

Concerning the stage of BBB maturation, it was clear that at 2 dpf the barrier is not mature and there is a leakage of the tested dye (EB) into the brain parenchyma, as expected. Whereas, on the 4th dpf the dye is excluded, although there may be some leakage. Even if this is residual, it compromised the evaluation of oxygen effects on the BBB. So, in future studies, a longer stage of maturation should be evaluated under the same conditions, as for example after the 10th dpf, knowing that the BBB continues to mature until that stage.

Also, the live imaging revealed a great improvement in background fluorescence associated to fixation. However, the method should be uniformized to obtain comparable images with larvae at the same position. This could be useful in 1) real time tracking of particles, 2) evaluation of different parameters, such as bioaccumulation in the brain and 3) blood clearance.

Upon the establishment of this in vivo model, dendriplex permeation through the BBB shall be tested in the blood vessel transgenic animals, to assess particle position in the brain area (brain parenchyma or blood vessels). In this study there are many challenges to overcome such as the particle labelling using a NA, which seemed weak in *in vitro* detection. Other labeling methods are being developed in the lab in order to have the dendrimer labelled instead of the NA. Also,

there is ongoing work in targeting particles to neurons, which theoretically will improve the uptake into the brain.

Furthermore, studies should be done concerning animal behavior during and after the treatment as well as after the particle injection. Behavior studies are usually done in animal models when assessing CNS therapies, since behavior phenotypes reflects alterations in normal CNS physiology. Collecting them, treatment and therapy effectiveness may be inferred by assessing behavior parameters such as motion profile and distance traveled. [130]–[132]

There are many emerging studies concerning toxicity drug screening throughout the use of the zebrafish as its main platform. [80], [81] So, a set of assays could be developed to use the model not only for biodistribution studies but also toxicity *in vivo* analysis.

Concerning the advantages of the zebrafish larvae and the obtained results, an ischemic model is a promising tool for our neuroprotection therapies after ischemic stroke. It will may reduce the distance between promising therapies to actual effective clinical therapies by an economical and simple *in vivo* screening.

This page was intentionally left in blank.

References

[1] A. D. Lopez, C. D. Mathers, M. Ezzati, D. T. Jamison, and C. J. Murray, "Global and regional burden of disease and risk factors, 2001: systematic analysis of population health data," *Lancet*, vol. 367, no. 9524, pp. 1747–1757, 2006.

[2] "The top 10 causes of death," *World Heath Organization*, 2017. [Online]. Available: http://www.who.int/mediacentre/factsheets/fs310/en/. [Accessed: 23-Feb-2018].

[3] G. A. Donnan, M. Fisher, M. Macleod, and S. M. Davis, "Stroke," *Lancet*, vol. 371, no. 9624, pp. 1612–23, 2008.

[4] D. T. Lackland *et al.*, "Factors Influencing the Decline in Stroke Mortality: A Statement From the American Heart Association," *Stroke*, vol. 45, no. 1, pp. 315–353, 2014.

[5] A. G. Thrift, H. M. Dewey, R. A. L. Macdonell, J. J. McNeil, and G. A. Donnan, "Incidence of the major stroke subtypes initial findings from the North East Melbourne Stroke Incidence Study (NEMESIS)," *Stroke*, vol. 32, no. 8, pp. 1732–1738, 2001.

[6] K. W. Muir, "Stroke," *Medicine*, vol. 37, no. 2. pp. 109–114, 2008.

[7] K. P. Doyle, R. P. Simon, and M. P. Stenzel-Poore, "Mechanisms of ischemic brain damage," *Neuropharmacology*, vol. 55, no. 3, pp. 310–318, 2008.

[8] L. Yang, K. K. Shah, and T. J. Abbruscato, *An in vitro model of ischemic stroke*, vol. 814. 2012.

[9] "Hemorrhagic stroke," *National Stroke Association*. [Online]. Available: http://www.stroke.org. [Accessed: 16-May-2018].

[10] P. Deb, S. Sharma, and K. M. Hassan, "Pathophysiologic mechanisms of acute ischemic stroke: An overview with emphasis on therapeutic significance beyond thrombolysis," *Pathophysiology*, vol. 17, no. 3. pp. 197–218, 2010.

[11] "World Stroke Campaign," *World Stroke Organization*. [Online]. Available: http://www.worldstrokecampaign.org/learn/the-facts-behind-1-in-6.html. [Accessed: 21-May-2018].

[12] B. T. Hawkins, "The Blood-Brain Barrier/Neurovascular Unit in Health and Disease," *Pharmacol. Rev.*, vol. 57, no. 2, pp. 173–185, 2005.

[13] U. Dirnagl, C. Iadecola, and M. A. Moskowitz, "Pathobiology of ischaemic stroke: an integrated view," *Trends Neurosci.*, vol. 22, pp. 391–397, 1999.

[14] R. Brouns and P. P. De Deyn, "The complexity of neurobiological processes in acute ischemic stroke," *Clinical Neurology and Neurosurgery*, vol. 111, no. 6. pp. 483–495, 2009.

[15] S. Grupke, J. Hall, M. Dobbs, G. J. Bix, and J. F. Fraser, "Understanding history, and not repeating it. Neuroprotection for acute ischemic stroke: From review to preview," *Clinical Neurology and Neurosurgery*, vol. 129. pp. 1–9, 2015.

[16] M. Fisher and J. H. Garcia, "Evolving stroke and the ischemic penumbra," *Neurology*, vol. 47, no. 4. pp. 884–888, 1996.

[17] B. B. Johansson, "Brain plasticity and stroke rehabilitation: The Willis lecture," *Stroke*, vol.

31, no. 1, pp. 223–230, 2000.
[18] K. E. Sandoval and K. A. Witt, “Blood-brain barrier tight junction permeability and ischemic stroke,” *Neurobiology of Disease*, vol. 32, no. 2. pp. 200–219, 2008.
[19] M. Fisher and J. L. Saver, “Future directions of acute ischaemic stroke therapy,” *The Lancet Neurology*, vol. 14, no. 7. pp. 758–767, 2015.
[20] J. H. Rha and J. L. Saver, “The impact of recanalization on ischemic stroke outcome: A meta-analysis,” *Stroke*, vol. 38, no. 3, pp. 967–973, 2007.
[21] J. Emberson *et al.*, “Effect of treatment delay, age, and stroke severity on the effects of intravenous thrombolysis with alteplase for acute ischaemic stroke: A meta-analysis of individual patient data from randomised trials,” *Lancet*, vol. 384, no. 9958, pp. 1929–1935, 2014.
[22] W. J. Powers *et al.*, “Guidelines for the Early Management of Patients With Acute Ischemic Stroke Regarding Endovascular Treatment,” *Stroke*, p. STR.0000000000000074, 2015.
[23] M. D. Hill and S. B. Coutts, “Alteplase in acute ischaemic stroke: the need for speed.,” *Lancet*, vol. 384, no. 9958, pp. 1904–6, 2014.
[24] W. Hacke *et al.*, “Thrombolysis with Alteplase 3 to 4.5 Hours after Acute Ischemic Stroke,” *N. Engl. J. Med.*, vol. 359, no. 13, pp. 1317–1329, 2008.
[25] N. M. Rao, S. R. Levine, J. a. Gornbein, and J. L. Saver, “Defining Clinically Relevant Cerebral Hemorrhage After Thrombolytic Therapy for Stroke: Analysis of the National Institute of Neurological Disorders and Stroke Tissue-Type Plasminogen Activator Trials,” *Stroke*, vol. 45, no. 9, pp. 2728–2733, 2014.
[26] J. L. Saver *et al.*, “Stent-Retriever Thrombectomy after Intravenous t-PA vs. t-PA Alone in Stroke,” *N. Engl. J. Med.*, vol. 372, no. 24, pp. 2285–2295, 2015.
[27] O. A. Berkhemer *et al.*, “A Randomized Trial of Intraarterial Treatment for Acute Ischemic Stroke,” *N. Engl. J. Med.*, vol. 372, no. 1, p. 141217070022009, 2014.
[28] A. M. Spiotta, M. I. Chaudry, F. K. Hui, R. D. Turner, R. T. Kellogg, and A. S. Turk, “Evolution of thrombectomy approaches and devices for acute stroke: A technical review,” *Journal of NeuroInterventional Surgery*, vol. 7, no. 1. pp. 2–7, 2015.
[29] R. Von Kummer *et al.*, “Desmoteplase 3 to 9 Hours after Major Artery Occlusion Stroke,” *Stroke*, vol. 47, no. 12, pp. 2880–2887, 2016.
[30] S. M. Davis, B. C. V. Campbell, and G. A. Donnan, “Endovascular Thrombectomy and Stroke Physicians: Equity, Access, and Standards,” *Stroke*, vol. 48, no. 8, pp. 2042–2044, 2017.
[31] G. N. *et al.*, “A multi-center study of safety and efficacy of mechanical thrombectomy for acute ischemic stroke patients with emergent large vessel occlusions not meeting top tier evidence criteria,” *Stroke*, vol. 48, 2017.
[32] C. V Campbell *et al.*, “Endovascular stent thrombectomy: the new standard of care for large vessel ischaemic stroke,” *www.thelancet.com/neurology Rapid Rev. Lancet Neurol*, vol. 14, pp. 846–54, 2015.
[33] T. G. Jovin *et al.*, “Thrombectomy within 8 Hours after Symptom Onset in Ischemic Stroke,” *N. Engl. J. Med.*, vol. 372, no. 24, pp. 2296–2306, 2015.
[34] P. A. Lapchak and J. H. Zhang, “Translational Stroke Research Guideline Projections: The 20/20 Standards,” *Translational Stroke Research*, vol. 9, no. 1. pp. 9–12, 2018.
[35] A. Moretti, F. Ferrari, and R. F. Villa, “Neuroprotection for ischaemic stroke: current status and challenges.,” *Pharmacol. Ther.*, vol. 146, pp. 23–34, 2015.
[36] M. D. Ginsberg, “Neuroprotection for ischemic stroke: Past, present and future,” *Neuropharmacology*, vol. 55, no. 3, pp. 363–389, 2008.
[37] J. Aparicio-Blanco, C. Martín-Sabroso, and A.-I. Torres-Suárez, “In vitro screening of nanomedicines through the blood brain barrier: A critical review,” *Biomaterials*, vol. 103, pp. 229–255, 2016.
[38] A. Domínguez, B. Suárez-Merino, and F. Goñi-de-Cerio, “Nanoparticles and Blood-Brain Barrier: The Key to Central Nervous System Diseases,” *J. Nanosci. Nanotechnol.*, vol. 14, no. 1, pp. 766–779, 2014.

[39] K. K. Jain, “Nanobiotechnology-based strategies for crossing the blood-brain barrier,” *Nanomedicine*, vol. 7, no. 8. pp. 1225–1233, 2012.
[40] V. Leiro, S. Duque Santos, C. D. F. Lopes, and A. Paula Pêgo, “Dendrimers as Powerful Building Blocks in Central Nervous System Disease: Headed for Successful Nanomedicine,” *Adv. Funct. Mater.*, vol. 28, no. 12, 2018.
[41] V. Leiro, S. D. Santos, and A. P. Pego, “Delivering siRNA with Dendrimers: In Vivo Applications,” *Curr. Gene Ther.*, vol. 17, no. 2, 2017.
[42] A. Z. Wilczewska, K. Niemirowicz, K. H. Markiewicz, and H. Car, “Nanoparticles as drug delivery systems,” *Pharmacological Reports*, vol. 64, no. 5. pp. 1020–1037, 2012.
[43] X. Li *et al.*, “Nano carriers for drug transport across the blood–brain barrier,” *Journal of Drug Targeting*, vol. 25, no. 1. pp. 17–28, 2017.
[44] J. Kreuter, “Drug delivery to the central nervous system by polymeric nanoparticles: What do we know?,” *Advanced Drug Delivery Reviews*, vol. 71. pp. 2–14, 2014.
[45] V. Leiro *et al.*, “Biodegradable PEG-dendritic block copolymers: Synthesis and biofunctionality assessment as vectors of siRNA,” *J. Mater. Chem. B*, vol. 5, no. 25, pp. 4901–4917, 2017.
[46] D. B. Stanimirovic, M. Bani-Yaghoub, M. Perkins, and A. S. Haqqani, “Blood-brain barrier models: in vitro to in vivo translation in preclinical development of CNS-targeting biotherapeutics.,” *Expert Opin. Drug Discov.*, vol. 10, no. 2, pp. 141–55, 2015.
[47] A. Wolff, M. Antfolk, B. Brodin, and M. Tenje, “In Vitro Blood-Brain Barrier Models - An Overview of Established Models and New Microfluidic Approaches,” *Journal of Pharmaceutical Sciences*, vol. 104, no. 9. pp. 2727–2746, 2015.
[48] H. C. Helms *et al.*, “In vitro models of the blood–brain barrier: An overview of commonly used brain endothelial cell culture models and guidelines for their use,” *J. Cereb. Blood Flow Metab.*, vol. 36, no. 5, pp. 862–890, 2016.
[49] N. A. Rahman *et al.*, “Immortalized endothelial cell lines for in vitro blood–brain barrier models: A systematic review,” *Brain Res.*, vol. 1642, pp. 532–545, 2016.
[50] J. Banerjee, Y. Shi, and H. S. Azevedo, “In vitro blood–brain barrier models for drug research: state-of-the-art and new perspectives on reconstituting these models on artificial basement membrane platforms,” *Drug Discovery Today*, vol. 21, no. 9. pp. 1367–1386, 2016.
[51] Y. Yang and G. A. Rosenberg, “Blood-brain barrier breakdown in acute and chronic cerebrovascular disease,” *Stroke*, vol. 42, no. 11, pp. 3323–3328, 2011.
[52] W. M. Pardridge, “Why is the global CNS pharmaceutical market so under-penetrated?,” *Drug Discovery Today*, vol. 7, no. 1, pp. 5–7, 2002.
[53] X. Jiang *et al.*, “Blood-brain barrier dysfunction and recovery after ischemic stroke,” *Prog. Neurobiol.*, 2017.
[54] K. Schoknecht, Y. David, and U. Heinemann, “The blood-brain barrier-Gatekeeper to neuronal homeostasis: Clinical implications in the setting of stroke,” *Seminars in Cell and Developmental Biology*, vol. 38. pp. 35–42, 2015.
[55] P. B. L. Pun, J. Lu, and S. Moochhala, “Involvement of ROS in BBB dysfunction,” *Free Radic. Res.*, vol. 43, no. 4, pp. 348–364, 2009.
[56] N. Weiss, F. Miller, S. Cazaubon, and P. O. Couraud, “The blood-brain barrier in brain homeostasis and neurological diseases,” *Biochimica et Biophysica Acta - Biomembranes*, vol. 1788, no. 4. pp. 842–857, 2009.
[57] R. Alyautdin, I. Khalin, M. I. Nafeeza, M. H. Haron, and D. Kuznetsov, “Nanoscale drug delivery systems and the blood-brain barrier,” *International Journal of Nanomedicine*, vol. 9, no. 1. pp. 795–811, 2014.
[58] P. Jeon, M. Choi, J. Oh, and M. Lee, “Dexamethasone-Conjugated Polyamidoamine Dendrimer for Delivery of the Heme Oxygenase-1 Gene into the Ischemic Brain,” *Macromol. Biosci.*, vol. 15, no. 7, pp. 1021–1028, 2015.
[59] D. Cui, Q. Xu, S. Gu, J. Shi, and X. Che, “PAMAM-drug complex for delivering anticancer

drug across blood-brain barrier in-vitro and in-vivo," *African J. Pharm. Pharmacol.*, vol. 3, no. 5, pp. 227–233, 2009.
[60] W. Ke *et al.*, "Gene delivery targeted to the brain using an Angiopep-conjugated polyethyleneglycol-modified polyamidoamine dendrimer," *Biomaterials*, vol. 30, no. 36, pp. 6976–6985, 2009.
[61] L. Zhang, S. Zhu, L. Qian, Y. Pei, Y. Qiu, and Y. Jiang, "RGD-modified PEG-PAMAM-DOX conjugates: In vitro and in vivo studies for glioma," *Eur. J. Pharm. Biopharm.*, vol. 79, no. 2, pp. 232–240, 2011.
[62] A. Zarebkohan, F. Najafi, H. R. Moghimi, M. Hemmati, M. R. Deevband, and B. Kazemi, "Synthesis and characterization of a PAMAM dendrimer nanocarrier functionalized by SRL peptide for targeted gene delivery to the brain," *Eur. J. Pharm. Sci.*, vol. 78, pp. 19–30, 2015.
[63] E. Nance *et al.*, "Systemic dendrimer-drug treatment of ischemia-induced neonatal white matter injury," *J. Control. Release*, vol. 214, pp. 112–120, 2015.
[64] A. Agrawal *et al.*, "Functional delivery of siRNA in mice using dendriworms," *ACS Nano*, vol. 3, no. 9, pp. 2495–2504, 2009.
[65] R. Hemmer *et al.*, "Analysis of biotinylated generation 4 poly(amidoamine) (PAMAM) dendrimer distribution in the rat brain and toxicity in a cellular model of the blood-brain barrier," *Molecules*, vol. 18, no. 9, pp. 11537–11552, 2013.
[66] I. D. Kim *et al.*, "Neuroprotection by biodegradable PAMAM ester (e-PAM-R)-mediated HMGB1 siRNA delivery in primary cortical cultures and in the postischemic brain," *J. Control. Release*, vol. 142, no. 3, pp. 422–430, 2010.
[67] H. Dai *et al.*, "Intrinsic targeting of inflammatory cells in the brain by polyamidoamine dendrimers upon subarachnoid administration," *Nanomedicine*, vol. 5, no. 9, pp. 1317–1329, 2010.
[68] A. Sharma, J. E. Porterfield, E. Smith, R. Sharma, S. Kannan, and R. M. Kannan, "Effect of mannose targeting of hydroxyl PAMAM dendrimers on cellular and organ biodistribution in a neonatal brain injury model," *J. Control. Release*, vol. 283, pp. 175–189, 2018.
[69] S. Kannan *et al.*, "Dendrimer-based postnatal therapy for neuroinflammation and cerebral palsy in a rabbit model," *Sci. Transl. Med.*, vol. 4, no. 130, 2012.
[70] M. K. Mishra *et al.*, "Dendrimer Brain Uptake and Targeted Therapy for Brain Injury in a Large Animal Model of Hypothermic Circulatory Arrest," *ACS Nano*, vol. 8, no. 3, pp. 2134–2147, 2014.
[71] R.-Q. Huang, Y.-H. Qu, W.-L. Ke, J.-H. Zhu, Y.-Y. Pei, and C. Jiang, "Efficient gene delivery targeted to the brain using a transferrin-conjugated polyethyleneglycol-modified polyamidoamine dendrimer," *FASEB J.*, vol. 21, no. 4, pp. 1117–1125, 2007.
[72] R. Huang, W. Ke, Y. Liu, C. Jiang, and Y. Pei, "The use of lactoferrin as a ligand for targeting the polyamidoamine-based gene delivery system to the brain," *Biomaterials*, vol. 29, no. 2, pp. 238–246, 2008.
[73] Y. K. Katare *et al.*, "Brain Targeting of a Water Insoluble Antipsychotic Drug Haloperidol via the Intranasal Route Using PAMAM Dendrimer," *Mol. Pharm.*, vol. 12, no. 9, pp. 3380–3388, 2015.
[74] F. Zhang *et al.*, "Generation-6 hydroxyl PAMAM dendrimers improve CNS penetration from intravenous administration in a large animal brain injury model," *J. Control. Release*, vol. 249, pp. 173–182, 2017.
[75] S. Somani, D. R. Blatchford, O. Millington, M. L. Stevenson, and C. Dufès, "Transferrin-bearing polypropylenimine dendrimer for targeted gene delivery to the brain," *J. Control. Release*, vol. 188, pp. 78–86, 2014.
[76] S. Somani, G. Robb, B. S. Pickard, and C. Dufès, "Enhanced gene expression in the brain following intravenous administration of lactoferrin-bearing polypropylenimine dendriplex," *J. Control. Release*, vol. 217, 2015.
[77] A. Janaszewska *et al.*, "The biodistribution of maltotriose modified poly(propylene imine)

(PPI) dendrimers conjugated with fluorescein - Proofs of crossing blood-brain-barrier," *New J. Chem.*, vol. 36, no. 2, pp. 350–353, 2012.
[78] M. J. Serramía *et al.*, "In vivo delivery of siRNA to the brain by carbosilane dendrimer," *J. Control. Release*, vol. 200, pp. 60–70, 2015.
[79] S. Li *et al.*, "Crossing the blood-brain-barrier with transferrin conjugated carbon dots: A zebrafish model study," *Colloids Surfaces B Biointerfaces*, vol. 145, pp. 251–256, 2016.
[80] J. B. Pryor, B. J. Harper, and S. L. Harper, "Comparative toxicological assessment of PAMAM and thiophosphoryl dendrimers using embryonic zebrafish," *Int. J. Nanomedicine*, vol. 9, no. 1, pp. 1947–1956, 2014.
[81] T. C. King Heiden, E. Dengler, W. J. Kao, W. Heideman, and R. E. Peterson, "Developmental toxicity of low generation PAMAM dendrimers in zebrafish," *Toxicol. Appl. Pharmacol.*, vol. 225, no. 1, pp. 70–79, 2007.
[82] J. Xie, E. Farage, M. Sugimoto, and B. Anand-Apte, "A novel transgenic zebrafish model for blood-brain and blood-retinal barrier development," *BMC Dev. Biol.*, vol. 10, 2010.
[83] R. A. Umans *et al.*, "CNS angiogenesis and barriergenesis occur simultaneously," *Dev. Biol.*, vol. 425, no. 2, pp. 101–108, 2017.
[84] A. V. Kalueff, A. M. Stewart, and R. Gerlai, "Zebrafish as an emerging model for studying complex brain disorders," *Trends in Pharmacological Sciences*, vol. 35, no. 2. pp. 63–75, 2014.
[85] W. B. Barbazuk *et al.*, "The synthenic relationship of the zebrafish and human genomes," *Genome Res.*, vol. 10, pp. 1351–1358, 2000.
[86] B. P. Walcott and R. T. Peterson, "Zebrafish models of cerebrovascular disease," *Journal of Cerebral Blood Flow and Metabolism*, vol. 34, no. 4. pp. 571–577, 2014.
[87] D. J. Milan, T. A. Peterson, J. N. Ruskin, R. T. Peterson, and C. A. MacRae, "Drugs that induce repolarization abnormalities cause bradycardia in zebrafish," *Circulation*, vol. 107, no. 10, pp. 1355–1358, 2003.
[88] C. Pardo-Martin, T. Y. Chang, B. K. Koo, C. L. Gilleland, S. C. Wasserman, and M. F. Yanik, "High-throughput in vivo vertebrate screening," *Nat. Methods*, vol. 7, no. 8, pp. 634–636, 2010.
[89] H. F. Cserr and M. Bundgaard, "Blood-brain interfaces in vertebrates: a comparative approach.," *Am. J. Physiol.*, vol. 246, no. 3 Pt 2, pp. R277–R288, 1984.
[90] M. Bundgaard and N. J. Abbott, "All vertebrates started out with a glial blood-brain barrier 4-500 million years ago," *Glia*, vol. 56, no. 7, pp. 699–708, 2008.
[91] R. A. Umans and M. R. Taylor, "Zebrafish as a model to study drug transporters at the bloodbrain barrier," *Clin. Pharmacol. Ther.*, vol. 92, no. 5, pp. 567–570, 2012.
[92] A. Fleming, H. Diekmann, and P. Goldsmith, "Functional Characterisation of the Maturation of the Blood-Brain Barrier in Larval Zebrafish," *PLoS One*, vol. 8, no. 10, 2013.
[93] W. R. Barrionuevo and W. W. Burggren, "O2 consumption and heart rate in developing zebrafish (Danio rerio): influence of temperature and ambient O2," *Am J Physiol Gastrointest Liver Physiol*, vol. 276, no. 2, pp. R505-504, 1999.
[94] X. Yu and Y. V. Li, "Zebrafish as an alternative model for hypoxic-ischemic brain damage," *Int. J. Physiol. Pathophysiol. Pharmacol.*, vol. 3, no. 2, pp. 88–96, 2011.
[95] J. McCarthy, Ken and Vellis, "Preparations of Separate Astrocglial and Oligodendroglial Cell Cultures from Rat Cerebral Tissue," *J. Cell Biol.*, vol. 85, no. June, 1980.
[96] D. N. Rocha, J. P. Ferraz-Nogueira, C. C. Barrias, J. B. Relvas, and A. P. Pêgo, "Extracellular environment contribution to astrogliosis—lessons learned from a tissue engineered 3D model of the glial scar," *Front. Cell. Neurosci.*, vol. 9, 2015.
[97] J. P. Martins, C. J. Alves, E. Neto, and M. Lamghari, "Communication from the periphery to the hypothalamus through the blood-brain barrier: An in vitro platform," *Int. J. Pharm.*, vol. 499, no. 1–2, pp. 119–130, 2016.
[98] D. Moreira, "Implementation of an in vitro blood-brain barrier model to study nanoparticle administration in stroke," Master thesis, FEUP/ICBAS, University of Porto,

2017.
[99] T. Yang, K. E. Roder, and T. J. Abbruscato, “Evaluation of bEnd5 cell line as an in vitro model for the blood-brain barrier under normal and hypoxic/aglycemic conditions,” *J. Pharm. Sci.*, vol. 96, no. 12, pp. 3196–3213, 2007.
[100] A. C. H. Yu, G. A. Gregory, and P. H. Chan, “Hypoxia-induced dysfunctions and injury of astrocytes in primary cell cultures,” *J. Cereb. Blood Flow Metab.*, vol. 9, no. 1, pp. 20–28, 1989.
[101] H. Zhu *et al.*, “Baicalin reduces the permeability of the blood-brain barrier during hypoxia in vitro by increasing the expression of tight junction proteins in brain microvascular endothelial cells,” *J. Ethnopharmacol.*, vol. 141, no. 2, pp. 714–720, 2012.
[102] Y. F. Wang, Y. T. Gu, G. H. Qin, L. Zhong, and Y. N. Meng, “Curcumin ameliorates the permeability of the blood-brain barrier during hypoxia by upregulating heme oxygenase-1 expression in brain microvascular endothelial cells,” *J. Mol. Neurosci.*, vol. 51, no. 2, pp. 344–351, 2013.
[103] K. Yamagata, M. Tagami, F. Takenaga, Y. Yamori, and S. Itoh, “Hypoxia-induced changes in tight junction permeability of brain capillary endothelial cells are associated with IL-1beta and nitric oxide,” *Neurobiol. Dis.*, vol. 17, no. 3, pp. 491–499, 2004.
[104] T. J. Abbruscato and T. P. Davis, “Combination of hypoxia/aglycemia compromises in vitro blood-brain barrier integrity.,” *J. Pharmacol. Exp. Ther.*, vol. 289, no. 2, pp. 668–75, 1999.
[105] T. Tilling, D. Korte, D. Hoheisel, and H. J. Galla, “Basement membrane proteins influence brain capillary endothelial barrier function in vitro.,” *J. Neurochem.*, vol. 71, no. 3, pp. 1151–1157, 1998.
[106] G. Li *et al.*, “Permeability of endothelial and astrocyte cocultures: In vitro Blood-brain barrier models for drug delivery studies,” *Ann. Biomed. Eng.*, vol. 38, no. 8, pp. 2499–2511, 2010.
[107] T. Koto *et al.*, “Hypoxia disrupts the barrier function of neural blood vessels through changes in the expression of claudin-5 in endothelial cells,” *Am. J. Pathol.*, vol. 170, no. 4, pp. 1389–1397, 2007.
[108] S. D. Santos *et al.*, “PAMAM Dendrimers: Blood-Brain Barrier Transport and Neuronal Uptake after Focal Brain Ischemia,” *J. Control. Release*, no. [in revision].
[109] H. S. Sharma, “Nanoneuroscience: Emerging concepts on nanoneurotoxicity and nanoneuroprotection,” *Nanomedicine*, vol. 2, no. 6, pp. 753–758, 2007.
[110] X. Tian *et al.*, “LRP-1-mediated intracellular antibody delivery to the Central Nervous System,” *Sci. Rep.*, vol. 5, 2015.
[111] W. J. Brownlee and F. P. Seib, “Impact of the hypoxic phenotype on the uptake and efflux of nanoparticles by human breast cancer cells,” *Sci. Rep.*, vol. 8, 2018.
[112] S. Page, A. Munsell, and A. J. Al-Ahmad, “Cerebral hypoxia/ischemia selectively disrupts tight junctions complexes in stem cell-derived human brain microvascular endothelial cells,” *Fluids Barriers CNS*, vol. 13, no. 1, 2016.
[113] D. Wang *et al.*, “Key role of 15-LO/15-HETE in angiogenesis and functional recovery in later stages of post-stroke mice,” *Sci. Rep.*, vol. 7, 2017.
[114] V. H. Tam, C. Sosa, R. Liu, N. Yao, and R. D. Priestley, “Nanomedicine as a non-invasive strategy for drug delivery across the blood brain barrier,” *International Journal of Pharmaceutics*, vol. 515, no. 1–2. pp. 331–342, 2016.
[115] Y. Wang *et al.*, “Regulation of endocytosis via the oxygen-sensing pathway,” *Nat. Med.*, vol. 15, no. 3, pp. 319–325, 2009.
[116] E. Bourseau-Guilmain *et al.*, “Hypoxia regulates global membrane protein endocytosis through caveolin-1 in cancer cells,” *Nat. Commun.*, vol. 7, 2016.
[117] Y. Nishimura *et al.*, “Identification of a novel indoline derivative for in vivo fluorescent imaging of blood-brain barrier disruption in animal models,” *ACS Chem. Neurosci.*, vol. 4, no. 8, pp. 1183–1193, 2013.
[118] B. P. Eliceiri, A. M. Gonzalez, and A. Baird, “Zebrafish Model of the Blood-Brain Barrier:

Morphological and Permeability Studies," *Methods Mol. Biol.*, no. 686, pp. 3171–378, 2011.
[119] K. Watanabe *et al.*, "In vivo assessment of the permeability of the blood-brain barrier and blood-retinal barrier to fluorescent indoline derivatives in zebrafish," *BMC Neurosci.*, vol. 13, no. 1, 2012.
[120] J. Y. Jeong *et al.*, "Functional and developmental analysis of the blood-brain barrier in zebrafish," *Brain Res. Bull.*, vol. 75, no. 5, pp. 619–628, 2008.
[121] "Mind the graph," 2016. [Online]. Available: https://blog.mindthegraph.com/scientific-illustrations-maker/#.W6i6QGhKg2w. [Accessed: 24-Apr-2018].
[122] M. Bacigaluppi, G. Comi, and D. M. Hermann, "Animal Models of Ischemic Stroke. Part Two: Modeling Cerebral Ischemia," *Open Neurol. J.*, vol. 4, no. 2, pp. 34–38, 2010.
[123] E. H. H. Shang and R. S. S. Wu, "Aquatic hypoxia is a teratogen and affects fish embryonic development," *Environ. Sci. Technol.*, vol. 38, no. 18, pp. 4763–4767, 2004.
[124] W. R. Barrionuevo, M. N. Fernandes, and O. Rocha, "Aerobic and anaerobic metabolism for the zebrafish, Danio rerio, reared under normoxic and hypoxic conditions and exposed to acute hypoxia during development.," *Braz. J. Biol.*, vol. 70, no. 2, pp. 425–34, 2010.
[125] T. Schwerte, D. Uberbacher, and B. Pelster, "Non-invasive imaging of blood cell concentration and blood distribution in zebrafish Danio rerio incubated in hypoxic conditions in vivo.," *J. Exp. Biol.*, vol. 206, pp. 1299–1307, 2003.
[126] "Expression Disruption Screen - ED141B," *Centro Andaluz de Biología del Desarollo*, 2013. [Online]. Available: https://www.upo.es/CABD/EDscreen/ED/ED00141B.html. [Accessed: 06-Sep-2018].
[127] R. E. Kast, "Using blood brain barrier disruption by methamphetamine for drug delivery," *Journal of Neuro-Oncology*, vol. 85, no. 1. pp. 109–110, 2007.
[128] R. T. Bartus, P. Elliott, N. Hayward, R. Dean, E. L. McEwen, and S. K. Fisher, "Permeability of the blood brain barrier by the bradykinin agonist, RMP-7: Evidence for a sensitive, auto-regulated, receptor-mediated system," in *Immunopharmacology*, 1996, vol. 33, no. 1–3, pp. 270–278.
[129] B. Malfroy-Camine, "Method for increasing blood-brain barrier permeability by administrating a bradykinin agonist of blood-brain barrier permeability," 5,112,596, 1992.
[130] A. M. Stewart, O. Braubach, J. Spitsbergen, R. Gerlai, and A. V. Kalueff, "Zebrafish models for translational neuroscience research: From tank to bedside," *Trends in Neurosciences*, vol. 37, no. 5. pp. 264–278, 2014.
[131] F. Ahmad, L. P. J. J. Noldus, R. A. J. Tegelenbosch, and M. K. Richardson, "Zebrafish embryos and larvae in behavioural assays," *Behaviour*, vol. 149, no. 10–12, pp. 1241–1281, 2012.
[132] M. M. Braga *et al.*, "Evaluation of spontaneous recovery of behavioral and brain injury profiles in zebrafish after hypoxia," *Behav. Brain Res.*, vol. 253, pp. 145–151, 2013.

This page was intentionally left in blank.

Supplementary Data

Section 3.2.1.

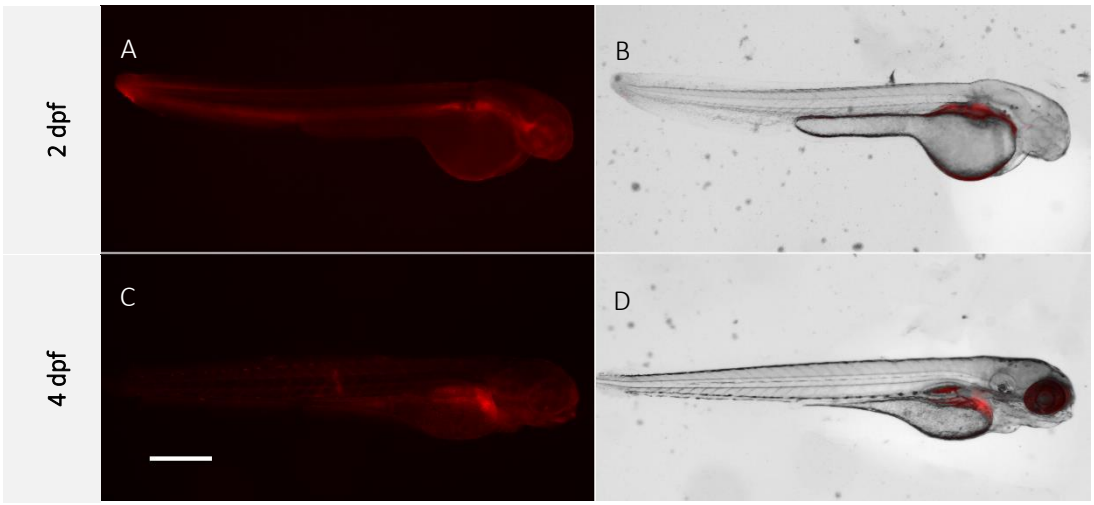

Figure S1 – *BBB maturation analysis after adding EB (0.1% (m/v)) in the swimming medium*. *In vivo* images of 2 and 4 dpf zebrafish under a fluorescence stereomicroscope. **A** and **C**: EB (red) channel; **B** and **D**: Brightfield merged with EB channel. Scale bar: 250 µm

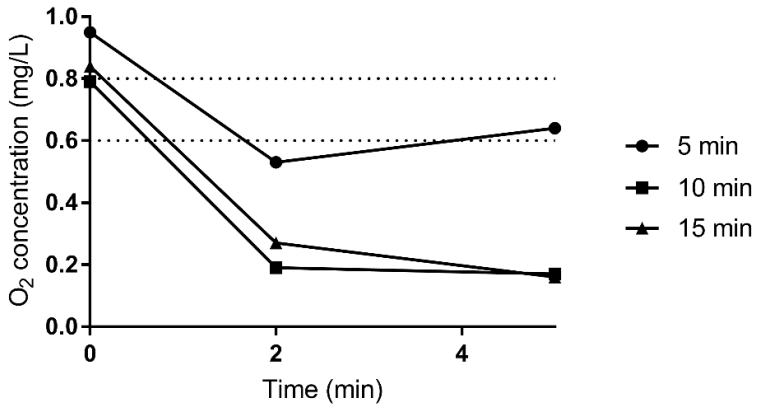

Figure S2 – *Preliminary oximeter measurements of the hypoxic chamber*. Oxygen levels in the hypoxia chamber by using different bubbling times (5, 10 and 15 min) and two methods of medium extraction from the chamber to the oximeter: with a needle and a syringe (timepoint 0 min) and after opening the lid and carefully with a pipette (timepoints 2 and 5 min).

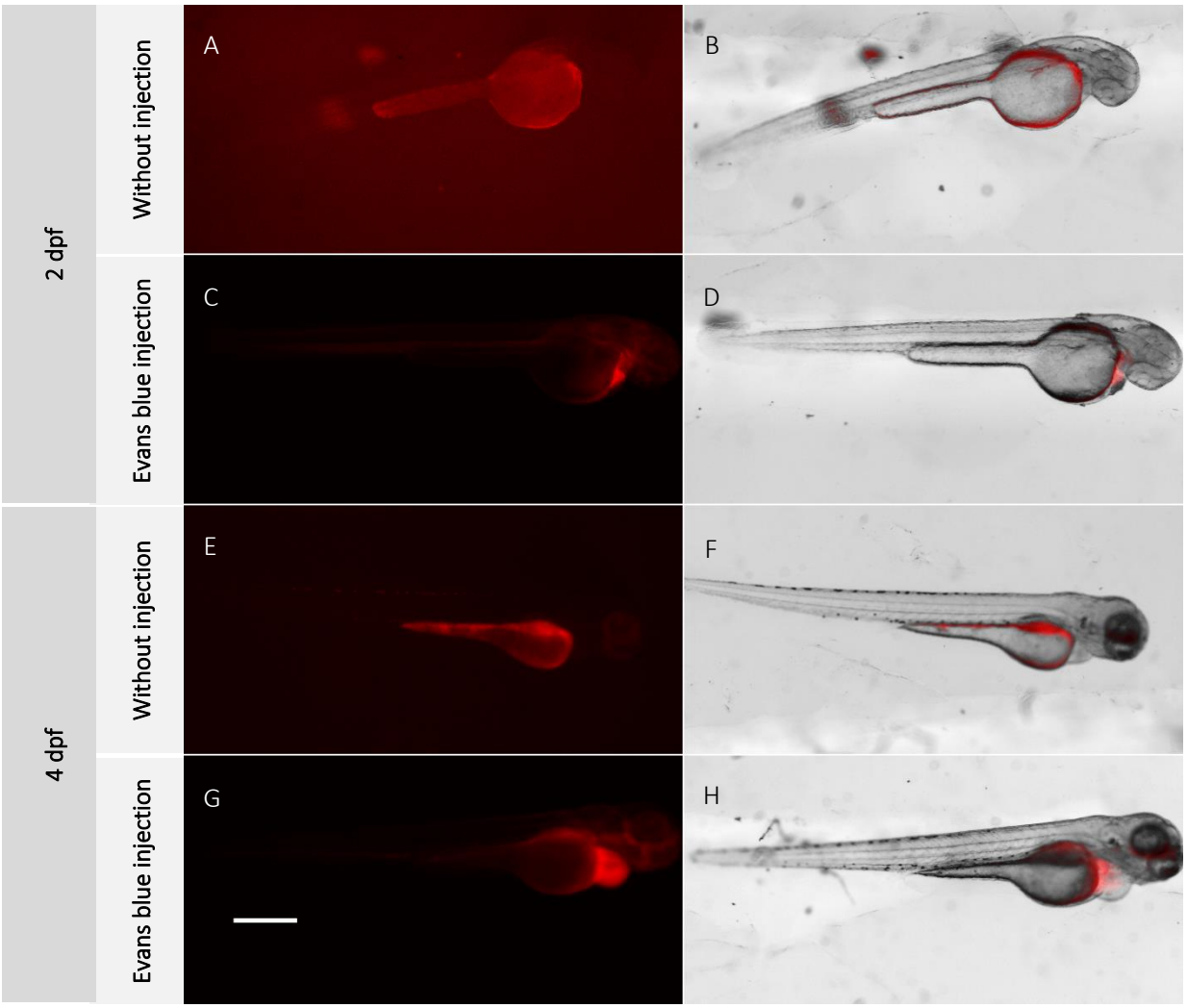

Figure S3 – *BBB maturation analysis after injecting EB in the pericardial site*. *In vivo* images of 2 and 4 dpf zebrafish under a fluorescence stereomicroscope with and without EB injection. **A**, **C, E** and **G**: EB (red) channel; **B**, **D, F** and **H**: Brightfield merged with EB channel. Scale bar: 250 µm

SECTION 3.2.2.2.

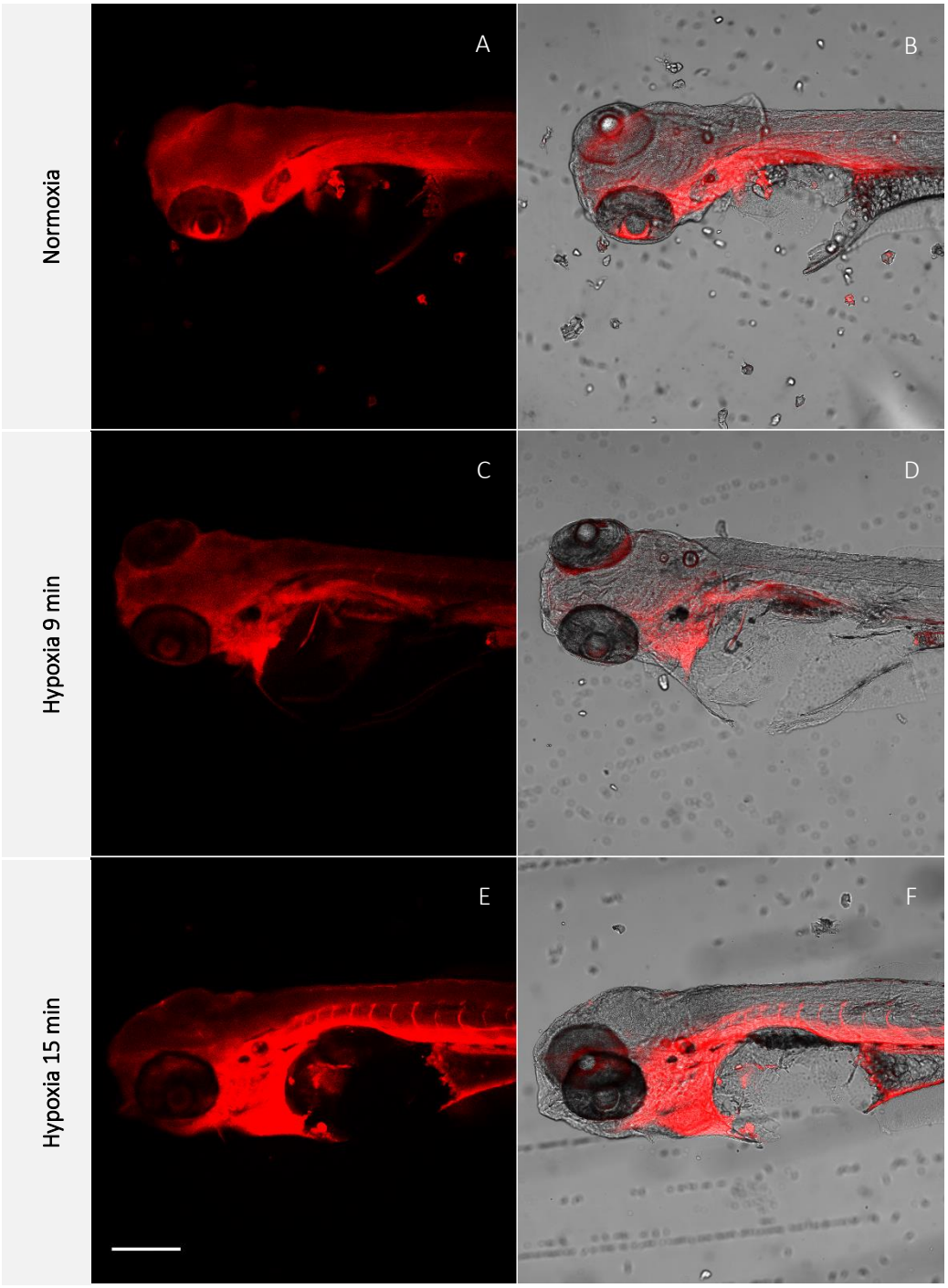

Figure S4 – *Short hypoxia effects in BBB tightness in zebrafish larvae*. *Ex vivo* images of zebrafish larvae subjected to normoxia – A, B and different hypoxia times (9 – C, D and 15 min – E, F) and after Eb injection under a stereomicroscope. **A**, **C** and **E**: EB (red) channel; **B**, **D** and **F**: Brightfield merged with EB channel. Scale bar: 250 µm

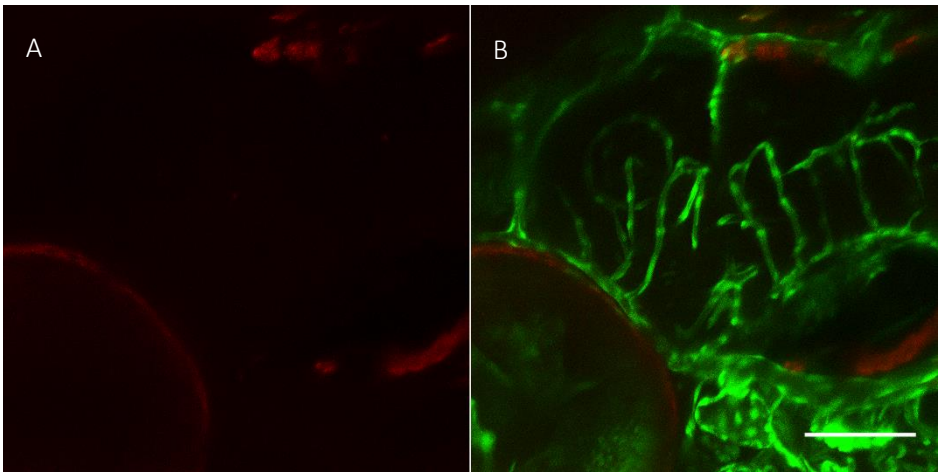

Figure S5 - *In vivo imaging of the transgenic animal with blood vessels stained*. Confocal microscope images of the transgenic animal without treatment in Evans blue channel (A) and EB and green channel (B). Scale bar: 100 µm

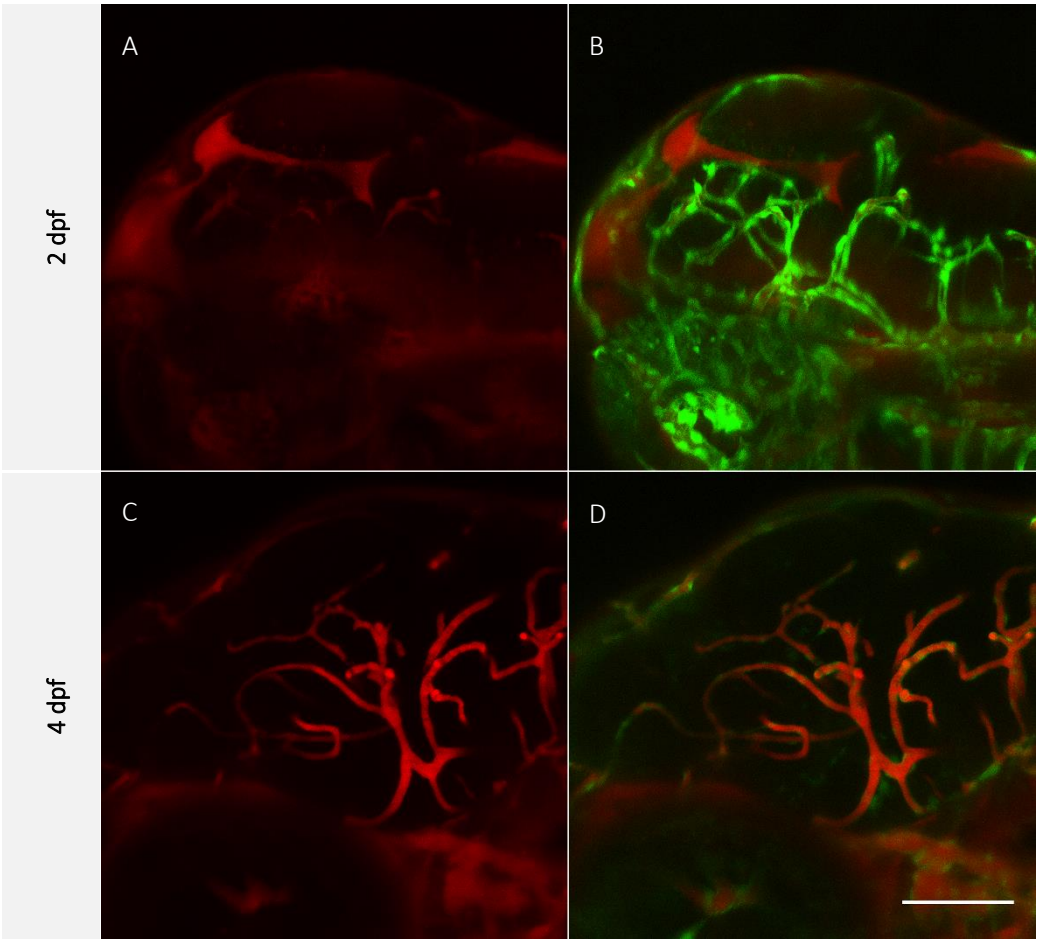

Figure S6 – *BBB maturation analysis of endogenous blood vessels labeled zebrafish*. *In vivo* images of 2 and 4 dpf after EB injection. **A** and **C**: EB channel; **B** and **D**: Blood vessels fluorescence merged with EB channel. Scale bar: 100 µm